SMOOTH SWITCHING LPV CONTROL AND ITS APPLICATIONS

Ву

Tianyi He

A DISSERTATION

Submitted to
Michigan State University
in partial fulfillment of the requirements
for the degree of

Mechanical Engineering – Doctor of Philosophy

ABSTRACT

SMOOTH SWITCHING LPV CONTROL AND ITS APPLICATIONS

By

Tianyi He

This dissertation studies the smooth switching LPV (Linear Parameter-Varying) system and control, as well as its applications in mechanical systems, aerospace systems to achieve the smooth transition between switching LPV controllers. Both state-feedback and dynamic output-feedback cases are addressed by the simultaneous design approach of smooth switching LPV control, and the proposed method has been applied to active vibration control of BWB (Blended-Wing-Body) aircraft flexible wing and the AMB (Active Magnetic Bearing) system. Moreover, a sequential design approach is developed to design smooth switching LPV controllers, where the high-dimensional optimization in the simultaneous design approach can be relaxed.

In conventional switching LPV control, switching controllers are designed on each subregion while guaranteeing safe switching, but without considering the smoothness during switching events. The abruptly varying control signal can exceed actuator authority; moreover, abrupt changes in system responses caused by unsmooth controller gains will be harmful to system components and hardware. The simultaneous design of smooth switching LPV control minimizes a combined cost of system output \mathcal{H}_2 performance and smooth-switching index subject to \mathcal{H}_2 constraints on control inputs and \mathcal{H}_∞ constraint on bounded model uncertainty. These stability and performance criteria are then formulated using a set of Parametric Linear Matrix Inequalities (PLMIs). Besides, a tunable weighting coefficient is introduced to provide an optimal trade-off design between system \mathcal{H}_2 performance and switching smoothness. Simulation results with the AMB model and BWB aircraft wing model are provided to demonstrate the effectiveness of the proposed smooth switching control.

In the above approach, switching controllers are synthesized by controller variables that simultaneously satisfy PLMIs on all subregions and switching stability conditions on all switching

surfaces. When the number of subregions goes large, simultaneous design approach leads to a high-dimensional optimization problem, with a high number of LMI constraints, decision variables, online computational load, and memory requirement. As a result, these drawbacks make simultaneous design practically infeasible for high-order systems with many divided subregions. An innovative sequential design approach is proposed by introducing interpolated controller decision variables and formulating independent PLMI conditions on each subregion such that system performances on overlapped subregions are guaranteed as well. In this way, the switching controller synthesis conditions are formulated as independent optimization problems and can be well solved sequentially.

Besides, this dissertation also utilizes the LPV framework to investigate optimal sensor placement to achieve optimal vibration suppression for a flexible BWB airplane wing. For a given flight speed range, vibration behaviors of the wing structure are evaluated by the guaranteed \mathcal{H}_2 performance with the \mathcal{H}_2 LPV controller. Candidate sensor locations are identified on each wing, and the optimal sensor placements can be found among these candidate sensor locations by the greedy algorithm. The searched optimal results are validated by globally searching through all possible combinations. With the LPV model of a flexible wing and \mathcal{H}_2 controller synthesis conditions, search results provide the optimal sensor locations, and besides, the trade-off between optimal system performance and the number of sensors can also be obtained.

ACKNOWLEDGMENTS

Many years later, as I face this dissertation, every detail will probably not be recalled, but that distant time devoted to it will be remembered.

Since joining Michigan State University as a Ph.D. student in 2015, I've been feeling so fortunate receiving so many encouragements, supports, and communications with beautiful minds from this community. There are so many people who deserve recognition, respect, and thanks for the contributions to the completion of this dissertation, as well as their kind help throughout my entire Ph.D. study.

Foremost, I would like to express my most enormous gratitude to my advisor, Professor Guoming George Zhu, who is more than an exceptional researcher with distinguished research taste both in control theory and applications, and also an uncommon educator with enthusiastic passion to communicate with and help students, to train students with outstanding engineering skills and research ethics. During my Ph.D. study, Professor Zhu has been open-minded for any new ideas, and always been there, offering discussions and suggestions. Thanks to his supervision and financial support, I've been able to get this research done and complete my Ph.D. study.

Besides, I would like to thank Senior Scientist Dr. Sean Swei at NASA Ames Research Center, and Professor Weihua Su at University of Alabama, for their guidance and help on the BWB airplane vibration control project, as well as their invaluable career advice. They have brought me the possibility of connecting control theory into aerospace engineering projects, which has provided me precise experience in control engineering.

I would also like to thank Professor Hassan Khalil, Professor Ranjan Mukherjee, Professor Brian Feeny, for serving on my guidance committee. They have always been ready to offer kind help and give wise advice for my research work. What's more, I've benefited so much from their lectures and talks, which draw me a 'big' picture of control theory and engineering, equip me with mathematical tools, and direct me into the right tracks to complete my Ph.D. degree.

Many thanks go to all the peers in the ERC lab at Michigan State University. We have had a good time taking lectures, collaborating, and discussing research problems, playing, and sporting. The time we get together is limited, but the joy is undoubtedly not. Their names are: Dr. Liang Liu, Dr. Ali Al-jiboory, Dr. Ruitao Song, Dr. Aqeel Salim, Dr. Yifan Men, Dr. Ali Alhajjar, Dr. Yingxu Wang, Ms. Ruixue Christine Li, Mr. Shen Qu, Mr. Wenpeng Wei, Mr. Anuj Pal, Mr. Jian Tang, Dr. Donghao Hao, Dr. Huan Li, Dr. Chengsheng Miao, Ms. Dawei Hu, Mr. Yu He and Mr. Lingyun Hua.

In particular, I would like to express special gratitude to the special one, Ms. Sijing Li, as well as Delta Airline for connecting us between DTW and BOS. Last but not least, my deep gratitude is given to my family. Without their support, completion of the Ph.D. degree couldn't be possible.

TABLE OF CONTENTS

LIST O	FTABL	ES
LIST O	F FIGUI	RES
LIST O	F ALGC	ORITHMS xiv
СНАРТ	ER 1	INTRODUCTION
1.1		ystem and Control
	1.1.1	Overview
	1.1.2	LPV system and performance
	1.1.3	Performance specifications and PLMI formulations
		1.1.3.1 \mathcal{H}_{∞} performance
		1.1.3.2 \mathcal{H}_2 performance
1.2	Switch	ing LPV System and Control
1.2	1.2.1	Overview
	1.2.2	Switching LPV system and performance
	1.2.3	Performance specifications in switching LPV system
	1.2.3	1.2.3.1 \mathcal{H}_{∞} performance
		1.2.3.2 \mathcal{H}_2 performance
	1.2.4	Switching strategies and stability conditions
	1.2.4	
		,
1.2	Matiria	
1.3		ations of Smooth Switching LPV Control
1.4	Organi	zation of This Dissertation
СНАРТ	ER 2	SMOOTH SWITCHING LPV CONTROL 2
2.1	Mixed	ICC/\mathcal{H}_{∞} Control
	2.1.1	State-feedback LPV control
	2.1.2	Dynamic output-feedback LPV control
		2.1.2.1 ICC condition
		2.1.2.2 Synthesis conditions
2.2	Simult	aneous Design Approach
	2.2.1	Continuous-time state-feedback case
		2.2.1.1 Problem formulation
		2.2.1.2 Controller synthesis PLMIs
	2.2.2	Continuous-time dynamic output-feedback (DOF) case
	2.2.2	2.2.2.1 Problem formulation
		2.2.2.2 Controller synthesis PLMIs
2.3	Seguer	ntial Design Approach
4.3	2.3.1	Motivations of sequential design
		Controller synthesis PLMIs
	41.4	- COMBOURD SYMMESIS FLAVIS

	2.3.2.1 One-dimensional scheduling parameter 50
	2.3.2.2 Two-dimensional scheduling parameters
	2.3.2.3 Scheduling parameter of any dimensions
2.4	PLMI Relaxation Method
	2.4.1 Modeling scheduling parameters 61
	2.4.2 PLMIs relaxation
CHADE	ED 2 A DDI ICATION EVANDI EG
CHAPT	
3.1	Active Magnetic Bearing (AMB) Model
	3.1.1 Trade-off between $trace(W)$ and ICC conditions
	3.1.2 Smooth switching LPV control by simultaneous design 67
	3.1.2.1 Trade-off between $trace(W)$ and switching smoothness 67
	3.1.2.2 Simulation results and discussions
3.2	Blended-Wing-Body (BWB) Airplane Flexible Wing
	3.2.1 LPV modeling of BWB airplane flexible wing
	3.2.2 Mixed ICC/ \mathcal{H}_{∞} LPV control
	3.2.2.1 Constraints and performance trade-off
	3.2.2.2 Mixed ICC and \mathcal{H}_{∞} Control Problem
	3.2.2.3 Time-domain simulation results 80
	3.2.3 Smooth switching LPV control by simultaneous design
	3.2.3.1 Time-domain simulation results
3.3	Numerical Examples for Sequential Design
	3.3.1 Example 1
	3.3.2 Example 2
СНАРТ	ER 4 OPTIMAL SENSOR PLACEMENT
4.1	Introduction
4.1	
	Problem formulation of sensor placement
4.3	Simulation results by global search
	4.3.1 Simulation results
4 4	4.3.2 Discussion
4.4	Sub-modular property of sensor placement problem
	4.4.1 Set function and sub-modular property
	4.4.2 Greedy algorithm
CHAPT	ER 5 CONCLUSIONS AND RECOMMENDED WORK
5.1	Conclusions
5.2	Recommended work
RIRI IA	GRAPHY
סוטעוט	OIMM 1111

LIST OF TABLES

Table 3.1:	Mode description in reduced-order model	74
Table 3.2:	Comparison of three different design methods in each design iteration	101
Table 3.3:	Comparison of three different design methods in each design iteration	108
Table 4.1:	Summary of optimal sensor candidate combinations	118

LIST OF FIGURES

Figure 1.1:	Classical gain-scheduling control	2
Figure 1.2:	LPV control-modern gain-scheduling control	3
Figure 1.3:	Closed-loop LPV system in LFT form with uncertainty block	5
Figure 1.4:	Switching LPV gain-scheduling control	9
Figure 1.5:	Three-subregion partition of scheduling parameter region	9
Figure 1.6:	Unsmooth control input signal from conventional switching LPV control [1]	17
Figure 1.7:	Illustration of motivations of smooth switching LPV control	18
Figure 1.8:	Roadmap of this dissertation	20
Figure 2.1:	Subregion division illustration of one-dimensional scheduling parameter	48
Figure 2.2:	Subregion division illustration of two-dimensional scheduling parameter	48
Figure 3.1:	Trajectory of scheduling parameter, rotor speed	65
Figure 3.2:	Trade-off relationship between \overline{U} and $trace(W)$	66
Figure 3.3:	x_1 response under different ICC conditions	66
Figure 3.4:	x_2 response under different ICC conditions	67
Figure 3.5:	u_1 response under different ICC conditions	67
Figure 3.6:	u_2 response under different ICC conditions	68
Figure 3.7:	Control inputs under infinite ICC conditions	68
Figure 3.8:	Trade-off relationship between switching smoothness and $trace(W)$ under \overline{U}_1 =10 7	69
Figure 3.9:	Trade-off relationship between switching smoothness and $trace(W)$ under \overline{U}_2 =10 ⁸	69
Figure 3.10:	State x_1 response by [1] and proposed method	70

Figure 3.11: State x_2 response by [1] and proposed method	70
Figure 3.12: Control input u_1 response by [1] and proposed method	71
Figure 3.13: Control input u_2 response by [1] and proposed method	71
Figure 3.14: Schematic layout of BWB airplane configuration	74
Figure 3.15: Root loci of open-loop system with varying flight speed	75
Figure 3.16: Three-subregion partition for scheduling parameter	76
Figure 3.17: Scheduling parameter (flight speed) trajectory	77
Figure 3.18: Trade-off between control limit \bar{U} and trace(W) at different robustness conditions	78
Figure 3.19: Bending displacement at wing root	81
Figure 3.20: Bending displacement at wing tip	81
Figure 3.21: Wing root bending under different \bar{U}	82
Figure 3.22: Wing tip bending under different \bar{U}	82
Figure 3.23: Control input 1 under different \bar{U}	83
Figure 3.24: Control input 2 under different \bar{U}	83
Figure 3.25: Control input 3 under different \bar{U}	84
Figure 3.26: Control input 4 under different \bar{U}	84
Figure 3.27: Control input 5 under different \bar{U}	85
Figure 3.28: Control input 6 under different \bar{U}	85
Figure 3.29: Wing root bending under different γ_{∞}	87
Figure 3.30: Wing tip bending under different γ_{∞}	87
Figure 3.31: Control input 1 under different γ_{∞}	88
Figure 3.32: Control input 2 under different γ_{∞}	88
Figure 3.33: Control input 1 under different γ_{∞}	89

Figure 3.34:	Control input 2 under different γ_{∞}	89
Figure 3.35:	Control input 1 under different γ_{∞}	90
Figure 3.36:	Control input 2 under different γ_{∞}	90
Figure 3.37:	Root loci of closed-loop system	91
Figure 3.38:	Closed-loop ICC cost with LPV and LTI models	91
Figure 3.39:	Scheduling parameter with switching events	92
Figure 3.40:	Unforced bending displacements at wing root (upper) and wing tip (lower)	93
Figure 3.41:	Trade-off between $trace(W)$ and smoothness index I_{sm}	93
Figure 3.42:	Upper: comparison at wing root with smooth/un-smooth switching controller; Lower: comparison at wing root with three control methods	94
Figure 3.43:	Upper: comparison at wing tip with smooth/un-smooth switching controller; Lower: comparison at wing tip with three control methods	95
Figure 3.44:	Upper: control 1 responses comparison with smooth/un-smooth switching controller; Lower: control 1 responses comparison with three control methods .	97
Figure 3.45:	Upper: control 2 responses comparison with smooth/un-smooth switching controller; Lower: control 2 responses comparison with three control methods .	97
Figure 3.46:	Upper: control 3 responses comparison with smooth/un-smooth switching controller; Lower: control 3 responses comparison with three control methods .	98
Figure 3.47:	Upper: control 4 responses comparison with smooth/un-smooth switching controller; Lower: control 4 responses comparison with three control methods .	98
Figure 3.48:	Upper: control 5 responses comparison with smooth/un-smooth switching controller; Lower: control 5 responses comparison with three control methods .	99
Figure 3.49:	Upper: control 6 responses comparison with smooth/un-smooth switching controller; Lower: control 6 responses comparison with three control methods .	99
Figure 3.50:	γ_1 obtained by sequential (black), simultaneous(blue) and non-switching(red) design approach	101
Figure 3.51:	γ_2 obtained by sequential (black), simultaneous(blue) and non-switching(red) design approach	102

Figure 3.52:	γ_3 obtained by sequential (black), simultaneous(blue) and non-switching(red) design approach	. 102
Figure 3.53:	Closed-loop system states responses by sequential (black), simultaneous(blue) and non-switching(red) design approaches	. 104
Figure 3.54:	γ_{11} obtained by sequential(black), simultaneous(blue) and non-switching(red) design approach	. 106
Figure 3.55:	γ_{12} obtained by sequential(black), simultaneous(blue) and non-switching(red) design approach	. 107
Figure 3.56:	γ_{21} obtained by sequential(black), simultaneous(blue) and non-switching(red) design approach	. 107
Figure 3.57:	γ_{22} obtained by sequential(black), simultaneous(blue) and non-switching(red) design approach	. 108
Figure 4.1:	Sensor location candidates	. 112
Figure 4.2:	trace(W) versus the number of available sensors, $U=6$. 114
Figure 4.3:	trace(W) versus the number of available sensors, $U=8$. 115
Figure 4.4:	trace(W) versus number of available sensors, at flight speed 115 m/s	. 117
Figure 4.5:	trace(W) versus number of available sensors, at flight speed 125 m/s	. 117
Figure 4.6:	Sensor contribution to each vibration mode at flight speed 110 $m/s \dots \dots$. 119
Figure 4.7:	Sensor contribution to each vibration mode at flight speed 113 m/s	. 120
Figure 4.8:	Sensor contribution to each vibration mode at flight speed 115 m/s	. 120
Figure 4.9:	Submodular property of sensor placement on flexible wing	. 123
Figure 5.1:	A controller scheme with compensating operator Q	. 127

LIST OF ALGORITHMS

Algorithm 1: Greedy algorithm for set function optimization	•				 			. 12	22
Algorithm 2: Greedy algorithm for optimal sensor placement								. 12	24

CHAPTER 1

INTRODUCTION

1.1 LPV System and Control

1.1.1 Overview

Linear Parameter-Varying (LPV) system and control have gained significant interest from the control community over the past two decades [2, 3, 4, 5, 6, 7, 8]. The main benefit of the LPV system is that the varying characteristics of system dynamics can be captured by the LPV model with its linear system matrices dependent on scheduling parameter. LPV controllers can be designed with its gain scheduled based on the scheduling parameters measured in real-time.

The LPV control method is seen as a "modern" gain-scheduling control, which is one of the most popular and effective approaches to address nonlinear systems. Gain-scheduling control has been widely used in a wide variety of dynamical systems with nonlinear and time-varying dynamics. The *classical* gain-scheduling control utilizes the idea of *divide and conquer*. The nonlinear system is firstly linearized at gridded operating points to a bundle of linear models, usually called *parametric* gridded model. Linear controllers are then designed based on each local model by linear control theory, which leads to a bundle of corresponding fixed-gain linear controllers. In controller implementation, controller gains are scheduled or switched according to operating points. As shown in Figure 1.1, one linear controller is active when the system is operating within the region close to its linearization point.

The classical gain-scheduling tackles the complicated nonlinear control problem by solving a bundle of simpler sub-problems, however, it has a few drawbacks and limitations in theory and applications.

• Classical gain-scheduling control designs linear controller at gridded operating points, thus stability, performance, and robustness can only be guaranteed locally, but not globally in the

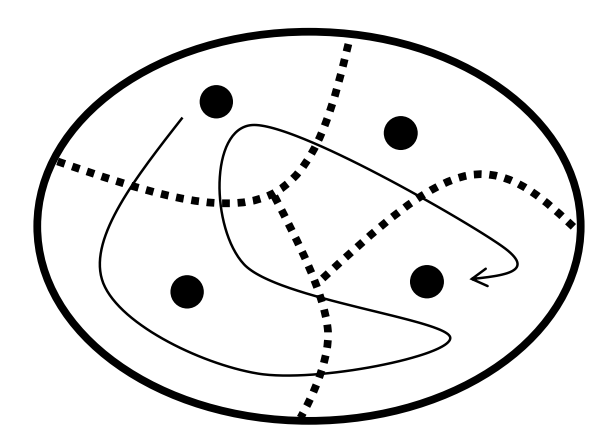


Figure 1.1: Classical gain-scheduling control

entire operating region. The closed-loop system performance by linear controllers designed at gridded points will degrade when the current operating point deviates from linearization points.

- Classical gain-scheduling control is only suitable for the slow-varying system, because the switching stability between local controllers will impose constraints on switching signals. This is well studied in switching stability conditions in switching LTI systems [9, 10].
- The trade-off between the density of gridding points and computational complexity needs to be well considered. In general, more gridding points are needed to more precisely describe the system dynamics, which inevitably increases computational complexity. Moreover, gridded linear controllers are designed beforehand and are restored in memory, then they are read from memory in controller implementation, which means that more memory is needed by more gridded operating points.

To avoid the drawbacks of classical gain-scheduling control and retain the gain-scheduling strategy, *modern* LPV control has been proposed in the early 90s' by Shamma [11] and extended by pioneering researchers Becker, Apkarian, Gahinet and Wu [12, 2, 3, 13, 14, 15, 16]. The modern gain-scheduling control-LPV control can be described in Figure 1.2. In modern gain-scheduling control, controllers are designed with scheduling gains over the entire operating region. The operating conditions are considered as scheduling parameters and assumed to be available in

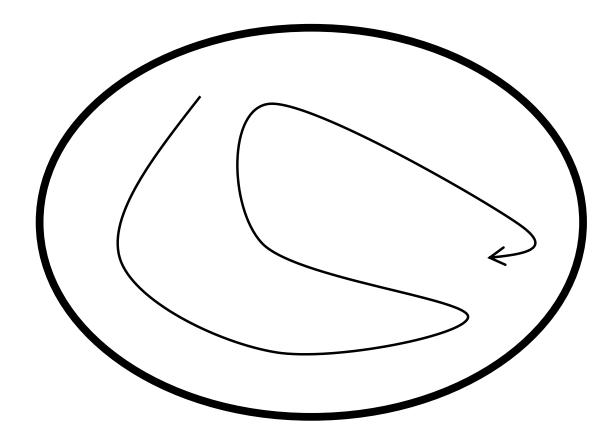


Figure 1.2: LPV control-modern gain-scheduling control

real-time. The controller matrices are designed as parameter-dependent and vary with scheduling parameters.

The mainstream approach of LPV gain-scheduling control design is to formulate control synthesis conditions in terms of Linear Matrix Inequalities (LMIs) or Parameterized Linear Matrix Inequalities (PLMIs) [12, 17, 3, 18, 19, 20, 13]. Numerically tractable optimization methods, such as convex optimization, can then be applied to solve for feasible or optimal LPV gain-scheduling controllers. LPV control designs with pole placement, guaranteed \mathcal{H}_2 and/or \mathcal{H}_∞ performance have been intensively studied in the literature [21, 22, 23, 24, 20, 13, 15], as well as the case of inexact scheduling parameters [25, 26, 27, 28, 29, 30, 31, 32], and LPV systems with delay [16].

As long as a solution to the formulated optimization problem is obtained, then the derived parameter-dependent LPV controller matrices will achieve the guaranteed system performance. Apparently, the modern LPV gain-scheduling control is able to guarantee stability globally over the scheduling parameter region, to achieve guaranteed closed-loop system performance, and to avoid repeating linearization and linear controller design.

This chapter introduces the non-switching LPV system and control, followed by the switching LPV system and control. The system description, system performance specifications, and multiple performance channels will be included in the following context.

1.1.2 LPV system and performance

Consider the closed-loop LPV system described by

$$\Sigma_{cl}(\theta) : \begin{cases} \dot{x}(t) = A_{cl}(\theta)x(t) + B_{\infty}(\theta)w_{\infty}(t) + B_{2}(\theta)w_{2}(t); \\ z_{\infty}(t) = C_{cl,\infty}(\theta)x(t) + D_{\infty}(\theta)w_{\infty}(t) \\ z_{2}(t) = C_{cl,2}(\theta)x(t) \end{cases}$$

$$(1.1)$$

where $\theta(t) = \left[\theta_1(t), \theta_2(t), \dots, \theta_q(t)\right]^T$ denotes the scheduling parameter vector of q elements, x(t) denotes the state, $w_\infty(t)$ the exogenous inputs (for instance, system uncertainty input, sensor noises, etc.), and w_2 the disturbance input; $z_\infty(t)$ the \mathcal{H}_∞ controlled output, $z_2(t)$ the \mathcal{H}_2 performance output. The system matrices depend on the scheduling parameter vector θ , which is assumed to be measurable in real-time. The magnitude and variational rate $\dot{\theta}$ are bounded as

$$\theta \in \Theta = \left\{ \underline{\theta}_i \le \theta_i(t) \le \overline{\theta}_i, i \in \{1, 2, ..., q\}, \right\}$$

$$\dot{\theta} \in \Lambda = \left\{ -\nu_i \le \dot{\theta}_i(t) \le \nu_i, i \in \{1, 2, ..., q\}. \right\}$$
(1.2)

There are two independent performance channels in this system, \mathcal{H}_2 channel from w_2 to z_2 and \mathcal{H}_∞ channel from w_∞ to z_∞ . In the next subsections, system performances are specified. Throughout this dissertation, we make use of the following standard definition of \mathcal{L}_2 and \mathcal{L}_∞ norms on $x(t) \in \mathbb{R}^n$ for all $t \geq 0$,

$$||x||_2^2 := \int_0^\infty x^T(t)x(t)dt, \quad ||x||_\infty^2 := \sup_{t>0} x(t)^T x(t).$$

1.1.3 Performance specifications and PLMI formulations

It should be noted that there are two separate input and output pairs defined in (1.1), and they are specifically designated for assessing the closed-loop LPV system performances, as shown in Figure 1.3. In the mixed $\mathcal{H}_{\infty}/\mathcal{H}_2$ control, the LPV system $\Sigma(\theta)$ achieves specific \mathcal{H}_2 performance while subject to \mathcal{H}_{∞} performance constraints. Note that the interconnection of Δ in Figure 1.3 is to capture the model uncertainties in $\Sigma(\theta)$, and the robustness against modeling uncertainty is addressed by \mathcal{H}_{∞} channel. The definitions of \mathcal{H}_{∞} , \mathcal{H}_2 performances are given below.

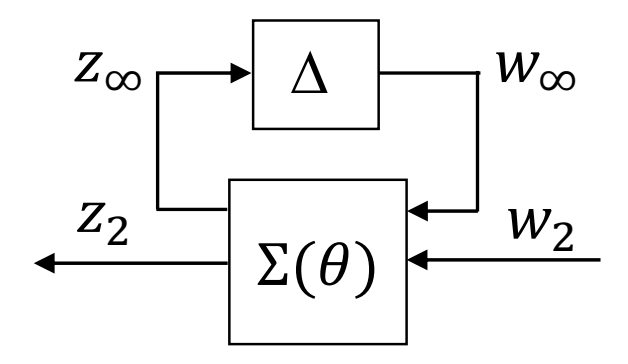


Figure 1.3: Closed-loop LPV system in LFT form with uncertainty block

1.1.3.1 \mathcal{H}_{∞} performance

The \mathcal{H}_{∞} performance, defined from $w_{\infty}(t)$ to $z_{\infty}(t)$ with \mathcal{L}_2 input and \mathcal{L}_2 output, is utilized to assess the closed-loop system robustness in the presence of model uncertainties. Mathematically, $T_{\infty}(\theta,s):=T_{z_{\infty}w_{\infty}}(\theta,s)$ denotes the parameter-dependent transfer function from w(t) to $z_{\infty}(t)$ and $||T_{\infty}||_{\infty}$ the \mathcal{H}_{∞} norm of T_{∞} . Then, the \mathcal{H}_{∞} performance for the $(w_{\infty}(t),z_{\infty}(t))$ pair is defined as \mathcal{L}_2 gain [14, 15], where

$$||T_{\infty}||_{\infty} = \sup_{\theta \in \Theta} \sup_{w_{\infty}, z_{\infty} \in \mathcal{L}_{2}, w_{\infty} \neq 0} \frac{||z_{\infty}(t)||_{2}}{||w_{\infty}(t)||_{2}}.$$

$$(1.3)$$

Physically, \mathcal{H}_{∞} norm is related to the robust stability of a given system with modeling error. Based on the Small Gain Theorem [33], the closed-loop system satisfying the condition $||T_{\infty}||_{\infty} \leq \gamma_{\infty}$ is well-posed and internally stable for all uncertainty satisfying the constrain $||\Delta||_{\infty} < 1/\gamma_{\infty}$, where Δ is system uncertain dynamics interconnected from z_{∞} to w_{∞} , see Figure 1.3. The following Lemma 1 for \mathcal{H}_{∞} performance is given [12, 2, 15].

Lemma 1. Suppose that there exists a parameter dependent positive-definite matrix $P_{\infty}(\theta)$, such that (1.4) holds for any admissible $(\theta, \dot{\theta}) \in \Theta^{(j)} \times \Lambda$. Then the closed-loop system (1.1) is exponentially stable with guaranteed performance $||z_{\infty}||_2 < \gamma ||w_{\infty}||_2$ for a given robustness level

 $\gamma>0$ and for all admissible trajectories $(\theta,\dot{\theta})\in\Theta imes\Lambda$. (* denotes symmetric terms.)

$$\begin{bmatrix} -\dot{P}_{\infty} + A_{cl}P_{\infty} + (*) & * & B_{\infty} \\ C_{cl,\infty}P_{\infty} & -\gamma I & D_{\infty} \\ * & * & -\gamma I \end{bmatrix} < 0$$

$$(1.4)$$

1.1.3.2 \mathcal{H}_2 performance

The \mathcal{H}_2 performance, defined from $w_2(t)$ to $z_2(t)$, is utilized to assess the closed-loop system output performance. Let $T_2(\theta,s):=T_{z_2w_2}(\theta,s)$ be the parameter-dependent transfer function from $w_2(t)$ to $z_2(t)$, and if the closed-loop system matrix A_{cl} is stable, then the \mathcal{H}_2 norm of $T_2(\theta,s)$ is defined as the worst-case \mathcal{H}_2 performance on the subregion Θ [34, 20],

$$||T_{2}(K(\theta), s)||_{2}^{2} = \sup_{\theta \in \Theta} \frac{1}{2\pi} \int_{-\infty}^{\infty} trace \left[T_{2}^{*}(\theta, j\omega) T_{2}(\theta, j\omega) \right] d\omega,$$

$$= \sup_{\theta \in \Theta} trace(C_{cl,2}(\theta) \overline{P}_{2}(\theta) C_{cl,2}^{T}(\theta)).$$
(1.5)

where \overline{P}_2 solves the differential Riccati equation,

$$\dot{\overline{P}}_2 = A_{cl}\overline{P}_2 + \overline{P}_2(A_{cl})^T + B_2(B_2)^T \tag{1.6}$$

with zero initial condition.

The \mathcal{H}_2 norm of a system has two interesting physical interpretations both stochastically and deterministically. To be more specific, stochastically, \mathcal{H}_2 norm of a system denotes the trace of the output covariance matrix, or in other words, the summation of RMS-value of the system outputs to a white noise input; and deterministically, \mathcal{H}_2 norm of a system denotes the square summation of \mathcal{L}_2 to \mathcal{L}_∞ gains of individual channels from exogenous disturbance inputs to system outputs. In vibration control, system \mathcal{H}_2 norm can be used as a measure of output magnitude (\mathcal{L}_∞ norm) due to energy limited (\mathcal{L}_2 norm) disturbance inputs.

Note that for LPV control case, $||T_2(\theta,s)||_2$ depends on varying scheduling parameter θ , leading to increased complexity due to unknown scheduling parameter trajectory. To reduce complexity and keep optimization as a unified approach to derive the \mathcal{H}_2 norm, the upper bound

 $trace(W) = \sup \left\{ trace(C_{cl,2}(\theta) \bar{P}_2(\theta) C_{cl,2}^T(\theta)) \right\}$ for all θ satisfying (1.2) is sought instead. W is an introduced auxiliary variable, which is a symmetric matrix with compatible dimensions with outputs . Using this constraint, the guaranteed \mathcal{H}_2 performance for all admissible scheduling parameter can be formulated.

The following Lemma 2 is given to evaluate the \mathcal{H}_2 performance for LPV system [20, 34].

Lemma 2. For a stable A_{cl} , if there exist a parameter dependent positive-definite matrix $P_2(\theta)$ and a constant matrix W, such that

$$\begin{bmatrix} -\dot{P}_2 + A_{cl}P_2 + (*) & B_{cl} \\ * & -I \end{bmatrix} < 0,$$
(1.7)

and

$$\begin{bmatrix} W & C_{cl,2}P_2 \\ * & P_2 \end{bmatrix} > 0, \tag{1.8}$$

hold for all $(\theta, \dot{\theta}) \in \Theta \times \Lambda$, then the \mathcal{H}_2 norm of the closed-loop system is bounded by trace(W), i.e.

$$trace(C_{cl,2}\overline{P}_2(C_{cl,2})^T) < trace(C_{cl,2}P_2(C_{cl,2})^T) < trace(W).$$
 (1.9)

1.2 Switching LPV System and Control

1.2.1 Overview

In the non-switching LPV controller design, if controller variables subject to PLMIs optimize the system performance index, the closed-loop system performance will be guaranteed over the entire scheduling parameter region. However, when the scheduling parameter region is very large, the formulated PLMIs could be extremely conservative, making it difficult or even impossible to achieve satisfactory closed-loop system performance. Moreover, describing system dynamics over a large scheduling parameter region by a single LPV model would lead to significant modeling errors, and hence inevitably degrades the closed-loop system performance [35, 36].

It is easy to observe in non-switching LPV controller synthesis that, a single Parameter-Dependent Lyapunov Matrix (PDLM) is utilized to derive system stability and performance conditions. To reduce the conservativeness, switching LPV control using multiple Lyapunov functions has been proposed by Lu and Wu [1]. The entire region of the scheduling parameter is divided into multiple subregions, and multiple PDLMs are utilized to formulate PLMIs conditions for controller synthesis. To ensure switching stability, additional switching stability constraints on PDLMs need to be satisfied on switching surfaces. The conservativeness of formulated PLMIs on the entire scheduling parameter region can be effectively reduced by a set of smaller subregions and multiple PDLMs, thus the resulting optimal performance will be improved. The switching LPV system borrows the idea and stability analysis method from [37, 38, 39, 40, 25, 10, 41, 42] to conduct the stability analysis and controller design. The switching LPV system and control have been demonstrated to achieve prominent performance over non-switching LPV control in multiple engineering practices [43, 44, 45, 46, 47, 48, 49].

As shown in Figure 1.4, the entire scheduling parameter region is divided into multiple subregions. An LPV gain-scheduling controller is designed for each subregion, and all controllers are often assumed to have the same form. It is essential to point out that switching controllers can have different order and form, but switching stability conditions will be difficult to derive. The assumption of same-order controllers will primarily simplify the stability issue and controller synthesis.

The switching LPV controllers are usually designed offline, and their switching logic is determined in terms of scheduling parameter region division. The switching stability is often proved by non-increasing Lyapunov functions in the switching sequence. In the earliest paper discussing switching LPV control by Lu and Wu [1], hysteresis switching and average-dwell-time switching strategies were focused, and associated controller synthesis conditions were developed. Besides that, the minimum switching strategy was reported in [50]. These switching strategies impose constraints on Lyapunov matrices or switching signals on switching surfaces and achieve guaranteed switching stability. The detailed description of switching strategies and their associated switching

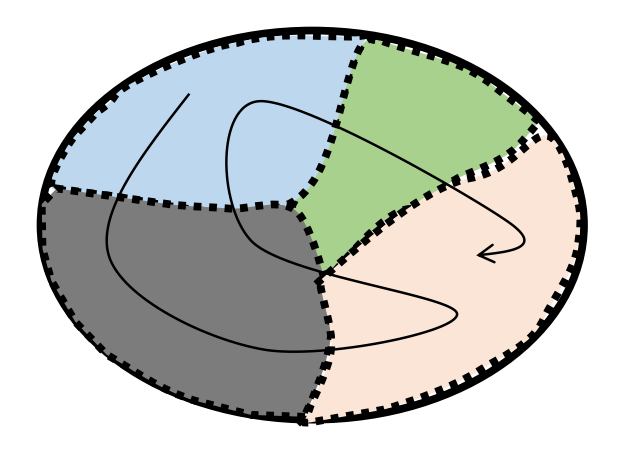


Figure 1.4: Switching LPV gain-scheduling control

stability conditions will be covered in the later subsection.

1.2.2 Switching LPV system and performance

Consider again the closed-loop system described in (1.1), but the scheduling parameter region is divided into J subregions. The sub-systems for adjacent subregions are to be switched according to different laws, including scheduling-parameter-dependent laws, state-dependent laws or external switching signals. The j^{th} subregion is denoted by $\Theta^{(j)}$ ($j \in N_J = \{1, 2, \ldots, J\}$), and switching surface from $\Theta^{(i)}$ to $\Theta^{(j)}$ is denoted by $S^{(i,j)}$. For example, Figure 1.5 shows a three-subregion partition of one-dimensional scheduling parameter and switching events by hysteresis switching . When θ crosses the switching surface $S^{(1,2)}$, the sub-system $\Sigma^1_{cl}(\theta)$ is switched to $\Sigma^2_{cl}(\theta)$, and when θ crosses the switching surface $S^{(2,1)}$, $\Sigma^2_{cl}(\theta)$ is switched back to $\Sigma^1_{cl}(\theta)$.

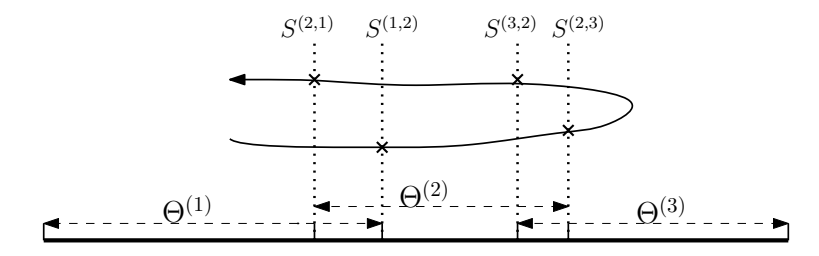


Figure 1.5: Three-subregion partition of scheduling parameter region

Then the closed-loop system with \mathcal{H}_{∞} and \mathcal{H}_2 performance channels on the subregion $(\theta, \dot{\theta}) \in \Theta^{(j)} \times \Lambda$ is described as

$$\Sigma_{cl}^{j}(\theta) : \begin{cases} \dot{x}(t) = A_{cl}^{j}(\theta)x(t) + B_{\infty}^{j}(\theta)w_{\infty}(t) + B_{2}^{j}(\theta)w_{2}(t); \\ z_{\infty}(t) = C_{cl,\infty}^{j}(\theta)x(t) + D_{\infty}^{j}(\theta)w_{\infty}(t) \\ z_{2}(t) = C_{cl,2}^{j}(\theta)x(t) \end{cases}$$
(1.10)

1.2.3 Performance specifications in switching LPV system

1.2.3.1 \mathcal{H}_{∞} performance

The \mathcal{H}_{∞} performance, defined from $w_{\infty}(t)$ to $z_{\infty}(t)$ with \mathcal{L}_2 input and \mathcal{L}_2 output, is utilized to assess the closed-loop system robustness in the presence of model uncertainties. Mathematically, let $T_{\infty}(\theta,s):=T_{z_{\infty}w_{\infty}}(\theta,s)$ denotes the parameter-dependent transfer function from w(t) to $z_{\infty}(t)$ and $||T_{\infty}||_{\infty}$ the \mathcal{H}_{∞} norm of T_{∞} . Then, the \mathcal{H}_{∞} performance for the $(w_{\infty}(t),z_{\infty}(t))$ pair is defined similar to that of non-switching LPV system \mathcal{L}_2 gain [15], where

$$||T_{\infty}||_{\infty} = \sup_{\theta \in \Theta(j), j \in N_I} \sup_{w_{\infty}, z_{\infty} \in \mathcal{L}_2, w_{\infty} \neq 0} \frac{||z_{\infty}(t)||_2}{||w_{\infty}(t)||_2}.$$
(1.11)

The following Lemma 3 can be used to formulate the \mathcal{H}_{∞} performance for Σ_{cl}^{j} [1, 32].

Lemma 3. Suppose that there exists a family of parameter-dependent positive-definite matrices $P_{\infty}^{j}(\theta)$ such that (1.12) holds for all admissible trajectories $(\theta, \dot{\theta}) \in \Theta^{(j)} \times \Lambda$, then the closed-loop subsystem (1.10) is exponentially stable on entire subregion with guaranteed performance $||z_{\infty}||_{2} < \gamma ||w_{\infty}||_{2}$ for a given robustness level $\gamma > 0$. (* denotes symmetric terms.)

$$\begin{bmatrix} -\dot{P}_{\infty}^{j} + A_{cl}^{j} P_{\infty}^{j} + (*) & * & B_{\infty}^{j} \\ C_{cl,\infty}^{j} P_{\infty}^{j} & -\gamma I & D_{\infty}^{j} \\ * & * & -\gamma I \end{bmatrix} < 0$$

$$(1.12)$$

1.2.3.2 \mathcal{H}_2 performance

The \mathcal{H}_2 performance, defined from $w_2(t)$ to $z_2(t)$, is utilized to assess the closed-loop system output performance. Let $T_2(\theta,s):=T_{z_2w_2}(\theta,s)$ be the parameter-dependent transfer function

from $w_2(t)$ to $z_2(t)$, and if each of subregion closed-loop system matrix A^j_{cl} is stable, then the \mathcal{H}_2 norm of is defined as the worst-case \mathcal{H}_2 performances on all the subregions $\Theta^{(j)}$,

$$||T_2||_2^2 = \sup_{\theta \in \Theta(j), j \in N_I} trace(C_{cl,2}^j(\theta) \overline{P}_2^j(\theta) C_{cl,2}^j(\theta)^T).$$
 (1.13)

where \overline{P}_2^j solves the differential Riccati equation,

$$\dot{\overline{P}}_{2}^{j} = A_{cl}^{j} \overline{P}_{2}^{j} + \overline{P}_{2}^{j} (A_{cl}^{j})^{T} + B_{2}^{j} (B_{2}^{j})^{T}, \qquad (1.14)$$

with zero initial condition.

The \mathcal{H}_2 norm of a stochastic system is the trace of output stochastic covariance matrix, or the summation of RMS-value of the outputs to a white noise input, whereas the \mathcal{H}_2 norm of a deterministic system denotes the square summation of \mathcal{L}_2 to \mathcal{L}_∞ gains of individual channel from exogenous inputs to system outputs. Alternatively, the \mathcal{H}_2 norm can be interpreted as deterministic outputs covariance in terms of time correlation [51]. With the following lemma, The \mathcal{H}_2 norm for $\theta \in \Theta^{(j)}$ subregion is bounded by its upper bound trace(W), and can be derived by minimizing trace(W), which falls into the typical min-max problem.

Lemma 4. [20] For any stable A_{cl}^{j} , if there exist a parameter dependent positive-definite matrix $P_{2}^{j}(\theta)$ and a constant matrix W, such that

$$\begin{bmatrix} -\dot{P}_{2}^{j} + A_{cl}^{j} P_{2}^{j} + (*) & B_{cl}^{j} \\ * & -I \end{bmatrix} < 0,$$
(1.15)

and

$$\begin{bmatrix} W & C_{cl,2}^{j} P_2^{j} \\ * & P_2^{j} \end{bmatrix} > 0,$$
 (1.16)

hold for all $(\theta, \dot{\theta}) \in \Theta^{(j)} \times \Lambda$, then the \mathcal{H}_2 norm of the closed-loop local subsystem in the j^{th} subregion is bounded by trace(W), i.e.,

$$trace(C_{cl,2}^{j}\overline{P}_{2}^{j}(C_{cl,2}^{j})^{T}) < trace(C_{cl,2}^{j}P_{2}^{j}(C_{cl,2}^{j})^{T}) < trace(W).$$
 (1.17)

If the condition (1.15) and (1.16) are valid on all subregions, then trace(W) is the universal upper bound of \mathcal{H}_2 norm on entire scheduling parameter region.

1.2.4 Switching strategies and stability conditions

Switching LPV system is a special case of switching system, which considers the switching of systems in a more general sense. Switching systems can be seen as a hybrid of the continuous-time system and discrete-time switching signal. The neighboring controllers to be switched are always assumed to be in the same form and order to simplify the stability problem and controller synthesis complexity. It is noted that this dissertation also follows this assumption.

In the literature, there are extensive studies about the switching strategies and associated switching stability conditions for linear systems [52, 10, 9]. These switching strategies have been extended to switching LPV systems [53, 1]. In this section, the state-of-art research about switching LPV system and control will be covered, then popular switching strategies and associated switching stability conditions of LPV systems will be given.

Consider the closed-loop autonomous LPV system without external inputs in (1.18) for analysis of switching stability,

$$\Sigma_{cl}^{j}(\theta): \left\{ \dot{x}(t) = A_{cl}^{j}(\theta)x(t). \right. \tag{1.18}$$

1.2.4.1 Hysteresis switching

Revisit Figure 1.5, there is an overlapped subregion between any two neighboring subregions. When θ crosses the switching surface $S^{(1,2)}$, the sub-system $\Sigma^1_{cl}(\theta)$ is switched to $\Sigma^2_{cl}(\theta)$, and when θ crosses the switching surface $S^{(2,1)}$, $\Sigma^2_{cl}(\theta)$ is switched back to $\Sigma^1_{cl}(\theta)$.

Direct Lyapunov method is often used to prove the switching stability. Due to that multiple controllers are designed on subregions, we suppose that there is a family of positive definite Lyapunov matrices $P^j(\theta)$ dependent on scheduling parameter θ . Then parameter-dependent Lyapunov functions are formulated as quadratic functions as

$$V^{j}(x,\theta) = x^{T} P^{j}(\theta) x \tag{1.19}$$

where j represents the active controller on the j^{th} subregion Θ_j , and its corresponding Lyapunov matrx $P^j(\theta)$ is used in formulating the Lyapnov function.

The switching stability can be achieved by non-increasing Lyapunov functions during each switching event [54, 1]. The non-increasing condition is proved to be a sufficient condition but not a necessary condition. In literature, there are proven results to relax this conservative result, in which the multiple Lyapunov functions may increase its value during a time interval, only if the increment is bounded by certain kinds of continuous functions. Interested readers are recommended to the reference [55, 56].

Consider one switching event on surface $S^{(i,j)}$ from i^{th} subregion to j^{th} subregion, if the hysteresis switching is utilized, the sufficient condition of globally exponentially stability of switching system is given by Theorem 1 and the proof is given following the reference [1].

Theorem 1. If there exists a family of parameter-dependent Lyapunov matrices satisfying condition (1.20), then the exponential stability is achieved within local subsystems $\Sigma_{cl}^{j}(\theta)$ with $(\theta, \dot{\theta}) \in \Theta^{(j)} \times \Lambda$. Moreover, if condition (1.21) is satisfied on the switching surface, then global exponential stability is achieved on entire scheduling parameter region $(\theta, \dot{\theta}) \in \Theta \times \Lambda$.

$$P^{j}(\theta)A_{cl}^{j}(\theta) + (A^{j})_{cl}^{T}(\theta)P^{j}(\theta) + \dot{P}^{j}(\theta) < 0$$
(1.20)

$$P^{i}(\theta) \ge P^{j}(\theta), \qquad \theta \in S^{(i,j)}, i, j \in N_{J}, i \ne j$$
 (1.21)

Proof. We assume that the sequence of switching time is t_0, t_1, \dots, t_N . If (1.20) is satisfied on local subregion, then there must exist a scalar $\lambda > 0$ that satisfies

$$P^{j}(\theta)A_{cl}^{j}(\theta) + (A^{j})_{cl}^{T}(\theta)P^{j}(\theta) + \dot{P}^{j}(\theta) < -\lambda P^{j}(\theta). \tag{1.22}$$

On the time interval $t \in [t_k, t_{k+1})$ which j^{th} controller is active, we have

$$V^{j}(x(t),\theta) \le e^{-\lambda(t-t_k)} V^{j}(x(t_k),\theta). \tag{1.23}$$

Moreover, the switching stability condition on switching surface (1.21) will lead to $V^j(x(t_k),\theta) \leq V^j(x(t_k^-),\theta)$. Therefore,

$$V^{j}(x(t),\theta) \leq e^{-\lambda(t-t_{k})}V^{j}(x(t_{k}^{-}),\theta)$$

$$\leq e^{-\lambda(t-t_{k})}e^{-\lambda(t_{k}^{-}t_{k-1})}V^{j}(x(t_{k-1}),\theta)$$

$$\cdots$$

$$\leq e^{-\lambda(t-t_{0})}V^{j}(x(t_{0}),\theta)$$

$$(1.24)$$

so the global exponential stability is achieved.

1.2.4.2 Average-Dwell-Time (ADT) switching

The Average-Dwell-Time (ADT) switching strategy enforces the "slow-switching" property of switching signals so that the closed-loop system achieves global stability under the switching sequence. By ADT switching strategy, only a limited number of switches are allowed within a finite time interval [1, 4, 57].

We assume that switching signal $\sigma(t)$ renders $N_{\sigma}(T,t)$ number of switching events within the time interval [t,T]. If there exist two positive numbers N_0 and τ_a such that

$$N_{\sigma}(T,t) \le N_0 + \frac{T-t}{\tau_a}, \qquad \forall T \ge t \ge 0$$
(1.25)

where N_0 is the chatter bound to avoid chattering phenomenon. Then sufficient condition for ADT switching is given in Theorem 2 and the proof is given following the reference [10, 57].

Theorem 2. Given positive scalar λ_0 and μ , if there exists a family of parameter-dependent Lyapunov matrices $P^j(\theta)$ satisfying condition (1.26) on each subregion $(\theta, \dot{\theta}) \in \Theta^{(j)} \times \Lambda$ and condition (1.27) on switching surface, then the exponentially stability is achieved by switching signal with average dwell time $\tau_a > \frac{\ln \mu}{\lambda_0}$ within the entire scheduling parameter region $(\theta, \dot{\theta}) \in \Theta \times \Lambda$.

$$P^{j}(\theta)A_{cl}^{j}(\theta) + (A^{j})_{cl}^{T}(\theta)P^{j}(\theta) + \dot{P}^{j}(\theta) + \lambda_{0}P^{j}(\theta) < 0$$
(1.26)

$$\frac{1}{\mu}P^{j}(\theta) \ge P^{i}(\theta) \ge \mu P^{j}(\theta), \qquad \theta \in S^{(i,j)}, i, j \in N_{j}, i \ne j$$
(1.27)

Proof. Without loss of generality, we assume that the sequence of switching time is t_0, t_1, \dots, t_N . By (1.26), it is easy to obtain

$$\dot{V}^{j}(x(t),\theta) < -\lambda_0 V^{j}(x(t),\theta) < 0, \tag{1.28}$$

thus local exponential stability on each subregion is achieved.

Consider the Lyapunov function $W(x(t),\theta)=e^{2\lambda_0t}V^j(x(t),\theta)$ when j^{th} controller is active, thus

$$\dot{W} = 2\lambda_0 W + e^{2\lambda_0 t} \dot{V}.$$

The function W is obviously positive and non-increasing between switching intervals. Then at the time interval $[t_i, t_{i+1})$, we arrive at

$$W(t_{i+1}) = e^{2\lambda_0 t_{i+1}} V^{j(t_{i+1})}(x(t_{i+1}), \theta) \le \mu e^{2\lambda_0 t_{i+1}} V^{j(t_i)}(x(t_{i+1}), \theta)$$

$$= \mu W(t_{i+1}^-) \le \mu W(t_i)$$
(1.29)

Sum up from t_0 to terminal time T, then we have

$$W(T) \le W(t_N) \le \mu^{N_{\sigma}(t_N, t_0)} W(t_0)$$
 (1.30)

From the defined W(t),

$$e^{2\lambda_0 T} V^{j(T)}(x(T), \theta) \le \mu^{N_{\sigma}(T, t_0)} V^{j(t_0)}(x(t_0), \theta)$$
(1.31)

$$V^{j(T)}(x(T), \theta) \leq e^{-2\lambda_0 T + \left(N_0 + \frac{T}{\tau_a}\right) \ln \mu} V^{j(t_0)}(x(t_0), \theta)$$

$$= e^{N_0 \ln \mu} e^{\left(\frac{\ln \mu}{\tau_a} - 2\lambda_0\right) T} V^{j(t_0)}(x(t_0), \theta)$$
(1.32)

Therefore, if the switching signal satisfies the limitation of average-dwell-time $\tau_a > \frac{\ln \mu}{\lambda_0}$, then it is concluded that $V^{j(T)}(x(T), \theta)$ converges to zero exponentially as $T \to \infty$, which indicates global exponential stability of switching LPV system.

1.3 Motivations of Smooth Switching LPV Control

As discussed in the above paragraphs, with given partitioned subregions, a family of LPV controllers is designed by constructing Parametric Linear Matrix Inequalities (PLMIs) with multiple parameter-dependent Lyapunov functions. Controllers are designed by solving the corresponding optimization problem associated with switching stability conditions and specific performance criteria. Many engineering applications of switching LPV control have shown system performance improvement over non-switching LPV controllers. These applications include active magnetic bearing (AMB) system [1], F-16 aircraft model [58], flexible ball-screw drives [59] and air-fuel ratio control of spark ignition engines [48].

However, in most of these applications, the drawback of unsmooth transient responses over the switching surfaces can be observed [1, 48, 32], and the un-smoothness can be attributed to sharp changes in control inputs or controller gains. In Figure 1.6, the conventional switching LPV control [1] resulted in the abrupt changes of control input, marked by red squares. These spikes in control command signals impose heavy-duty tasks on actuators, which will be harmful to hardware and sometimes exceed actuator's authority.

Only a few smooth switching techniques have been proposed in the literature to compensate for sharp jumps. Chen [60] considered the hysteresis switching state-feedback LPV control and conducted linear interpolation of controller variables on switching surfaces to achieve smooth switching during switch-in and switch-out on the overlapping region. However, this method cannot quantitatively evaluate switching smoothness, and only relative stability is achieved. Hanifzadegan and Nagamune [61] followed the idea of linear interpolation of controller matrices on switching surfaces, and introduced a measure of smoothness index and imposed constraints on controller matrix derivative to compensate for the drawbacks found in Chen [60]. The design of stabilizing controllers was formulated into a non-convex optimization problem, and an iterative descent algorithm was then applied to find a local LPV controller for each subregion. The linear interpolations of controller matrices on switching surfaces were conducted to obtain switching LPV controller on the overlapping region. This method relies heavily on iterative computations to solve multi-objective

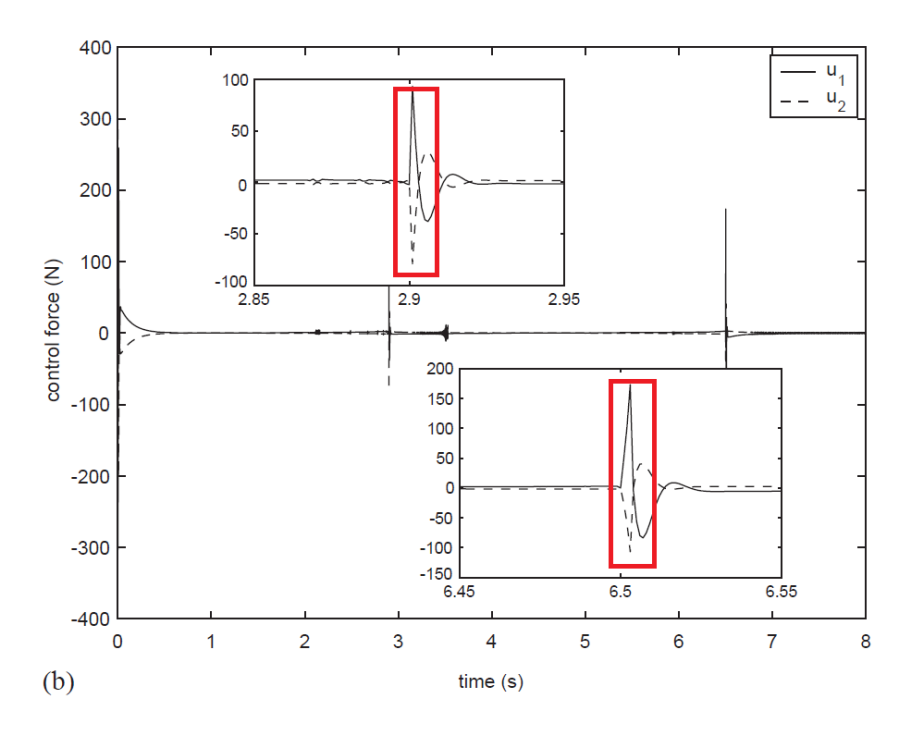


Figure 1.6: Unsmooth control input signal from conventional switching LPV control [1]

non-convex problems. Moreover, the introduced smoothness index lacks physical meaning, and the smoothness constraints on controller matrices are selected through trial and error.

Considering that existing methods cannot efficiently address the design of smooth switching LPV controller, it is highly needed to develop an efficient and systematic approach to achieve smooth switching between adjacent LPV controllers. In the authors' point of view, the leading cause of un-smooth control inputs and system responses is due to the sudden change of control variables during switching events. The ultimate reason is that un-smooth switching LPV control optimizes closed-loop system performance over each subregion, nevertheless switching smoothness between adjacent controllers is not considered. The system performance optimization over each subregion, but ignoring switching often leads to high-gain controllers with jumped controller gains. This can be easily validated by checking the control gain difference between two neighboring subregions over the switching surface.

The core idea of smooth switching LPV controller can be illustrated by the comparison of Figures 1.7a and 1.7b. The smooth switching LPV controller minimizes the gap between controller

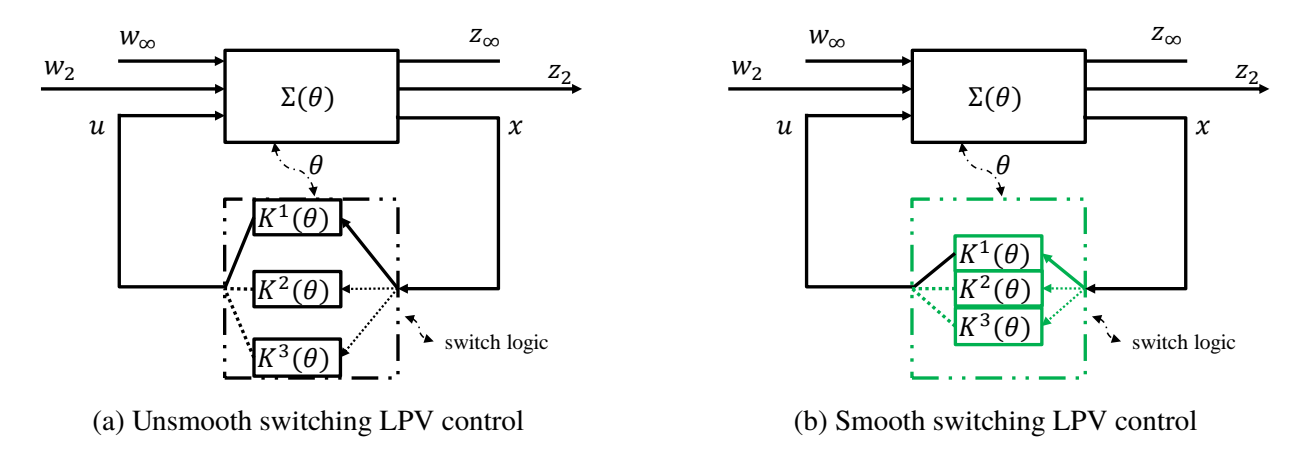


Figure 1.7: Illustration of motivations of smooth switching LPV control

gains and achieves smooth switching, whereas the conventional LPV controller only considers the switching stability but not the switching smoothness. Two approaches, simultaneous design and sequential design, are proposed in this dissertation and the design strategies are summarized in the following paragraphs.

In the simultaneous design approach, a convex optimization problem is formulated to design all switching controllers at the same time. A numerically tractable smoothness index is introduced into the cost function by using the norm of deviation of controller parameters between any two switching surfaces. By means of minimizing this smoothness index, it can be demonstrated that sharp changes in control states or outputs can be significantly reduced, but at the cost of degraded \mathcal{H}_2 and \mathcal{H}_∞ system performance. In other words, there exists a trade-off relationship between system performance and switching smoothness. Intuitively, a tunable weighting coefficient can be adopted to balance the system performance and switching smoothness in the cost function. By tuning the weighting coefficient, i.e., line search, an optimal trade-off can be obtained, leading to a smooth-switching LPV controller with acceptable system performance.

Controller synthesis conditions by the simultaneous design approach are not independent on adjacent subregions due to the switching stability condition. When the number of subregions goes large, the simultaneous design approach leads to a high-dimensional optimization problem, with a high amount of LMI (Linear Matrix Inequality) constraints, decision variables, online

computational load, and memory requirement [62, 63]. As a result, the simultaneous design would be practically infeasible for high-order systems with many divided subregions.

To reduce the computational complexity, a sequential controller design approach is proposed. Interpolated controller variables for overlapped subregions and newly formulated PLMIs are utilized to synthesize switching LPV controllers on each subregion independently. On each overlapped subregion, the Lyapunov matrix is formulated by convexly combining PDLM on adjacent subregions. The PLMIs for \mathcal{H}_{∞} performance on each subregion is formulated, such that the convex combination of adjacent PLMIs leads to a guaranteed \mathcal{H}_{∞} performance on every overlapped subregion. Moreover, the proposed method guarantees that the overlapped subregion has intermediate performance between its neighboring subregions. The proposed method designs an individual controller for each subregion in sequential order, instead of synthesizing all controllers simultaneously. By iteratively solving the reduced-dimensional optimization problem for each subregion, switching controllers with guaranteed \mathcal{H}_{∞} performance on all subregions and overlapped subregions can be obtained.

1.4 Organization of This Dissertation

In this dissertation, two approaches of smooth switching LPV controller design are proposed, including simultaneous design and sequential design. After the introduction of switching LPV system and control in Chapter 1, simultaneous design and sequential design of smooth switching LPV control are discussed, and controller synthesis conditions are given in Chapter 2. In Chapter 3, a few application examples are given to demonstrate the effectiveness of smooth switching LPV control designs. Simultaneous design approach is applied to the AMB model and BWB aircraft flexible wing, then another two numerical examples are applied with sequential design approach. Also, the optimal sensor placement problem using the LPV framework is investigated in Chapter 4. At last, conclusions and future work are discussed in Chapter 5.

The structure of this dissertation is shown in Figure 1.8.

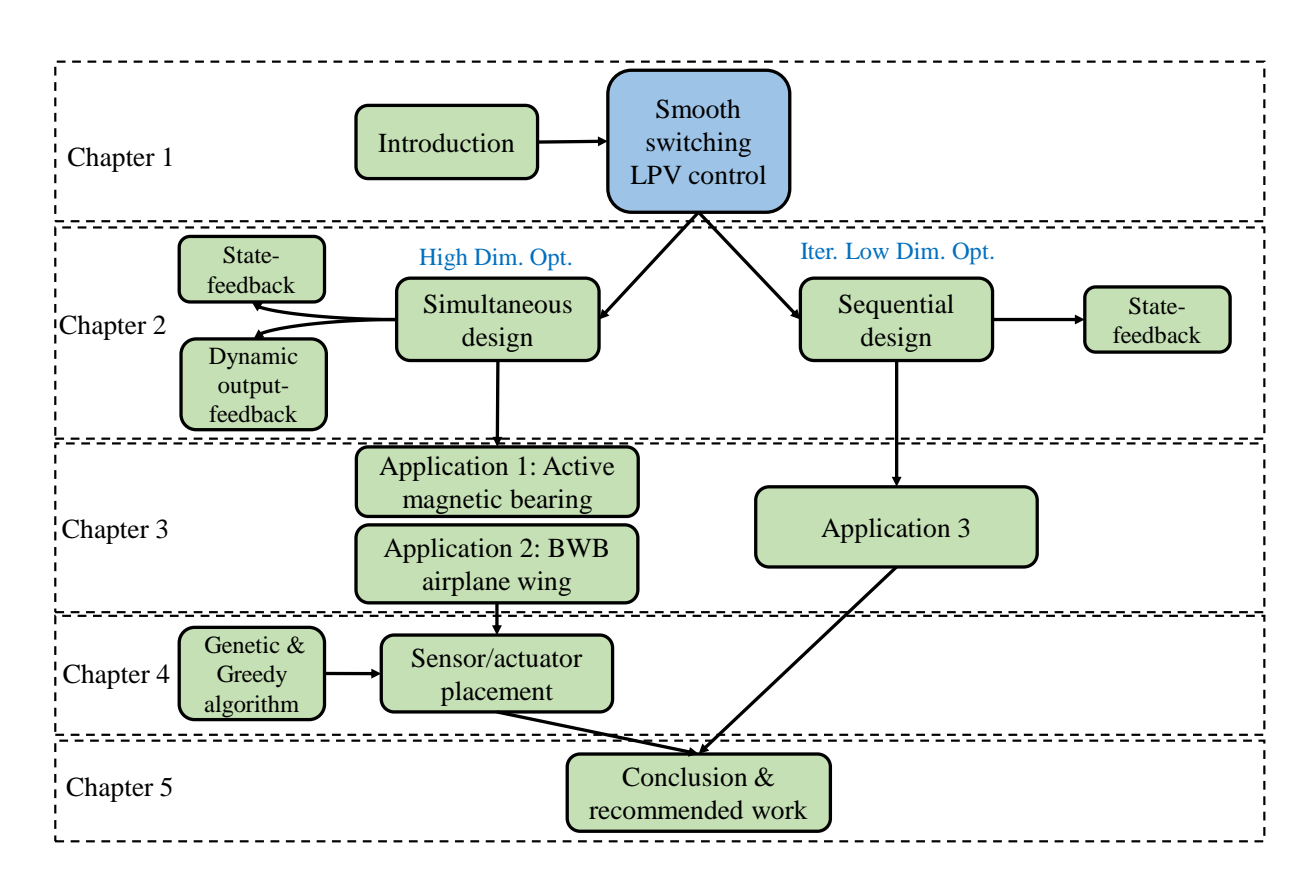


Figure 1.8: Roadmap of this dissertation

CHAPTER 2

SMOOTH SWITCHING LPV CONTROL

As discussed in Chapter 1, smooth switching LPV control is needed to remedy for unsmooth responses in conventional switching LPV control. This chapter will give the theoretical derivations and controller synthesis conditions for smooth switching LPV controllers.

Before we get into the smooth switching LPV control, the mixed Input Covariance Constraint (ICC) and \mathcal{H}_{∞} LPV control is firstly introduced. The mixed ICC/ \mathcal{H}_{∞} LPV control is able to achieve multi-objective performance of closed-loop system. The \mathcal{H}_2 performance is optimized while the closed-loop system satisfying \mathcal{H}_{∞} performance and input covariance constraint. The ICC/ \mathcal{H}_{∞} control is able to avoid high-gain controller by setting upper limit of control input covariance.

2.1 Mixed ICC/ \mathcal{H}_{∞} Control

2.1.1 State-feedback LPV control

Consider the following affine LPV systems,

$$\Sigma(\theta) : \begin{cases} \dot{x}(t) &= A(\theta(t))x(t) + B_{\infty}(\theta(t))w_{\infty}(t) + B_{2}(\theta(t))w_{2}(t) + B_{u}(\theta(t))u(t) \\ z_{\infty}(t) &= C_{\infty}(\theta(t))x(t) + D_{\infty}(\theta(t))w_{\infty}(t) + E_{\infty}(\theta(t))u(t) \\ z_{2}(t) &= C_{2}(\theta(t))x(t) \end{cases}$$
(2.1)

where $\theta(t) = \left[\theta_1(t), \theta_2(t), \dots, \theta_q(t)\right]^T$ denotes the scheduling parameter vector of q elements, $x(t) \in R^{n_x}$ denotes the state, $w_\infty(t) \in R^{n_w\infty}$ the \mathcal{H}_∞ disturbance input due to modeling error, $w_2(t) \in R^{n_w2}$ the \mathcal{H}_2 disturbance input, $u(t) \in R^{n_u}$ the control input, $z_\infty(t) \in R^{n_{z\infty}}$ the \mathcal{H}_∞ controlled output, and $z_2(t) \in R^{n_{z2}}$ the \mathcal{H}_2 performance output. All system matrices are assumed to have compatible dimensions and in affine parameter-dependent form. For example, $A(\theta)$ can be described by

$$A(\theta(t)) = A_0 + \sum_{i=1}^{q} A_i \theta_i$$
, (2.2)

where A_0 and A_i , i = 1, 2, ..., q, are constant matrices. It is assumed that the scheduling parameters are measurable in real-time, and their magnitude and variational rate are bounded. Specifically, the scheduling parameter set is formulated as:

$$\theta \in \Theta = \left\{ \underline{\theta}_i \le \theta_i(t) \le \overline{\theta}_i, i \in \{1, 2, ..., q\}, \right\}$$

$$\dot{\theta} \in \Lambda = \left\{ -\nu_i \le \dot{\theta}_i(t) \le \nu_i, i \in \{1, 2, ..., q\}. \right\}$$
(2.3)

Assume we are seeking for a gain-scheduling state-feedback controllers of the form

$$u(t) = K(\theta(t))x(t), \tag{2.4}$$

where $K(\theta)$ is the parameter-dependent control gain matrix. Note that u(t) can be partitioned as $u(t) = [u_1(t), u_2(t), \dots, u_{n_u}(t)]^T$. Then, substituting (2.52) into (2.1) yields the closed-loop LPV system described by

$$\Sigma_{cl}(\theta) : \begin{cases} \dot{x}(t) = A_{cl}(\theta)x(t) + B_{\infty}(\theta)w_{\infty}(t) + B_{2}(\theta)w_{2}(t); \\ z_{\infty}(t) = C_{cl,\infty}(\theta)x(t) + D_{\infty}(\theta)w_{\infty}(t) \\ z_{2}(t) = C_{2}(\theta)x(t) \end{cases}$$

$$(2.5)$$

where $A_{cl}(\theta) = A(\theta) + B_u(\theta)K(\theta), C_{cl,\infty}(\theta) = C_{\infty}(\theta) + E_{\infty}(\theta)K(\theta).$

The control input is given as

$$u(t) = K(\theta(t))x(t).$$

Hence, the variance of kth control input of jth controller is bounded as [64, 65]

$$cov(u_k(\theta(t))) \le \sup_{\theta \in \Theta} e_k K(\theta) \bar{P}_2(\theta) K^T(\theta) e_k^T = U_k,$$
(2.6)

where e_k is a selection row vector such that $e_kK(\theta)$ equals to the kth row of matrix $K(\theta)$, and \bar{P}_2 is given by (1.6). The following lemma provides hard constraint on variance of the kth control input for any $\theta \in \Theta$.

Lemma 5. The ICC condition of the kth control input of the state-feedback controller

$$U_k = e_k K \bar{P}_2 K^T e_k^T < e_k K P_2 K^T e_k^T < \bar{U}_k$$
 (2.7)

is equivalent to

$$\begin{bmatrix} \bar{U}_k & e_k K P_2 \\ * & P_2 \end{bmatrix} > 0, \quad k = 1, 2, \dots, n_u, \tag{2.8}$$

where n_u is the number of control inputs.

The following lemma gives the synthesis conditions for mixed ICC/ \mathcal{H}_{∞} LPV state-feedback controller.

Theorem 3. Given the input covariance constraints \bar{U}_k , $k=1,2,\cdots,n_u$, and a positive scalar γ_{∞} , if there exist continuously differentiable parameter-dependent matrices $0 < P_2(\theta) = P_2^T(\theta) \in R^{n_x \times n_x}$, $0 < P_{\infty}(\theta) = P_{\infty}^T(\theta) \in R^{n_x \times n_x}$, $G(\theta) \in R^{n_x \times n_x}$, $Z(\theta) \in R^{n_u \times n_x}$, small scalars $\epsilon_2 > 0$ and $\epsilon_{\infty} > 0$, and matrix $W = W^T \in R^{n_{z_2} \times n_{z_2}}$ that minimize the following cost function with a given scaling matrix Q > 0,

$$\min trace(QW) \tag{2.9}$$

subject to the following inequalities (* denotes symmetric terms),

$$\begin{bmatrix} \Phi_{11} & * & * \\ \Phi_{12} & -\epsilon_2 (G(\theta) + G(\theta)^T) & * \\ B_2(\theta)^T & \boldsymbol{\theta}_{n_w \times n_w} & -\boldsymbol{I}_{n_w} \end{bmatrix} < 0,$$
 (2.10)

$$\begin{bmatrix} W & C_2(\theta)G(\theta) \\ * & G(\theta) + G(\theta)^T - P_2(\theta) \end{bmatrix} > 0,$$
(2.11)

$$\begin{bmatrix} \bar{U}_k & e_k Z(\theta) \\ * & G(\theta) + G(\theta)^T - P_2(\theta) \end{bmatrix} > 0, \ k = 1, 2, \dots, n_u,$$
 (2.12)

$$\begin{bmatrix} \Phi_{\infty 1} & * & * & * \\ \Phi_{\infty 2} & -\epsilon_{\infty} (G(\theta) + G(\theta)^{T}) & * & * \\ \Phi_{\infty 3} & \epsilon_{\infty} \Phi_{\infty 3} & -\mathbf{I}_{n_{z}} & * \\ B_{\infty}(\theta)^{T} & \mathbf{0}_{n_{w} \times n_{x}} & D_{\infty}(\theta)^{T} & -\gamma_{\infty}^{2} \mathbf{I}_{n_{w}} \end{bmatrix} < 0, \qquad (2.13)$$

where $\Phi_{11} = A(\theta)G(\theta) + B_u(\theta)Z(\theta) + (A(\theta)G(\theta) + B_u(\theta)Z(\theta))^T - \frac{\partial P_2(\theta)}{\partial \theta}\dot{\theta}$, $\Phi_{12} = P_2(\theta) - G(\theta) + \epsilon_2(A(\theta)G(\theta) + B_u(\theta)Z(\theta))^T$, and e_k is input channel selection matrix for control input of interest, and $\Phi_{\infty 1} = A(\theta)G(\theta) + B_u(\theta)Z(\theta) + (A(\theta)G(\theta) + B_u(\theta)Z(\theta))^T - \frac{\partial P_\infty(\theta)}{\partial \theta}\dot{\theta}$, $\Phi_{\infty 2} = P_\infty(\theta) - G(\theta) + \epsilon_\infty(A(\theta)G(\theta) + B_u(\theta)Z(\theta))^T$, and $\Phi_{\infty 3} = C_\infty(\theta)G(\theta) + E_\infty(\theta)Z(\theta)$. Then, the gain-scheduling controller

$$u(t) = K(\theta)x(t), \ K(\theta) = Z(\theta)G^{-1}(\theta)$$
(2.14)

exponentially stabilizes the LPV system $\Sigma(\theta)$ for any $(\theta, \dot{\theta}) \in \Theta \times \Lambda$ with a guaranteed \mathcal{H}_{∞} performance bound γ_{∞} . In addition, the ICC cost is bounded by

$$trace(W) > trace\left\{C_2(\theta)P_2(\theta)C_2(\theta)^T\right\},$$
 (2.15)

and the constraint (2.6) is satisfied.

Proof. For closed-loop LPV system (2.5), assume $A_{cl}(\theta)$ is stable for any pair $(\theta, \dot{\theta}) \in \Lambda \times \Omega$, then there is a continuously differentiable parameter-dependent positive-definite matrix $\bar{P}_2(\theta) = \bar{P}_2(\theta)^T > 0$, such that

$$\dot{\bar{P}}_{2}(\theta) + A_{cl}(\theta)\bar{P}_{2}(\theta) + \bar{P}_{2}(\theta)A_{cl}(\theta)^{T} + B_{2}(\theta)B_{2}(\theta)^{T} = 0$$
(2.16)

where $\bar{P}_2(\theta)$ is the controllability Gramian of the LPV system. In other words, there is a parameter-dependent positive-definite matrix $P_2(\theta) > \bar{P}_2(\theta)$ satisfying the following inequality

$$\dot{P}_{2}(\theta) + A_{cl}(\theta)P_{2}(\theta) + P_{2}(\theta)A_{cl}(\theta)^{T} + B_{2}(\theta)B_{2}(\theta)^{T} < 0.$$
(2.17)

To decouple $A_{cl}(\theta)$ and $P_2(\theta)$ in (2.17), we utilize *Finsler's Lemma* [66] to obtain the following,

$$\Gamma(\theta) + X(\theta)V(\theta) + V^{T}(\theta)X^{T}(\theta) < 0, \qquad (2.18)$$

where

$$\Gamma(\theta) = \begin{bmatrix} \dot{P}_2(\theta) & P_2(\theta) & 0 \\ P_2(\theta) & 0 & 0 \\ 0 & 0 & I \end{bmatrix}, \ X(\theta) = \begin{bmatrix} G^T(\theta) & 0 \\ R^T(\theta) & 0 \\ 0 & I \end{bmatrix}, \ V(\theta) = \begin{bmatrix} A_{cl}^T(\theta) & -I & 0 \\ B_2^T & 0 & -I \end{bmatrix},$$

and $G(\theta)$ and $R(\theta)$ are introduced as slack variables. To maintain convex parametrization property, $R(\theta)$ is chosen to be $R(\theta) = \epsilon_2 G(\theta)$, where $\epsilon_2 > 0$ is a scalar that is used to provide an extra degree-of-freedom when performing the line search and to reduce conservativeness. Letting $Z(\theta) = K(\theta)G(\theta)$ yields (2.62).

Now, consider (2.63). Pre- and post-multiplying (2.63) by $[I, C_2]$ and $[I, C_2]^T$ renders

$$\begin{bmatrix} I & C_2 \end{bmatrix} \begin{bmatrix} W & C_2(\theta)G(\theta) \\ * & G(\theta) + G(\theta)^T - P_2(\theta) \end{bmatrix} \begin{bmatrix} I \\ C_2^T \end{bmatrix} > 0$$
 (2.19)

from which we obtain

$$W > C_2(\theta)P_2(\theta)C_2(\theta)^T, \qquad (2.20)$$

hence (2.20) leads to (2.67). Since $C_2(\theta)P_2(\theta)C_2(\theta)^T > C_2(\theta)\bar{P}_2(\theta)C_2(\theta)^T$, as a result, minimizing trace(QW) implies minimizing the upper bound of the weighted ICC cost.

Similarly, pre- and post-multiplying (2.64) by $[I, e_k K(\theta)]$ and $[I, e_k K(\theta)]^T$ to obtain

$$\begin{bmatrix} I & e_k K(\theta) \end{bmatrix} \begin{bmatrix} \bar{U}_k & e_k Z(\theta) \\ * & G(\theta) + G(\theta)^T - P_2(\theta) \end{bmatrix} \begin{bmatrix} I \\ (e_k K(\theta))^T \end{bmatrix} > 0, \qquad (2.21)$$

which yields

$$\bar{U}_k > e_k K(\theta) P(\theta) K(\theta)^T e_k^T, \ k = 1, 2, \cdots, n_u.$$

This implies that the selected control input covariance is upper bounded by \bar{U}_k .

Now, for \mathcal{H}_{∞} performance inequality (2.65), we consider the following transformation matrix

$$T(\theta) = \begin{bmatrix} I & A_{cl}(\theta) & 0 & 0 \\ 0 & C_{cl,\infty}(\theta) & I & 0 \\ 0 & 0 & 0 & I \end{bmatrix}.$$

Pre- and post-multiplying (2.65) by $T(\theta)$ and $T(\theta)^T$ leads to the \mathcal{H}_{∞} performance criterion based upon the well-known *Real Bounded Lemma* [15] that the \mathcal{H}_{∞} norm of the closed-loop system is bounded by γ_{∞} . This can be easily verified by plugging in search variables and operating matrix multiplication.

Remark 1. For each given pair of small positive scalar variables ϵ_2 and ϵ_∞ , the minimization leads to a sub-optimal solution. Fixing both scalar variables would lead to conservativeness, however, the line search of scalar variables can reduce conservativeness significantly. Note that constraining $P_\infty = P_2$ for multi-objective control design, as commonly found in the literature, could lead to large conservativeness. The optimization process can be repeated for a set of gridded scalar values to minimize trace(QW). The line search process may burden the computational load, but with current advanced computational capacity, this should not be an issue.

2.1.2 Dynamic output-feedback LPV control

Suppose a LPV system with independent \mathcal{H}_2 and \mathcal{H}_∞ channels :

$$\Sigma(\theta) : \begin{cases} \dot{x}_{p}(t) = A(\theta(t))x_{p}(t) + B_{1}(\theta(t))w(t) + B_{2}(\theta(t))u(t) \\ z_{\infty}(t) = C_{\infty}(\theta(t))x_{p}(t) + D_{11}(\theta(t))w(t) + D_{12}(\theta(t))u(t) \\ z_{2}(t) = C_{2}(\theta(t))x_{p}(t) + E_{2}(\theta(t))u(t) \\ y(t) = C_{y}(\theta(t))x_{p}(t) + D_{y}(\theta(t))w(t) \end{cases}$$
(2.22)

Without loss of generality, $D_{yu} = 0$. System matrices represent in affine form as:

$$A(\theta) = A_0 + \sum_{i=1}^{q} A_i \theta_i \tag{2.23}$$

Each parameter and the rate of variations are assumed to be bounded as by $\theta_i \in \left[\underline{\theta_i}, \bar{\theta_i}\right], \dot{\theta_i} \in \left[\underline{v_i}, \bar{v_i}\right]$. The proposed gain-scheduling output-feedback controller is defined as (2.24) and $D_K = 0$ so that the closed-loop system is strictly proper and has meaningful \mathcal{H}_2 norm.

$$\begin{cases} \dot{x}_K = A_K(\theta, \dot{\theta})x_K + B_K(\theta, \dot{\theta})y \\ u = C_K(\theta, \dot{\theta})x_K \end{cases}$$
(2.24)

which ensures internal stability and a guaranteed \mathcal{H}_{∞} performance $||T_{z_{\infty}w}||_{\infty} < \gamma$ from disturbance w to performance output z_{∞} , and minimize the \mathcal{H}_2 performance $||T_{z_2w}||_2$, while control covariance $Cov(u_k(t)) < \bar{U}_k, k = 1, 2, \cdots, n_u$, for all admissible trajectories $(\theta, \dot{\theta})$ and zero-state initial conditions.

The resulted closed-loop system is:

$$\Sigma_{cl}(\theta) : \begin{cases} \dot{x}_{cl}(t) = A_{cl}(\theta(t))x_{cl}(t) + B_{cl}(\theta(t))w(t) \\ z_{\infty}(t) = C_{cl,\infty}(\theta(t))x_{cl}(t) + D_{cl,\infty}(\theta(t))w(t) \\ z_{2}(t) = C_{cl,2}(\theta(t))x_{cl}(t) \end{cases}$$
(2.25)

 $\boldsymbol{x}_{cl}^T = [\boldsymbol{x}_p^T, \boldsymbol{x}_K^T],$ where $\boldsymbol{\theta}$ is omitted in following notations:

$$A_{cl} = \begin{bmatrix} A & B_2 C_K \\ B_K C_y & A_K \end{bmatrix}, B_{cl} = \begin{bmatrix} B_1 \\ B_K D_y \end{bmatrix}$$
 (2.26)

$$C_{cl,\infty} = \begin{bmatrix} C_{\infty} & D_{12}C_K \end{bmatrix}, D_{cl,\infty} = D_{11}$$
(2.27)

$$C_{cl,2} = \begin{bmatrix} C_2 & E_2 C_K \end{bmatrix}, D_{cl,2} = 0$$
 (2.28)

2.1.2.1 ICC condition

The control input is calculated as $u(t)=C_Kx_K=C_ux_{cl}=\left[\begin{array}{cc} 0 & C_K \end{array}\right]\left[\begin{array}{c} x_p \\ x_K \end{array}\right].$

The ICC condition of the k^{th} control input

$$U_{k} = \Phi_{k} C_{u} \tilde{P}_{2} C_{u}^{T} \Phi_{k}^{T} < \Phi_{k} C_{u} P_{2} C_{u}^{T} \Phi_{k}^{T} < \bar{U}_{k}$$
(2.29)

is equivalent to LMI [67]

$$\begin{bmatrix} \bar{U}_k & \Phi_k C_u P_2 \\ * & P_2 \end{bmatrix} > 0, \quad k = 1, 2, \dots, n_u.$$
 (2.30)

2.1.2.2 Synthesis conditions

Theorem 4. Consider the LPV system (2.22), there exists a gain-scheduling output-feedback controller (2.24), which minimize output performance bound trace(Q), while ICC constrained (2.29) control input enforcing internal stability and guaranteed \mathcal{H}_{∞} performance of closed-loop system, if

exist parameter-dependent symmetric matrices R, S, and a parameter-dependent state-space data $(\hat{A}_K, \hat{B}_K, \hat{C}_K)$ such that the LMIs hold for all admissible $(\theta, \dot{\theta})$ set.

$$\min_{\hat{A}_K, \hat{B}_K, \hat{C}_K R, S} trace(Q) \tag{2.31}$$

$$\begin{bmatrix} AR + B_2 \hat{C}_K + (*) - \dot{R} & * & * & * \\ A^T + \hat{A}_K & SA + \hat{B}_K C_y + (*) + \dot{S} & * & * \\ B_1^T & (SB_1 + \hat{B}_K D_y)^T & -\gamma I & * \\ C_{\infty} R + D_{12} \hat{C}_K & C_{\infty} & D_{11} & -\gamma I \end{bmatrix} < 0$$
 (2.32)

$$\begin{bmatrix} R & I \\ I & S \end{bmatrix} > 0 \tag{2.33}$$

$$\begin{bmatrix} AR + B_2 \hat{C}_K + (*) - \dot{R} & * & * \\ A^T + \hat{A}_K & SA + \hat{B}_K C_y + (*) + \dot{S} & * \\ B_1^T & (SB_1 + \hat{B}_K D_y)^T & -I \end{bmatrix} < 0$$
 (2.34)

$$\begin{bmatrix} Q & C_1 R + D_{12} \hat{C}_K & C_1 \\ * & R & I \\ * & I & S \end{bmatrix} > 0$$

$$(2.35)$$

$$\begin{bmatrix} \bar{U}_k & \Phi_k \hat{C}_K & 0 \\ * & R & I \\ * & I & S \end{bmatrix} > 0, \quad k = 1, 2, \dots, n_u.$$
 (2.36)

If the parameter-dependent matrices are found to satisfy the PLMI conditions, the gainscheduling output-feedback controller can be obtained by two-step scheme:

• Solve for N,M, the factorization problem $I - RS = NM^T$.

• compute A_K, B_K, C_K, D_K with

$$A_{K} = N^{-1}(\hat{A}_{K} - S\dot{R} - N\dot{M}^{T} - SAR - \hat{B}_{K}C_{y}R - SB_{2}\hat{C}_{K})M^{-T}$$

$$B_{K} = N^{-1}\hat{B}_{K}$$

$$C_{K} = \hat{C}_{K}M^{-T}$$
(2.37)

Proof. \mathcal{H}_{∞} channel

Suppose Lyapunov matrix for \mathcal{H}_{∞} channel, partition $P = \Pi_1 \Pi_2^{-1} = \Pi_2^{-T} \Pi_1^T$.

$$\Pi_{1} = \begin{bmatrix} R & I \\ M^{T} & 0 \end{bmatrix}, \Pi_{2} = \begin{bmatrix} I & S \\ 0 & N^{T} \end{bmatrix}, P = \begin{bmatrix} R & M \\ M^{T} & U \end{bmatrix}, P^{-1} = \begin{bmatrix} S & N \\ N^{T} & V \end{bmatrix}$$
(2.38)

Define nonsingular congruence matrix $T_{\infty} = diag(\Pi_2, I, I)$, which means that reverse derivation is valid. Pre- and post-multiply T_{∞}^T and T_{∞} on left and right side of (1.4).

$$\begin{bmatrix} \Pi_{2}^{T} & \\ & I \end{bmatrix} \begin{bmatrix} A_{cl}P + PA_{cl}^{T} - \dot{P} & B_{cl} & PC_{cl,\infty}^{T} \\ B_{cl}^{T} & -\gamma I & D_{cl,\infty}^{T} \end{bmatrix} \begin{bmatrix} \Pi_{2} & \\ & I \end{bmatrix} < 0$$
 (2.39)

$$\begin{bmatrix} \Pi_{2}^{T} A_{cl} \Pi_{1} + (*) - \Pi_{2}^{T} \dot{P} \Pi_{2} & * & * \\ B_{cl}^{T} \Pi_{2} & -\gamma I & * \\ C_{cl,\infty} \Pi_{1} & D_{cl,\infty} & -\gamma I \end{bmatrix} < 0$$
 (2.40)

By change of variables

y change of variables
$$\begin{cases} \hat{A}_K = SAR + NB_K C_y R + SB_2 C_K M^T + NA_K M^T + S\dot{R} + N\dot{M}^T \\ \hat{B}_K = NB_K \\ \hat{C}_K = C_K M^T \end{cases} \tag{2.41}$$

Then (1.4) is transformed to

$$\begin{bmatrix} AR + B_2 \hat{C}_K + (*) + \dot{R} & * & * & * \\ A^T + \hat{A}_K & SA + \hat{B}_K C_y + (*) - \dot{S} & * & * \\ B_1^T & (SB_1 + \hat{B}_K D_y)^T & -\gamma I & * \\ CR + D_{12} \hat{C}_K & C & D_{11} & -\gamma I \end{bmatrix} < 0$$
 (2.42)

Inequality (2.33) ensures P > 0, and I - RS is nonsingular, leading to unique mapping of change of variables.

$$\begin{bmatrix} R & I \\ I & S \end{bmatrix} > 0 \Rightarrow P = \Pi_1 \Pi_2^{-1} > 0 \tag{2.43}$$

\mathcal{H}_2 channel

In order to convexify the controller variables, same Lyapunov matrix is used for \mathcal{H}_2 channel, partition $P = \Pi_1 \Pi_2^{-1} = \Pi_2^{-T} \Pi_1^T$.

$$\Pi_{1} = \begin{bmatrix} R & I \\ M^{T} & 0 \end{bmatrix}, \Pi_{2} = \begin{bmatrix} I & S \\ 0 & N^{T} \end{bmatrix}, P = \begin{bmatrix} R & M \\ M^{T} & U \end{bmatrix}, P^{-1} = \begin{bmatrix} S & N \\ N^{T} & V \end{bmatrix}$$
(2.44)

Define congruence matrix $T_2 = diag(\Pi_2, I)$. Pre- and post-multiply T_2^T and T_2 on left and right side of (1.7).

$$\begin{bmatrix} \Pi_2^T \\ I \end{bmatrix} \begin{bmatrix} \dot{P} + A_{cl}P + PA_{cl} & B_{cl} \\ * & -I \end{bmatrix} \begin{bmatrix} \Pi_2 \\ I \end{bmatrix} < 0$$
 (2.45)

$$\Rightarrow \begin{bmatrix} AR + B\hat{C}_K + (*) + \dot{R} & * & * \\ A^T + \hat{A}_K & SA + \hat{B}_K C_y + (*) - \dot{S} & * \\ B_1^T & (SB_1 + \hat{B}_K D_y)^T & -I \end{bmatrix} < 0$$
 (2.46)

Define $T_3 = diag(I, \Pi_2)$, Pre- and post-multiply T_1^T and T_1 on left and right side of (1.8).

$$\begin{bmatrix} I \\ \Pi_2^T \end{bmatrix} \begin{bmatrix} Q & C_{cl2}P \\ * & P \end{bmatrix} \begin{bmatrix} I \\ \Pi_2 \end{bmatrix} > 0$$
 (2.47)

$$\Rightarrow \begin{bmatrix} Q & CR + E_2 \hat{C}_K & C \\ * & R & I \\ * & I & S \end{bmatrix} > 0$$
(2.48)

ICC condition

Pre- and post-multiply T_3^T and T_3 on left and right side of (2.30).

$$\begin{bmatrix} I \\ \Pi_2^T \end{bmatrix} \begin{bmatrix} \bar{U}_k & \Phi_k C_u P \\ * & P \end{bmatrix} \begin{bmatrix} I \\ \Pi_2 \end{bmatrix} > 0, \tag{2.49}$$

$$\Rightarrow \begin{bmatrix} \bar{U}_k & \Phi_k \hat{C}_K & 0 \\ * & R & I \\ * & I & S \end{bmatrix} > 0, \quad k = 1, 2, \dots, n_u.$$
 (2.50)

Remark 2. To remove the $\dot{\theta}$ information introduced by \dot{R} and \dot{M} , practical validity approach from [68] is applied. Due to factorization problem doesn't influence existence of controller but with introduced conservativeness. Set one of them as constant matrix, then derivative term will be eliminated. For example, set $N(\theta) = R(\theta) = R^0$ (constant), $M^T(\theta) = (I - R^0 S(\theta))$. then controller matrix \hat{A}_K is now

$$A_{K} = N^{-1}(\hat{A}_{K} - SAR - \hat{B}_{K}C_{y}R - SB_{2}\hat{C}_{K})M^{-T}$$

$$R^{0} = R_{0}$$

$$S(\theta) = S_{0} + \sum_{i=1}^{q} S_{i}\theta_{i}$$
(2.51)

Determine variables \hat{A}_K , \hat{B}_K , \hat{C}_K are chosen in affine form as plant matrix.

$$\hat{A}_K(\theta) = \hat{A}_{K0} + \sum_{i=1}^q \hat{A}_{Ki}\theta_i$$
$$\hat{B}_K(\theta) = \hat{B}_{K0} + \sum_{i=1}^q \hat{B}_{Ki}\theta_i$$
$$\hat{C}_K(\theta) = \hat{C}_{K0} + \sum_{i=1}^q \hat{C}_{Ki}\theta_i$$

2.2 Simultaneous Design Approach

2.2.1 Continuous-time state-feedback case

The scheduling parameter region is divided into J subregions, with J-1 overlapped region between any two adjacent subregions. A J number of gain-scheduling state-feedback controllers designed on J subregions for switching are given by

$$u^{j}(t) = K^{j}(\theta(t))x(t), j \in N_{J} = \{1, 2, \dots, J\};$$
 (2.52)

where $u^j(t)$ is partitioned as $u^j(t) = \left[u^j_1(t), u^j_2(t), \dots, u^j_{n_u}(t)\right]^T$. Then, the closed-loop LPV system involved with the j^{th} controller is now written as [69]

$$\begin{cases} \dot{x}(t) &= A_{cl}^{j}(\theta(t))x(t) + B_{\infty}(\theta(t))w_{\infty}(t) + B_{2}(\theta(t))w_{2}(t); \\ z_{\infty}(t) &= C_{cl,\infty}^{j}(\theta(t))x(t) + D_{\infty}(\theta(t))w_{\infty}(t) \\ z_{2}(t) &= C_{2}(\theta(t))x(t) \end{cases}$$
(2.53)

where
$$A_{cl}(\theta(t)) = A(\theta(t)) + B_u(\theta(t))K^j(\theta(t)), C_{cl,\infty}(\theta(t)) = C_{\infty}(\theta(t)) + E_{\infty}(\theta(t))K^j(\theta(t)).$$

There are two separated input and output pairs defined in (2.53), and they are specifically designated for assessing the closed-loop LPV system performances, as described below: (1) \mathcal{H}_{∞} performance is defined from $w_{\infty}(t)$ to $z_{\infty}(t)$ with \mathcal{L}_2 input and \mathcal{L}_2 output used to handle model uncertainties; (2) \mathcal{H}_2 performance is defined from $w_2(t)$ to $z_2(t)$ with \mathcal{L}_2 input and \mathcal{L}_{∞} output (or \mathcal{L}_2 - \mathcal{L}_{∞} gains), for improving system performance.

The control objective is to design a family of smooth switching ICC/\mathcal{H}_{∞} LPV controllers to robustly stabilize system in (2.1). This control problem can be divided into two parts: mixed ICC/\mathcal{H}_{∞} control for each subregion and smooth switching with hysteresis switching strategy.

2.2.1.1 Problem formulation

The mixed ICC/ \mathcal{H}_{∞} control problem is to find a state-feedback gain-scheduling controller (2.52) on each subregion for the LPV system (2.1) that minimizes the upper bound of \mathcal{H}_2 performance

cost:

$$\min \sup_{K^{j}(\theta)} ||T_{z_{2},w_{2}}(K^{j}(\theta),s)||_{2}, j \in N_{J};$$
(2.54)

such that the closed-loop system (2.53) is exponentially stable, and in addition, the following constraints are satisfied,

$$||T_{z_{\infty},w_{\infty}}(K^{j}(\theta),s)||_{\infty} \le \gamma_{\infty},$$
 (2.55)

$$Cov(u_k(t)) \le \bar{U}_k, k = 1, 2, \dots, n_u,$$
 (2.56)

where γ_{∞} is the given \mathcal{H}_{∞} -norm bound on system robustness subject to model uncertainties, and \bar{U}_k is the given bound on the control covariance $Cov(u_k(t))$ for the k^{th} control input $u_k(t)$ defined below,

$$Cov(u_k(t)) = \left[\frac{1}{2\pi} \int_{-\infty}^{\infty} T_{u_k}^*(K^j(\theta), j\omega) T_{u_k}(K^j(\theta), j\omega) d\omega \right], \qquad (2.57)$$

where $T_{u_k}(K_j(\theta),s):=T_{w_2\to u_k}(K^j(\theta),s)$ denotes the transfer function from $w_2(t)$ to $u_k(t)$ for the closed-loop LPV system (2.53). If the exogenous input $w_2(t)$ is an unknown disturbance that belongs to a bounded \mathcal{L}_2 set, the covariance $Cov(u_k(t))$ defined in (2.56) becomes the time correlation of control signal $u_k(t)$. Then, the mixed ICC and \mathcal{H}_∞ control problem is to minimize the summation of \mathcal{L}_2 to \mathcal{L}_∞ gains from $w_2(t)$ to individual output channel $z_{2,k}(t)$ for $k=1,2,\ldots,n_{z2}$ subject to the \mathcal{L}_2 to \mathcal{L}_∞ gain constraints on $u_k(t)$ for $k=1,2,\ldots,n_u$ and the \mathcal{H}_∞ constraint. In other words, the mixed ICC and \mathcal{H}_∞ problem minimizes the weighted sum of the worst case peak values of performance output subject to the constraints on the worst-case peak values of control inputs and the \mathcal{H}_∞ constraint.

To design a family of switching LPV controllers, hysteresis switching strategy is utilized to switch between adjacent controllers, ensuring the switching stability over any two neighboring subregions.

For the j^{th} subregion, consider a continuously differentiable parameter-dependent matrix $P^j(\theta) = P^j(\theta)^T > 0$ in \mathcal{H}_{∞} channel, or more precisely, the Lyapunov matrix $\{P^j(\theta)\}_{j \in N_J}$.

Then the Lyapunov function can be expressed as,

$$V_j(x,\theta) = x^T P^j(\theta) x \tag{2.58}$$

where x is the closed-loop system state. On the switching surfaces $S^{(i,j)}$, the condition below should be satisfied,

$$P^{i}(\theta) \ge P^{j}(\theta) \tag{2.59}$$

indicating that the Lyapunov function of the closed-loop system is non-increasing when switching from $\Theta^{(i)}$ to $\Theta^{(j)}$. The condition of Lyapunov matrices implies that

$$V^{i}(x,\theta) \ge V^{j}(x,\theta). \tag{2.60}$$

Then, switching from the i^{th} controller to the j^{th} controller is safe [1].

To smoothen the potential sharp change in controller gains, a cost function to be minimized is formulated as

$$F = trace(W) + \mu \sum ||(K_i - K_j)|_{\theta \in S(i,j)}||_2^2, \ i, j \in N_J, i \neq j.$$
 (2.61)

where $\sum ||(K_i - K_j)|_{\theta \in S^{(i,j)}}||_2^2$ denotes the gain differences on switching surfaces $\theta \in S^{(i,j)}$. The first term trace(W) in Eqn. (2.61) is viewed as an index of output \mathcal{H}_2 performance, while second term is the measure of switching smoothness. $\mu \geq 0$ is the tunable variable to balance these two indexes, leading to a trade-off relationship between output performance and switching smoothness.

2.2.1.2 Controller synthesis PLMIs

This section provides the synthesis PLMI conditions for the proposed smooth switching ICC/ \mathcal{H}_{∞} controllers. The upper bound of the \mathcal{H}_2 -norm, instead of actual \mathcal{H}_2 -norm, is minimized in order to make optimization numerically tractable. Theorem 5 gives the PLMIs conditions for controller synthesis with guaranteed $\mathcal{H}_2/\mathcal{H}_{\infty}$ performance. Combining mixed ICC/ \mathcal{H}_{∞} controller synthesis conditions and hysteresis switching conditions, Theorem 6 then provides conditions for designing switching controllers design.

Theorem 5. Given the input covariance constraints \bar{U}_k $(k=1,2,\cdots,n_u)$ and a positive scalar γ_∞ , in the j^{th} subregion of scheduling parameter, if there exist continuously differentiable parameter-dependent matrices $0 < P_2^j(\theta) = P_2^j(\theta)^T \in R^{n_x \times n_x}$, $0 < P_\infty^j(\theta) = P_\infty^j(\theta)^T \in R^{n_x \times n_x}$, $G^j(\theta) \in R^{n_x \times n_x}$, $Z^j(\theta) \in R^{n_u \times n_x}$, small scalars $\epsilon_2^j > 0$ and $\epsilon_\infty^j > 0$, and symmetric matrix $W^j \in R^{n_z \times n_z}$ subject to the following inequalities (* denotes symmetric terms),

$$\begin{bmatrix} \Phi_{11} & * & * \\ \Phi_{12} & -\epsilon_2^j (G^j(\theta) + G^j(\theta)^T) & * \\ B_2(\theta)^T & \boldsymbol{\theta} & -\boldsymbol{I} \end{bmatrix} < 0;$$
 (2.62)

$$\begin{bmatrix} W^j & C_2(\theta)G^j(\theta) \\ * & G^j(\theta) + G^j(\theta)^T - P_2^j(\theta) \end{bmatrix} > 0;$$

$$(2.63)$$

$$\begin{bmatrix} \bar{U}_k & e_k Z^j(\theta) \\ * & G^j(\theta) + G^j(\theta)^T - P_2^j(\theta) \end{bmatrix} > 0, k = 1, 2, \dots, n_u$$
 (2.64)

$$\begin{bmatrix} \Phi_{\infty 1} & * & * & * \\ \Phi_{\infty 2} & -\epsilon_{\infty}^{j} (G^{j}(\theta) + G^{j}(\theta)^{T}) & * & * \\ \Phi_{\infty 3} & \epsilon_{\infty}^{j} \Phi_{\infty 3} & -\gamma_{\infty} \mathbf{I} & * \\ B_{\infty}(\theta)^{T} & \mathbf{0} & D_{\infty}(\theta)^{T} & -\gamma_{\infty} \mathbf{I} \end{bmatrix} < 0,$$
 (2.65)

where $\Phi_{11} = A(\theta)G^j(\theta) + B_u(\theta)Z^j(\theta) + (A(\theta)G^j(\theta) + B_u(\theta)Z^j(\theta))^T - \frac{\partial P_2^j(\theta)}{\partial \theta}\dot{\theta}$, $\Phi_{12} = P_2^j(\theta) - G^j(\theta) + \epsilon_2^j(A(\theta)G^j(\theta) + B_u(\theta)Z^j(\theta))^T$, and e_k is input channel selection matrix for control input of interest, and $\Phi_{\infty 1} = A(\theta)G^j(\theta) + B_u(\theta)Z^j(\theta) + (A(\theta)G^j(\theta) + B_u(\theta)Z^j(\theta))^T - \frac{\partial P_\infty^j(\theta)}{\partial \theta}\dot{\theta}$, $\Phi_{\infty 2} = P_\infty^j(\theta) - G^j(\theta) + \epsilon_\infty^j(A(\theta)G^j(\theta) + B_u(\theta)Z^j(\theta))^T$, and $\Phi_{\infty 3} = C_\infty(\theta)G^j(\theta) + E_\infty(\theta)Z^j(\theta)$, then the gain-scheduling controller

$$u(t) = K^{j}(\theta)x(t), K^{j}(\theta) = Z^{j}(\theta)G^{j}(\theta)^{-1}$$
 (2.66)

exponentially stabilizes the LPV system $\Sigma(\theta)$ for any $(\theta, \dot{\theta}) \in \Lambda \times \Omega$ with a guaranteed \mathcal{H}_{∞}

performance bound γ_{∞} , and in addition, the ICC cost is bounded by

$$trace(W) > trace(C_2(\theta)P(\theta)C_2(\theta)^T)$$

$$> trace(C_2(\theta)\bar{P}(\theta)C_2(\theta)^T) = J_{ICC}$$
(2.67)

and the constraint (3.3) is satisfied.

Proof. The proof is omitted because it is similar to that of 3.

Theorem 6. For any two adjacent subregions Θ^i and Θ^j $(i, j \in N_J)$, if PLMIs in Theorem 5 are satisfied simultaneously over switching surfaces $S^{(i,j)}$ and the following PLMIs are satisfied,

$$P_{\infty}^{i}(\theta) \ge P_{\infty}^{j}(\theta), \theta \in S^{(i,j)}$$
(2.68)

then switching mixed ICC/ \mathcal{H}_{∞} controller exponentially stabilizes LPV system $\Sigma(\theta)$, for any $(\theta, \dot{\theta}) \in \Lambda \times \Omega$ with a guaranteed \mathcal{H}_{∞} performance bound γ_{∞} , guaranteed ICC cost bound W^j on j^{th} subregion.

The proof is omitted because it can be easily proved by combining switching stability and Theorem 5 [25].

In Theorem 5, controller is formulated as $K^j(\theta) = Z^j(\theta)G^j(\theta)^{-1}$. Thus, parameter dependent matrices $Z(\theta)$ and $G(\theta)$ determine the controller gain deviation on switching surfaces. To optimizing switching smoothness, the smoothness index is introduced as sum of $Z(\theta)$ and $G(\theta)$ deviations over all switching surfaces, as shown in the following formula.

$$\sum (||Z^{i}(\theta) - Z^{j}(\theta)||_{2}^{2} + ||G^{i}(\theta) - G^{j}(\theta)||_{2}^{2}),$$

$$i, j \in N_{J}, \theta \in S^{(i,j)}.$$
(2.69)

By then, smooth switching LPV control has been transformed into a convex optimization problem with a tunable cost function

$$F = \sum tr(W^{j}) + \mu \sum (||Z^{i}(\theta) - Z^{j}(\theta)||_{2}^{2} + ||G^{i}(\theta) - G^{j}(\theta)||_{2}^{2}),$$

$$i, j \in N_{I}, \theta \in S^{(i,j)}.$$
(2.70)

while inequalities (2.62), (2.63), (2.64), (2.65), and (2.68) are satisfied simultaneously.

2.2.2 Continuous-time dynamic output-feedback (DOF) case

Consider the following affine LPV system,

$$\dot{x}_{p}(t) = A(\theta(t))x_{p}(t) + B_{1}(\theta(t))w(t) + B_{2}(\theta(t))u(t)
z_{\infty}(t) = C_{1}(\theta(t))x_{p}(t) + D_{1}(\theta(t))w(t) + D_{2}(\theta(t))u(t)
z_{2}(t) = C_{2}(\theta(t))x_{p}(t)
y(t) = C_{y}(\theta(t))x_{p}(t) + D_{y}(\theta(t))w(t)$$
(2.71)

where $\theta(t) = \left[\theta_1(t), \theta_2(t), \dots, \theta_q(t)\right]^T$ denotes the scheduling parameter vector of q elements, $x_p(t)$ denotes the state, w(t) the exogenous inputs (for instance, disturbance inputs, sensor noises, etc.), u(t) the control input; $z_\infty(t)$ the \mathcal{H}_∞ controlled output, $z_2(t)$ the \mathcal{H}_2 performance output, and y(t) the measurement output. All system matrices have compatible dimensions and are in the affine parameter-dependent form. For example, $A(\theta(t))$ can be described by

$$A(\theta(t)) = A_0 + \sum_{i=1}^{q} A_i \theta_i(t).$$
 (2.72)

It is assumed that the scheduling parameters are measurable in real-time, and their magnitudes and variational rates are bounded as $(\theta, \dot{\theta}) \in \Theta \times \Lambda$:

$$\theta \in \Theta = \left\{ \underline{\theta}_i \le \theta_i(t) \le \overline{\theta}_i, i \in \{1, 2, ..., q\}, \right\}$$

$$\dot{\theta} \in \Lambda = \left\{ -\nu_{\theta_i} \le \dot{\theta}_i(t) \le \nu_{\theta_i}, i \in \{1, 2, ..., q\}. \right\}$$
(2.73)

The scheduling parameter region is divided into J subregions, with an overlapping region between any two adjacent subregions. A gain-scheduling DOF controller is to be designed for each subregion, and the controllers for adjacent subregions are to be switched according to hysteresis switching logic. The j^{th} subregion is denoted by $\Theta^{(j)}$ ($j \in N_J = \{1, 2, \dots, J\}$), and switching surface from $\Theta^{(i)}$ to $\Theta^{(j)}$ is denoted by $S^{(i,j)}$.

The j^{th} DOF controller $K^j(\theta)$ for the j^{th} subregion is given by

$$K^{j}(\theta): \begin{cases} \dot{x}_{K} = A_{K}^{j}(\theta)x_{K} + B_{K}^{j}(\theta)y \\ u = C_{K}^{j}(\theta)x_{K} \end{cases}$$

$$(2.74)$$

where x_K denotes the controller state and (A_K^j, B_K^j, C_K^j) are controller variables to be determined. Note that there is no direct feedthrough term in u, because a strictly proper DOF controller leads to a finite \mathcal{H}_2 norm for transfer functions T_{z_2w} and input covariance. The state vector for the closed-loop LPV system associated with the j^{th} controller becomes $x_{cl}^T = [x_p^T, x_K^T]$, with the following state space realization

$$\begin{bmatrix}
A_{cl}^{j} & B_{cl}^{j} \\
C_{cl,\infty}^{j} & D_{cl,\infty}^{j} \\
C_{cl,2}^{j} & \mathbf{0}
\end{bmatrix} = \begin{bmatrix}
A & B_{2}C_{K}^{j} & B_{1} \\
B_{K}^{j}C_{y} & A_{K}^{j} & B_{K}^{j}D_{y} \\
C_{1} & D_{2}C_{K}^{j} & D_{1} \\
C_{2} & E_{2}C_{K}^{j} & \mathbf{0}
\end{bmatrix}.$$
(2.75)

For simplicity, the dependency on scheduling parameter θ will be omitted unless necessary in the rest of thesis.

The proposed control input u(t) associated with the j^{th} controller can be equivalently rewritten as

$$u(t) = C_u^j x_{cl} = \begin{bmatrix} 0 & C_K^j \end{bmatrix} \begin{bmatrix} x_p \\ x_K \end{bmatrix}.$$

Hence, the variance of the k^{th} $(k \in N_{nu} = \{1, 2, \dots, n_u\})$ control input of the j^{th} controller is constrained as

$$cov(u_k(t)) \le \sup_{\theta \in \Theta(j), j \in N_J} e_k C_u^j \overline{P}_2^j (C_u^j)^T e_k^T < \overline{U}_k,$$

where e_k is a selection row vector with 1 at the k^{th} entry and 0 elsewhere, such that $e_k C_u^j$ equals to the k^{th} control. We have the following lemma providing hard constraint on variance of control input for any scheduling parameter trajectory $\theta \in \Theta^{(j)}$.

Lemma 6. [67] The ICC condition on the k^{th} control input of the j^{th} controller,

$$\sup_{\theta \in \Theta(j)} e_k C_u^j \overline{P}_2^j (C_u^j)^T e_k^T < \sup_{\theta \in \Theta(j)} e_k C_u^j P_2^j (C_u^j)^T e_k^T < \overline{U}_k,$$
(2.76)

is equivalent to the following PLMI to be held for any $\theta \in \Theta^{(j)}$,

$$\begin{bmatrix} \overline{U}_k & e_k C_u^j P_2^j \\ * & P_2^j \end{bmatrix} > 0, \quad k \in N_{n_u}.$$

$$(2.77)$$

2.2.2.1 Problem formulation

For a given divided subregion set, the smooth-switching ICC/ \mathcal{H}_{∞} DOF LPV control problem is to find a family of gain-scheduling DOF controllers $K^{j}(\theta), j \in N_{J}$, defined in (2.74), over all subregions for the LPV system (2.71) that minimizes the following cost function,

$$\min_{A_K^j(\theta), B_K^j(\theta), C_K^j(\theta)} \epsilon * trace(W) + I_{sm}, \qquad (2.78)$$

subject to the following constraints

$$||T_{\infty}||_{\infty} < \gamma, \tag{2.79}$$

$$cov(u_k(t)) < \overline{U}_k, \quad k \in N_{n_u},$$
 (2.80)

where I_{sm} denotes the smoothness index to be defined in the next section, trace(W) is the upper bound of the system \mathcal{H}_2 norm over all subregions, and $\epsilon > 0$ is a tunable weighting coefficient to be used to trade-off between switching smoothness and system performance. In order to ensure that the control design problem is convex, I_{sm} is chosen as the deviation norm of controller parameters over all switching surfaces that is a convex function describing the smoothness of controller variables over switching surfaces.

2.2.2.2 Controller synthesis PLMIs

The following theorem contains the main result. Note that cost function (2.81) is a linear combination of two convex functions of output performance trace(W) and smoothness index I_{sm} associated with controller parameters. The tunable parameter $\epsilon > 0$ is used to balance the output performance and smoothness of controller parameters over switching surfaces. A line search for ϵ is needed in order to find the optimal trade-off relationship.

Theorem 7. Consider LPV system (2.71). There exists a family of gain-scheduling DOF controllers (2.74) that minimizes the ϵ -balanced cost function

$$\min_{\hat{A}_K^j, \hat{B}_K^j, \hat{C}_K^j X^j, Y^j} \epsilon * trace(W) + I_{sm}$$
(2.81)

subject to the ICC condition (2.80) and \mathcal{H}_{∞} constraint (2.79), if there exists a family of parameter-dependent symmetric matrices X^j and Y^j , and a family of parameter-dependent controller variables \hat{A}_K^j , \hat{B}_K^j , and \hat{C}_K^j ($j \in N_J$), such that PLMIs (2.83) - (2.87) hold with a given robustness level $\gamma > 0$ for all admissible $(\theta, \dot{\theta}) \in \Theta^{(j)} \times \Lambda$, and one of the two conditions in (2.88) holds on the switching surfaces $S^{(i,j)}$ for $\epsilon > 0$ with I_{sm} given by

$$I_{sm} = \sum_{i,j,i\neq j} \begin{pmatrix} ||\hat{A}_K^i - \hat{A}_K^j||_2 + ||\hat{B}_K^i - \hat{B}_K^j||_2 \\ +||\hat{C}_K^i - \hat{C}_K^j||_2 + ||Y^i - Y^j||_2 \\ +||X^i - X^j||_2 \end{pmatrix} \Big|_{\theta \in S(i,j)}.$$
 (2.82)

$$\begin{bmatrix} M_{11} & * & * & * \\ A^T + \hat{A}_K^j & M_{22} & * & * \\ B_1^T & M_{32} & -\gamma I & * \\ C_1 X^j + D_2 \hat{C}_K^j & C_1 & D_1 & -\gamma I \end{bmatrix} < 0$$
(2.83)

where

$$M_{11} = AX^{j} + B_{2}\hat{C}_{K}^{j} + (*) - \dot{X}^{j},$$

$$M_{22} = Y^{j}A + \hat{B}_{K}^{j}C_{y} + (*) + \dot{Y}^{j},$$

$$M_{32} = (Y^{j}B_{1} + \hat{B}_{K}^{j}D_{y})^{T}.$$

$$\begin{bmatrix} X^{j} & I \\ I & Y^{j} \end{bmatrix} > 0,$$
(2.84)

$$\begin{bmatrix} M_{11} & * & * \\ A^T + \hat{A}_K^j & M_{22} & * \\ B_1^T & M_{32} & -I \end{bmatrix} < 0,$$
(2.85)

$$\begin{bmatrix} W & C_1 X^j + D_2 \hat{C}_K^j & C_1 \\ * & X^j & I \\ * & I & Y^j \end{bmatrix} > 0$$
 (2.86)

$$\begin{bmatrix} \overline{U}_k & e_k \hat{C}_K^j & 0 \\ * & X^j & I \\ * & I & Y^j \end{bmatrix} > 0, \quad k \in N_{n_u}.$$

$$(2.87)$$

$$\begin{cases} Y^{i} \ge Y^{j} \\ X^{i} - (Y^{i})^{-1} \le X^{j} - (Y^{j})^{-1} \end{cases}$$

$$or$$

$$\begin{cases} X^{i} \le X^{j} \\ Y^{i} - (X^{i})^{-1} \ge Y^{j} - (X^{j})^{-1} \end{cases}$$

$$(2.88)$$

Proof. To convexify control strategy with \mathcal{H}_2 and \mathcal{H}_∞ channels, let $P^j=P_2^j=P_\infty^j$ for the j^{th} subregion. Suppose that the Lyapunov matrix P^j can be partitioned as

$$P^{j} = \begin{bmatrix} Y^{j} & N^{j} \\ (N^{j})^{T} & \star \end{bmatrix}, (P^{j})^{-1} = \begin{bmatrix} X^{j} & M^{j} \\ (M^{j})^{T} & \star \end{bmatrix}, \tag{2.89}$$

where \star denotes the elements which are not used.

Furthermore, define the congruence matrices as

$$\Pi_1^j = \begin{bmatrix} X^j & I \\ (M^j)^T & 0 \end{bmatrix}, \Pi_2^j = \begin{bmatrix} I & Y^j \\ 0 & (N^j)^T \end{bmatrix},$$

such that $P^j\Pi_1^j=\Pi_2^j$. For the \mathcal{H}_∞ performance channel, the PLMIs (2.83) can be easily obtained by following the procedures in [68, 12, 13, 32]. Define nonsingular congruence matrix $T_\infty^j=diag(\Pi_2^j,I,I)$, which means that reverse derivation is valid. Pre- and post-multiply $(T_\infty^j)^T$ and T_∞^j on left and right side of the \mathcal{H}_∞ performance condition (1.12) for each subregion.

$$\begin{bmatrix} \Pi_{2}^{j} & \\ & I \\ & & I \end{bmatrix}^{T} \begin{bmatrix} A_{cl}^{j} P^{j} + P^{j} (A_{cl}^{j})^{T} - \dot{P}^{j} & B_{cl}^{j} & * \\ & * & -\gamma I & * \\ & C_{cl,\infty}^{j} P & D_{cl,\infty}^{j} & -\gamma I \end{bmatrix} \begin{bmatrix} \Pi_{2}^{j} & \\ & I \\ & & I \end{bmatrix} < 0 \quad (2.90)$$

By $P^j = \Pi_1^j(\Pi_2^j)^{-1}$, the above LMI can be converted to

$$\begin{bmatrix}
(\Pi_{2}^{j})^{T} A_{cl}^{j} \Pi_{1}^{j} + (*) - (\Pi_{2}^{j})^{T} \dot{P}^{j} \Pi_{2}^{j} & * & * \\
(B_{cl}^{j})^{T} \Pi_{2}^{j} & -\gamma I & * \\
C_{cl,\infty}^{j} \Pi_{1}^{j} & D_{cl,\infty}^{j} & -\gamma I
\end{bmatrix} < 0$$
(2.91)

Introduce the change of controller variables as

$$\begin{cases} \hat{A}_{K}^{j} = N^{j} A_{K}^{j} (M^{j})^{T} + N^{j} B_{K}^{j} C_{y} X^{j} + Y^{j} B_{2} C_{K}^{j} (M^{j})^{T} + Y^{j} A X^{j} \\ \hat{B}_{K}^{j} = N^{j} B_{K}^{j} \\ \hat{C}_{K}^{j} = C_{K}^{j} (M^{j})^{T}, \end{cases}$$

$$(2.92)$$

then the PLMI condition (2.83) can be obtained.

For the \mathcal{H}_2 performance channel, define the congruence matrix $T_2^j = diag(\Pi_2^j, I)$. Pre- and post-multiply (1.15) by T_2^T and T_2 to obtain,

$$(T_2^j)^T \begin{bmatrix} -\dot{P}^j + A_{cl}^j P^j + (*) & B_{cl}^j \\ * & -I \end{bmatrix} T_2^j < 0,$$
 (2.93)

which yields (2.85) by means of change of variables in (2.92). Define $T_3^j = diag(I, \Pi_2^j)$, and preand post-multiply (1.16) by $(T_3^j)^T$ and T_3^j , we obtain

$$\begin{bmatrix} I \\ \Pi_2^j \end{bmatrix}^T \begin{bmatrix} W & C_{cl,2}^j P^j \\ * & P^j \end{bmatrix} \begin{bmatrix} I \\ \Pi_2^j \end{bmatrix} > 0,$$
 (2.94)

which yields (2.86) by means of change of variables in (2.92). For the ICC condition, pre- and post-multiplying T_3^T and T_3 to (2.77) yields

$$\begin{bmatrix} I \\ \Pi_2^T \end{bmatrix} \begin{bmatrix} \bar{U}_k & e_k C_u^j P_2^j \\ * & P_2^j \end{bmatrix} \begin{bmatrix} I \\ \Pi_2 \end{bmatrix} > 0,$$
 (2.95)

which gives (2.87).

Remark 3. The PLMIs formulated in Theorem 7 renders an optimization problem of infinite dimensions and un-defined decision variable structures. To numerically tackle this optimization problem, affine decision variable structure is assumed, for example, $\hat{A}_K^j(\theta)$ is expressed as $\hat{A}_K^j(\theta) = \hat{A}_{K0}^j + \sum_{i=1}^q \hat{A}_{Ki}^j \theta_i$. Coefficient check in multi-simplex domain [19, 70, 71] has been adopted to successfully obtain a finite set of LMIs but with introduced conservativeness. Other options [72, 73] can also be applied, for instance, sum-of-square relaxation [74] and enforcing multi-convexity method [75].

Remark 4. If the controller variables are obtained by minimizing the ϵ -balanced cost function subject to formulated PLMIs, the gain-scheduling DOF controller can be constructed by first solving the factorization problem $I - Y^j X^j = N^j (M^j)^T$ for N^j and M^j , and then computing A_K^j , B_K^j , and C_K^j from the following equations

$$\begin{cases}
A_K^j = (N^j)^{-1} \left[\hat{A}_K^j - Y^j \dot{X}^j - N^j (\dot{M}^j)^T - Y^j A X^j - \hat{B}_K^j C_y X^j - Y^j B_2 \hat{C}_K^j \right] (M^j)^{-T} \\
B_K^j = N^{-1} \hat{B}_K^j \\
C_K^j = \hat{C}_K (M^j)^{-T}
\end{cases} (2.96)$$

Remark 5. In order to remove the $\dot{\theta}$ dependency introduced by \dot{X}^j and \dot{Y}^j , the practical validity approach presented in [68] is applied. Either X^j or Y^j is set to be a constant matrix eliminates the derivative terms. For example, we may set $X(\theta) = X_0$ and N = I for all $\theta \in \Theta$, then $Y^j = Y^j(\theta)$

and $(M^j)^T = (I - Y^j(\theta)X_0)$. As a result, the reconstructed controller variables can be simplified

$$\begin{cases}
A_K^j = (N^j)^{-1} \left[\hat{A}_K^j - Y^j A X^j - \hat{B}_K^j C_y X^j - Y^j B_2 \hat{C}_K^j \right] (M^j)^{-T} \\
B_K = N^{-1} \hat{B}_K^j \\
C_K = \hat{C}_K (M^j)^{-T}
\end{cases} (2.97)$$

Note that the switching stability condition (2.88) is non-convex and freezing $X(\theta) = X_0$ will convexify it into

$$Y^{i}(\theta) \ge Y^{j}(\theta), \ \theta \in S^{(i,j)}. \tag{2.98}$$

Therefore, variables $(\hat{A}_{Ki}^j, \hat{B}_{Ki}^j, \hat{C}_{Ki}^j, Y_i^j, X_0)$ can be iteratively searched to optimize the cost function with the tuning parameter ϵ . The operation of PLMIs and optimization problem are solved by using the parser YALMIP [76] jointly with optimization algorithm SeDuMi [77].

2.3 Sequential Design Approach

2.3.1 Motivations of sequential design

In conventional switching LPV control design, switching controllers are synthesized by controller variables that simultaneously satisfy PLMIs for both \mathcal{H}_{∞} performance on all subregions and switching stability conditions on all switching surfaces. In other words, controller synthesis conditions on each subregion are not independent with adjacent ones due to the switching stability condition imposed on switching surfaces. When the number of subregions goes large, simultaneous design approach leads to a high-dimensional optimization problem, with a high amount of LMI constraints, decision variables, online computational load, and memory requirement [78, 79]. As a result, these drawbacks make simultaneous design practically infeasible for high-order systems with many divided subregions. For example, in the polytopic synthesis approach, it's well known that the number of LMIs grows with $\mathcal{O}(2^q)$, where q is the dimension of scheduling parameter [78, 63].

Chen [60] considered the hysteresis switching state-feedback LPV control and conducted linear interpolation of controller variables on switching surfaces. However, only the relative stability is achieved on the overlapping subregion by this method. Hanifzadegan and Nagamune [61] followed the idea of linear interpolation of controller matrices on switching surfaces, and imposed constraints on controller matrix derivative. The design of stabilizing controllers was formulated into a nonconvex optimization problem, and an iterative descent algorithm was then applied to find a local LPV controller for each subregion. Their approach relies heavily on iterative computations to solve multi-objective non-convex problems. Moreover, the interpolation of controller matrices cannot guarantee the \mathcal{H}_{∞} robust performance over the overlapped region. Jiang et.al [80] provided a systematic approach for developing switching LPV controller by linearly interpolating controller variables for average-dwell-time switching strategy. However, the formulated PLMIs are not numerically tractable, due to the scheduling parameter term in the denominator, which induces infinity term on switching surfaces. Bianchi [81] proposed a new design approach based on Youla parametrization that closed-loop system stability is not affected by the inclusion of any stable

switched LPV system. This makes it possible to design switched controllers independently ,but this method cannot be extended to parameter-dependent quadratically stable systems.

A sequential controller design approach is proposed in this thesis to design switching controllers with higher efficiency and less computational burden than simultaneous design. Interpolated controller variables for overlapped subregions and newly formulated PLMIs are utilized to synthesize switching LPV controllers on each subregion independently. On each overlapped subregion, the Lyapunov matrix is formulated by convexly combining PDLM on adjacent subregions. The PLMIs for \mathcal{H}_{∞} performance on each subregion is formulated, such that the convex combination of adjacent PLMIs leads to a guaranteed \mathcal{H}_{∞} performance on every overlapped subregion. Moreover, the guaranteed system performance on overlapped subregion is no worse than its neighboring subregions. In this way, an individual controller for each subregion can be designed in sequential order, instead of synthesizing all controllers simultaneously. By iteratively solving the reduced-dimensional optimization problem on each subregion, switching controllers for all subregions with guaranteed \mathcal{H}_{∞} performance on all subregions and overlapped subregions can be obtained.

Note that, in order to simplify the design problem, all sequential LPV controllers are assumed to have access to full states and that they share the same parametric controller form, while controller gains are different on each subregion. In this thesis, switching \mathcal{H}_{∞} LPV state-feedback control is considered, we will present the basic ideas of the proposed sequential design method by one-dimensional and two-dimensional cases. After that, the proposed approach will be extended to the general case of any dimensional scheduling parameters. The main contributions of this work are three-fold: (1) proposition of sequential design of switching LPV controllers; (2) formulation of synthesis conditions for sequential design of switching \mathcal{H}_{∞} state-feedback LPV controllers; (3) demonstration of the benefits of the proposed sequential design approach by numerical examples.

Consider the affine LPV system in Eqn. (2.99),

$$\dot{x}_p(t) = A(\theta(t))x_p(t) + B_1(\theta(t))w(t) + B_2(\theta(t))u(t)
z(t) = C(\theta(t))x_p(t) + D_1(\theta(t))w(t) + D_2(\theta(t))u(t)$$
(2.99)

where the system state is denoted as $x_p(t)$, the exogenous inputs denoted as w(t) (for instance distur-

bance inputs, sensor noise, etc.), the control input as u(t), and the controlled output as z(t). System matrices are assumed to depend on scheduling parameter vector $\theta(t) = \left[\theta_1(t), \theta_2(t), \dots, \theta_q(t)\right]^T$ and be in the affine parameter-dependent form. For example, $A(\theta(t))$ is described as

$$A(\theta(t)) = A_0 + \sum_{i=1}^{q} A_i \theta_i(t), \tag{2.100}$$

where A_0 and A_i , i = 1, 2, ..., q, are constant matrices.

The real-time measurable scheduling parameters are assumed to vary within parameter region which is formulated by bounds of magnitudes and variational rates,

$$\theta_{i} \in \Theta_{i} = \left\{ \underline{\theta}_{i} \leq \theta_{i}(t) \leq \overline{\theta}_{i}, i = 1, 2, \dots, q, \right\},$$

$$\dot{\theta}_{i} \in \Lambda_{i} = \left\{ -\nu_{i} \leq \dot{\theta}_{i}(t) \leq \nu_{i}, i = 1, 2, \dots, q. \right\}$$
(2.101)

Now consider the switched LPV system, which consists of M numbers of divided scheduling parameters $[\theta_1,\theta_2,\ldots,\theta_m,\ldots,\theta_M]$, and S numbers of un-divided scheduling parameters $[\theta_{M+1},\theta_{M+2},\ldots,\theta_{M+s},\ldots,\theta_{M+S}]$. Hence, M+S=q. For each of divided scheduling parameters, θ_m is divided into N_m numbers of subregions with its variational rate remained undivided as $\Lambda=\Lambda_1\times\cdots\times\Lambda^q$, and neighboring subregions will produce overlapped subregions. The entire scheduling parameter is divided into $\Pi_{m=1}^M N_m$ numbers of subregions, among which the (n_1,n_2,\ldots,n_M) th subregion, denoted as $\Theta^{(n_1,n_2,\ldots,n_M)}$, is formed by Cartesian product of subregions $\Theta_1^{(n_1)}\times\Theta_2^{(n_2)}\times\cdots\times\Theta_M^{(n_M)}\times\Theta_{M+1}\times\cdots\times\Theta_q$. The overlapped subregion formed by $\Theta_m^{(n_m)}$ and $\Theta_m^{(n_m+1)}$, is denoted as $\Theta_m^{([n_m,n_m+1])}$. Figure 2.1 and Figure 2.2 illustrate the divisions scenarios of one- and two-dimensional scheduling parameters.

In Figure 2.1, three adjacent subregions $\Theta^{(i-1)}, \Theta^{(i)}, \Theta^{(i+1)}$ produce two overlapped subregion $\Theta^{([i-1,i])}$ and $\Theta^{([i,i+1])}$, with switching surfaces $S^{([i-1,i])}$ and $S^{([i,i+1])}$ defined as region boundaries of overlapped subregions. In Figure 2.2, any four adjacent subregions $\Theta^{(i,j)}, \Theta^{(i+1,j)}, \Theta^{(i+1,j)}$, $\Theta^{(i,j+1)}, \Theta^{(i+1,j+1)}$ produce two kinds of overlapped subregions. The center subregion denoted by $\Theta^{([i,i+1],[j,j+1])}$ is formed by 2^2 overlapped subregions in two dimensions, whereas other overlapped subregions are individually formed by 2^1 overlapping subregions in one dimension, denoted

as $\Theta^{([i,i+1],j)}$, $\Theta^{([i,i+1],j+1)}$, $\Theta^{(i,[j,j+1])}$, $\Theta^{(i+1,[j,j+1])}$. In the case of M-dimensional divided scheduling parameter, the center-overlapped subregion is formed by 2^M overlapping subregions.

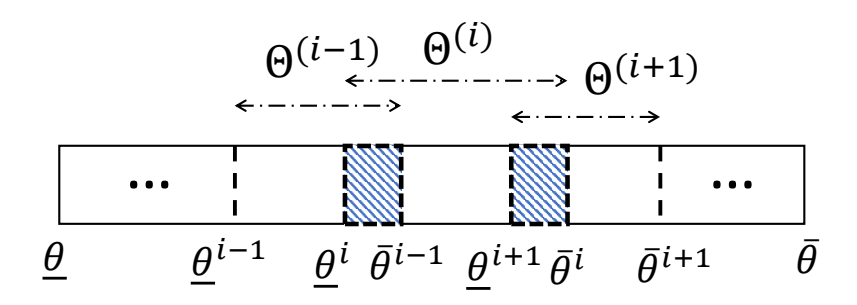


Figure 2.1: Subregion division illustration of one-dimensional scheduling parameter

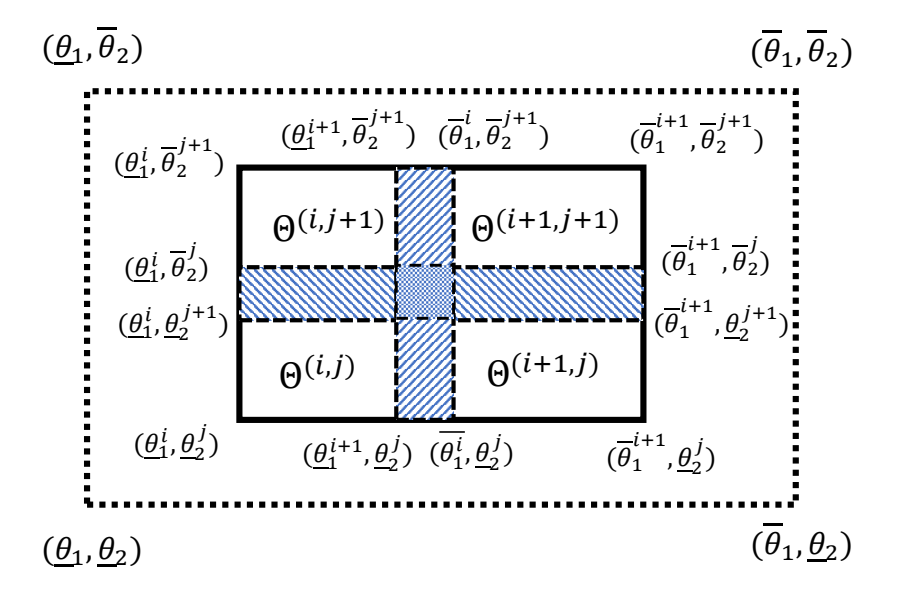


Figure 2.2: Subregion division illustration of two-dimensional scheduling parameter

For the given switching LPV system, we are seeking for a gain-scheduling state-feedback switching controller

$$u(t) = K_i(\theta)x(t) \tag{2.102}$$

stabilizing the LPV system (2.99) with guaranteed \mathcal{H}_{∞} performance, and controller gain $K_i(\theta)$ is to be switched according to switching signal i(t). The switched closed-loop system matrices are derived as

The \mathcal{H}_{∞} performance, defined as \mathcal{L}_2 -induced norms from w(t) to z(t), is utilized to assess the closed-loop system robustness in the presence of model uncertainties. Mathematically, let $T_{\infty}(\theta,s):=T_{zw}(\theta,s)$ denotes the parameter-dependent transfer function from w(t) to z(t) and $||T_{\infty}||_{\infty}$ as the worst-case \mathcal{H}_{∞} norm of T_{∞} defined in $\theta \in \Theta$. Then, the \mathcal{H}_{∞} performance for the (w(t),z(t)) pair is defined as \mathcal{L}_2 gain [15], where

$$||T_{\infty}||_{\infty} = \sup_{\theta \in \Theta} \sup_{w \in \mathcal{L}_2, ||w||_2 \neq 0} \frac{||z(t)||_2}{||w(t)||_2}.$$
 (2.104)

The following lemma provides PLMI conditions for simultaneously designing switching LPV \mathcal{H}_{∞} state-feedback controller with average-dwell-time switching logic [52, 53, 1], which has been well proven and widely used in literature.

Lemma 7. Given scalars $\lambda_0 > 0$, $\mu > 1$, if there exist parameter dependent matrices $P_i(\theta) > 0$, $Z_i(\theta)$ such that (2.105) holds for all admissible trajectories $(\theta, \dot{\theta}) \in \Theta^{(i)} \times \Lambda$ and (2.106) holds for any switching surface, then the closed-loop system (2.103) is exponentially stabilized by switching LPV state-feedback controller gains $K_i(\theta) = Z_i(\theta)P_i^{-1}(\theta)$ for every switching signal i(t) with average dwell time $\tau_a > \frac{\ln(\mu)}{\lambda_0}$ and $||z||_2 < \gamma ||w||_2$ is achieved with robustness level $\gamma = \max\{\gamma_i\} > 0$,

$$\begin{bmatrix} -\dot{P}_i + \langle AP_i + B_2Z_i \rangle + \lambda_0 P_i & * & B_1 \\ CP_i + D_2Z_i & -\gamma_i I & D_1 \\ * & * & -\gamma_i I \end{bmatrix} < 0, \qquad (2.105)$$

$$\frac{1}{\mu}P_{i+1}(\theta) \le P_i(\theta) \le \mu P_{i+1}(\theta), \ \theta \in S^{([i,i+1])}.$$
(2.106)

Remark 6. This simultaneous design method requires that PLMI conditions for all subregions and switching stability are satisfied at the same time. All switched controllers for subregions are designed simultaneously, leading to a very high-dimensional optimization problem, especially in the scenario of multi-dimensional scheduling parameters.

2.3.2 Controller synthesis PLMIs

A novel sequential design method is proposed to overcome the disadvantages of the conventional design method. The main idea is introducing interpolated controller decision variables and formulating independent PLMI conditions on each subregion such that system performances on overlapped subregions are guaranteed as well. In this way, the switching controller synthesis conditions are formulated as independent optimization problems and can be well solved sequentially. One- and two-dimensional scheduling parameter scenarios are provided as motivation examples for a more general *q*-dimensional scheduling parameter scenario.

2.3.2.1 One-dimensional scheduling parameter

Consider three neighboring subregions $\Theta^{(i-1)}$, $\Theta^{(i)}$, $\Theta^{(i+1)}$ as shown in Figure 2.1 and designate controller decision variable pairs $P_{i-1}(\theta)$, $Z_{i-1}(\theta)$, $P_i(\theta)$, $Z_i(\theta)$, and $P_{i+1}(\theta)$, $Z_{i+1}(\theta)$ for controller synthesis. On the overlapped subregion of $\Theta^{(i-1)} \cap \Theta^{(i)} = \Theta^{([i-1,i])}$, define the interpolated parameter-dependent positive definite matrix $P_{(i-1,i)}(\theta)$ and interpolated $Z_{(i-1,i)}(\theta)$ as

$$P_{(i-1,i)} = \varepsilon_{11}^{(i-1,i)}(\theta)P_i(\theta) + \varepsilon_{12}^{(i-1,i)}(\theta)P_{i-1}(\theta),$$

$$Z_{(i-1,i)} = \varepsilon_{11}^{(i-1,i)}(\theta)Z_i(\theta) + \varepsilon_{12}^{(i-1,i)}(\theta)Z_{i-1}(\theta),$$
(2.107)

where interpolation function $\varepsilon(\theta)$ is chosen as a sigmoid function as

$$\varepsilon_{11}^{(i-1,i)}(\theta) = \frac{e^{\alpha(\theta)}}{e^{\alpha(\theta)} + 1}, \ \varepsilon_{12}^{(i-1,i)}(\theta) = \frac{1}{e^{\alpha(\theta)} + 1},$$

and $\alpha(\theta) = \frac{\beta[2(\theta-\underline{\theta}^i)-(\overline{\theta}^{i-1}-\underline{\theta}^i)]}{\overline{\theta}^{i-1}-\underline{\theta}^i} = \frac{\beta[2(\theta-\underline{\theta}^i)-L^{(i-1,i)}]}{L^{(i-1,i)}}$. The variable $L^{(i-1,i)}$ denotes the size of the overlapped subregion and β is a tunable scalar which determines the interpolation function shape.

Then the time derivative of interpolated parametric matrix can be written as

$$\dot{P}_{(i-1,i)} = \left\{ \varepsilon_{12}^{(i-1,i)}(\theta) \dot{P}_{i-1}(\theta) + \varepsilon_{11}^{(i-1,i)}(\theta) \dot{P}_{i}(\theta) \right\}
+ \left\{ \varepsilon_{12}^{(i-1,i)}(\theta) \frac{-e^{\alpha(\theta)} \cdot 2\beta \dot{\theta}}{(e^{\alpha(\theta)} + 1)L^{(i-1,i)}} P_{i-1}(\theta) + \varepsilon_{11}^{(i-1,i)}(\theta) \frac{2\beta \dot{\theta}}{(e^{\alpha(\theta)} + 1)L^{(i-1,i)}} P_{i}(\theta) \right\}.$$
(2.108)

The associated PLMI conditions for $(\theta, \dot{\theta}) \in \Theta^{(i-1)} \times \Lambda$ and $(\theta, \dot{\theta}) \in \Theta^{(i)} \times \Lambda$ can be accordingly formulated as

$$\begin{bmatrix} \langle AP_{i-1} + B_2 Z_{i-1} \rangle - \dot{P}_{i-1} + \lambda_0 P_{i-1} + \frac{e^{\alpha(\theta)} \cdot 2\beta \dot{\theta}}{(e^{\alpha(\theta)} + 1)L^{(i-1,i)}} P_{i-1} & * & B_1 \\ CP_{i-1} + D_2 Z_{i-1} & -\gamma_{i-1} I & D_1 \\ * & * & -\gamma_{i-1} I \end{bmatrix} < 0$$

$$(2.109)$$

$$\begin{bmatrix} \langle AP_{i} + B_{2}Z_{i} \rangle - \dot{P}_{i} + \lambda_{0}P_{i} + \frac{-2\beta\dot{\theta}}{(e^{\alpha(\theta)} + 1)L^{(i-1,i)}}P_{i} & * & B_{1} \\ CP_{i} + D_{2}Z_{i} & -\gamma_{i}I & D_{1} \\ * & * & -\gamma_{i}I \end{bmatrix} < 0$$
 (2.110)

such that $\varepsilon_{12}^{(i-1,i)}\cdot$ (2.109) + $\varepsilon_{11}^{(i-1,i)}\cdot$ (2.110) yielding the following standard PLMI condition, which indicates the guaranteed \mathcal{H}_{∞} performance for any $(\theta, \dot{\theta}) \in \Theta^{([i-1,i])} \times \Lambda$,

which indicates the guaranteed
$$\mathcal{H}_{\infty}$$
 performance for any $(\theta,\dot{\theta})\in\Theta^{([i-1,i])}\times\Lambda$,
$$\begin{bmatrix} \left\langle AP_{(i-1,i)}+B_2Z_{(i-1,i)}\right\rangle -\dot{P}_{(i-1,i)}+\lambda_0P_{(i-1,i)} &* &B_1\\ CP_{(i-1,i)}+D_2Z_{(i-1,i)} &-\gamma_{(i-1,i)}I &D_1\\ &* &* &-\gamma_{(i-1,i)}I \end{bmatrix}<0 \ \ (2.111)$$
 where $\gamma_{(i-1,i)}=\varepsilon_{12}^{(i-1,i)}\gamma_{i-1}+\varepsilon_{11}^{(i-1,i)}\gamma_{i}<\max\{\gamma_{i-1},\gamma_{i}\}$.

where $\gamma_{(i-1,i)} = \varepsilon_{12}^{(i-1,i)} \gamma_{i-1} + \varepsilon_{11}^{(i-1,i)} \gamma_i < \max \left\{ \gamma_{i-1}, \gamma_i \right\}$.

In order to convert Eqns. (2.109) and (2.110) into numerically tractable ones, the bounds that, $-\nu \leq \dot{\theta}(t) \leq \nu, \frac{1}{e^{\alpha(\theta)}+1} < 1$, and $\frac{e^{\alpha(\theta)}}{e^{\alpha(\theta)}+1} < 1$ are used to modify the controller synthesis PLMI conditions with upper bound constant $\sigma^{(i-1,i)} = \frac{2\beta\nu}{L(i-1,i)} > 0$,

$$\begin{bmatrix} \langle AP_{i-1} + B_2 Z_{i-1} \rangle - \dot{P}_{i-1} + (\lambda_0 + \sigma^{(i-1,i)}) P_{i-1} & * & B_1 \\ CP_{i-1} + D_2 Z_{i-1} & -\gamma_{i-1} I & D_1 \\ * & * & -\gamma_{i-1} I \end{bmatrix} < 0, \quad (2.112)$$

$$\begin{bmatrix} \langle AP_{i} + B_{2}Z_{i} \rangle - \dot{P}_{i} + (\lambda_{0} + \sigma^{(i-1,i)})P_{i} & * & B_{1} \\ CP_{i} + D_{2}Z_{i} & -\gamma_{i}I & D_{1} \\ * & * & -\gamma_{i}I \end{bmatrix} < 0.$$
 (2.113)

If there exist feasible controller decision matrices P_{i-1} , Z_{i-1} and P_{i-1} , Z_{i-1} , and scalars γ_{i-1} , γ_i such that PLMI conditions (2.112) and (2.113) are valid on subregion $\Theta^{(i-1)} \times \Lambda$ and $\Theta^{(i)} \times \Lambda$, respectively, then the standard PLMI conditions as of Eqn. (2.105) will be also valid on these subregions, leading to the guaranteed \mathcal{H}_{∞} performance on each subregion. Furthermore, conditions (2.112) and (2.113) lead to conditions (2.109) and (2.110), and hence, result in (2.111) on the overlapped subregion $\Theta^{([i-1,i])}$, leading to guaranteed \mathcal{H}_{∞} performance $\gamma_{(i-1,i)}$ no worse than that of neighboring subregions.

Now designate controller decision matrices $P_{i+1}(\theta)$ and $Z_{i+1}(\theta)$ for subregion $\Theta^{(i+1)}$, and on the overlapped subregion of $\Theta^{(i)}\cap\Theta^{(i+1)}=\Theta^{([i,i+1])}$, define the interpolated parameter-dependent matrix $P_{(i,i+1)}(\theta)$ and $Z_{(i,i+1)}(\theta)$ as

$$P_{(i,i+1)}(\theta) = \varepsilon_{11}^{(i,i+1)}(\theta)P_{i+1}(\theta) + \varepsilon_{12}^{(i,i+1)}(\theta)P_{i}(\theta),$$

$$Z_{(i,i+1)}(\theta) = \varepsilon_{11}^{(i,i+1)}(\theta)Z_{i+1}(\theta) + \varepsilon_{12}^{(i,i+1)}(\theta)Z_{i}(\theta),$$
(2.114)

where similarly sigmoid function is chosen for interpolation as

$$\varepsilon_{11}^{(i,i+1)}(\theta) = \frac{e^{\alpha(\theta)}}{e^{\alpha(\theta)}+1}, \varepsilon_{12}^{(i,i+1)}(\theta) = \frac{1}{e^{\alpha(\theta)}+1}, \ \alpha(\theta) = \frac{\beta[2(\theta-\underline{\theta}^{i+1})-L^{(i,i+1)}]}{L^{(i,i+1)}},$$

where $L^{(i,i+1)}=\overline{\theta}^i-\underline{\theta}^{i+1}$. Then the PLMI conditions for controller synthesis on subregion $\Theta^{(i)}$ and $\Theta^{(i+1)}$ are formulated similarly with $\sigma^{(i,i+1)}=\frac{2\beta\nu}{L^{(i,i+1)}}>0$,

$$\begin{bmatrix} \langle AP_i + B_2 Z_i \rangle - \dot{P}_i + (\lambda_0 + \sigma^{(i,i+1)}) P_i & * & B_1 \\ CP_i + D_2 Z_i & -\gamma_i I & D_1 \\ * & * & -\gamma_i I \end{bmatrix} < 0, \tag{2.115}$$

$$\begin{bmatrix} \langle AP_{i+1} + B_2 Z_{i+1} \rangle - \dot{P}_{i+1} + (\lambda_0 + \sigma^{(i,i+1)}) P_{i+1} & * & B_1 \\ CP_{i+1} + D_2 Z_{i+1} & -\gamma_{i+1} I & D_1 \\ * & * & -\gamma_{i+1} I \end{bmatrix} < 0. \quad (2.116)$$

If there exist feasible controller decision variables P_{i+1} , Z_{i+1} and scalar γ_{i+1} such that PLMI condition (2.116) is valid on subregion $\Theta^{(i+1)}$, then the standard PLMI conditions as of Eqn. (2.105)

will be valid on subregion $\Theta^{(i+1)}$. In other words, controller gain $K_{i+1} = Z_{i+1}P_{i+1}^{-1}$ guarantees the \mathcal{H}_{∞} performance γ_{i+1} on subregion $\Theta^{(i+1)}$. At the same time, the interpolated controller variables $P_{(i,i+1)}, Z_{(i,i+1)}$ will satisfy the following PLMI condition obtained by $\varepsilon_{12}^{(i,i+1)} \cdot (2.115) + \varepsilon_{11}^{(i,i+1)} \cdot (2.116)$,

$$\begin{bmatrix}
\langle AP_{(i,i+1)} + B_2 Z_{(i,i+1)} \rangle - \dot{P}_{(i,i+1)} + \lambda_0 P_{(i,i+1)} & * & B_1 \\
CP_{(i,i+1)} + D_{12} Z_{(i,i+1)} & -\gamma_{(i,i+1)} I & D_{11} \\
* & * & -\gamma_{(i,i+1)} I
\end{bmatrix} < 0 \quad (2.117)$$

where $\gamma_{(i,i+1)} = \varepsilon_{11}^{(i,i+1)} \gamma_{i+1} + \varepsilon_{12}^{(i,i+1)} \gamma_i < \max\left\{\gamma_i, \gamma_{i+1}\right\}$. In other words, controller $K_{(i,i+1)} = Z_{(i,i+1)} P_{(i,i+1)}^{-1}$ also guarantees \mathcal{H}_{∞} performance $\max\{\gamma_i, \gamma_{i+1}\}$ over the overlapped subregion $\Theta^{([i,i+1])}$.

Note that $\sigma^{(i-1,i)}$ and $\sigma^{(i,i+1)}$ depend on the size of overlapped subregions, thus they may not be identical. In order to identify the common controller $K_i(\theta)$ on $\Theta^{(i)}$, the maximum value of two variables $\overline{\sigma}^{(i)} = \max{\{\sigma^{(i-1,i)}, \sigma^{(i,i+1)}\}}$ is used to replace the coefficients of introduced terms in Eqns. (2.113) and (2.115).

To ensure switching stability, the minimum dwell time for switching signal can be calculated as $\tau_a^* = \frac{\ln \mu^*}{\lambda_0}$, $\mu^* = \max \left\{ 1 + \frac{1}{e^\beta}, 1 + \frac{\overline{\lambda_i} - 1}{e^\beta + 1}, 1 + \frac{\overline{\lambda_i} - 1}{e^\beta + 1} \right\}$, such that (2.106) is satisfied on switching surfaces. $\overline{\lambda_i}$ and $\underline{\lambda_i}$ denote the maximum and minimum eigenvalues of matrix $P_i(\theta)$ at switching surfaces. If the interpolation variable β is chosen large enough, then μ^* is close to 1, and the minimum dwell time is close to 0. In other words, the average dwell time signal is almost arbitrary. At this point, we are ready to obtain the following theorem.

Theorem 8. With given λ_0 and given scheduling parameter subregions, if there exist parameter-dependent positive-definite matrices $P_i(\theta)$, parameter-dependent matrices $Z_i(\theta)$, and positive scalars γ_i , satisfying the PLMIs (2.118) for any $(\theta, \dot{\theta}) \in \Theta^{(i)} \times \Lambda$, then the switching controller gain $K_i(\theta) = Z_i(\theta)P_i^{-1}(\theta)$ guarantees the closed-loop system \mathcal{H}_{∞} performance γ_i , and the interpolated controllers with its adjacent controllers by Eqn. (2.114) also guarantee same performance for switching signals with average dwell time τ_a larger than τ_a^* which can be close to 0.

$$\begin{bmatrix} \langle AP_i + B_2 Z_i \rangle - \dot{P}_i + (\lambda_0 + \overline{\sigma}^{(i)}) P_i & * & B_1 \\ CP_i + D_2 Z_i & -\gamma_i I & D_1 \\ * & * & -\gamma_i I \end{bmatrix} < 0, \tag{2.118}$$

Remark 7. The constant $\overline{\sigma}^{(i)}$ in the PLMI condition illustrate the introduced relative stability of the closed-loop system, which is known in literature as σ -stability [60]. It is determined by the sizes of overlapped subregions $\min\left\{L^{(i,i+1)},L^{(i-1,i)}\right\}$ and interpolation rate β of sigmoid function. The introduced relative stability, together with interpolation of controller decision variables, provide independent synthesis conditions for each individual subregion, but with introduced design conservativeness.

2.3.2.2 Two-dimensional scheduling parameters

Suppose that entire scheduling parameter region is divided into $N_1 \cdot N_2$ subregions, and consider a subregion $\Theta^{(i,j)}$, $i \in N_1, j \in N_2$, as well as its adjacent subregions $\Theta^{(i+1,j)}$, $\Theta^{(i,j+1)}$, $\Theta^{(i+1,j+1)}$. As illustrated by shadows in Figure 2.2, the overlapped subregions are categorized into two types: single-overlapped subregion (slash shadow) and double-overlapped subregion(cross shadow). The double-overlapped subregion is firstly focused and associate PLMI conditions will be derived. Designate parameter-dependent controller variables for each subregion is $P_{(i,j)}, Z_{(i,j)}, P_{(i+1,j)}, Z_{(i+1,j)}, P_{(i,j+1)}, Z_{(i,j+1)}, P_{(i+1,j+1)}, Z_{(i+1,j+1)}$, then the controller decision variables on the double-overlapped subregion $\theta = (\theta_1, \theta_2) \in \Theta^{([i,i+1],[j,j+1])}$ are interpolated as

$$P = \varepsilon_{11}(\theta_{1}, \theta_{2})P_{(i,j)} + \varepsilon_{21}(\theta_{1}, \theta_{2})P_{(i+1,j)} + \varepsilon_{12}(\theta_{1}, \theta_{2})P_{(i,j+1)} + \varepsilon_{22}(\theta_{1}, \theta_{2})P_{(i+1,j+1)},$$

$$Z = \varepsilon_{11}(\theta_{1}, \theta_{2})Z_{(i,j)} + \varepsilon_{21}(\theta_{1}, \theta_{2})Z_{(i+1,j)} + \varepsilon_{12}(\theta_{1}, \theta_{2})Z_{(i,j+1)} + \varepsilon_{22}(\theta_{1}, \theta_{2})Z_{(i+1,j+1)},$$
(2.119)

$$\begin{split} \varepsilon_{11}(\theta_1,\theta_2) &= \left[\frac{e^{\alpha(\theta_1)}}{e^{\alpha(\theta_1)}+1}\right] \left[\frac{e^{\alpha(\theta_2)}}{e^{\alpha(\theta_2)}+1}\right], \varepsilon_{21}(\theta_1,\theta_2) = \left[\frac{1}{e^{\alpha(\theta_1)}+1}\right] \left[\frac{e^{\alpha(\theta_2)}}{e^{\alpha(\theta_2)}+1}\right], \\ \varepsilon_{12}(\theta_1,\theta_2) &= \left[\frac{e^{\alpha(\theta_1)}}{e^{\alpha(\theta_1)}+1}\right] \left[\frac{1}{e^{\alpha(\theta_2)}+1}\right], \varepsilon_{22}(\theta_1,\theta_2) = \left[\frac{1}{e^{\alpha(\theta_1)}+1}\right] \left[\frac{1}{e^{\alpha(\theta_2)}+1}\right]. \end{split}$$

$$\dot{P} = \varepsilon_{11} \left[\frac{2\beta_{1}\dot{\theta}_{1}}{(e^{\alpha(\theta_{1})} + 1)L_{1}^{(i,i+1)}} + \frac{2\beta_{2}\dot{\theta}_{2}}{(e^{\alpha(\theta_{2})} + 1)L_{2}^{(j,j+1)}} \right] P_{(i,j)} + \varepsilon_{11}\dot{P}_{(i,j)}
+ \varepsilon_{21} \left[\frac{-e^{\alpha(\theta_{1})} \cdot 2\beta_{1}\dot{\theta}_{1}}{(e^{\alpha(\theta_{1})} + 1)L_{1}^{(i,i+1)}} + \frac{2\beta_{2}\dot{\theta}_{2}}{(e^{\alpha(\theta_{2})} + 1)L_{2}^{(j,j+1)}} \right] P_{(i+1,j)} + \varepsilon_{21}\dot{P}_{(i+1,j)}
+ \varepsilon_{12} \left[\frac{2\beta_{1}\dot{\theta}_{1}}{(e^{\alpha(\theta_{1})} + 1)L_{1}^{(i,i+1)}} + \frac{-e^{\alpha(\theta_{2})} \cdot 2\beta_{2}\dot{\theta}_{2}}{(e^{\alpha(\theta_{2})} + 1)L_{2}^{(j,j+1)}} \right] P_{(i,j+1)} + \varepsilon_{12}\dot{P}_{(i,j+1)}
+ \varepsilon_{22} \left[\frac{-e^{\alpha(\theta_{1})} \cdot 2\beta_{1}\dot{\theta}_{1}}{(e^{\alpha(\theta_{1})} + 1)L_{1}^{(i,i+1)}} + \frac{-e^{\alpha(\theta_{2})} \cdot 2\beta_{2}\dot{\theta}_{2}}{(e^{\alpha(\theta_{2})} + 1)L_{2}^{(j,j+1)}} \right] P_{(i+1,j+1)} + \varepsilon_{22}\dot{P}_{(i+1,j+1)}$$

$$(2.120)$$

It's obvious that, $\varepsilon_{11} + \varepsilon_{12} + \varepsilon_{21} + \varepsilon_{22} = 1$. Moreover, $\alpha(\theta_m) = \frac{\beta_m[2(\theta_m - \underline{\theta}_m^{i+1}) - L_m^{(i,i+1)}]}{L_m^{(i,i+1)}}$, m = 1, 2, where $L_m^{(i,i+1)} = \overline{\theta}_m^i - \underline{\theta}_m^{i+1}$ denotes the size of overlapped subregion in θ_m direction, β_m determines the interpolation rate in θ_m direction.

With the expression of time derivative of interpolated parametric matrix in Eqn. (2.120), the coefficients of these additional terms are bounded as

$$\frac{2\beta_1\dot{\theta}_1}{(e^{\alpha(\theta_1)}+1)L_1^{(i,i+1)}} + \frac{2\beta_2\dot{\theta}_2}{(e^{\alpha(\theta_2)}+1)L_2^{(j,j+1)}} < \frac{2\beta_1\nu_1}{L_1^{(i,i+1)}} + \frac{2\beta_2\nu_2}{L_2^{(j,j+1)}} = \sigma_1^{(i,i+1)} + \sigma_2^{(j,j+1)}.$$

The other three coefficients are also bounded by $\sigma_1^{(i,i+1)} + \sigma_2^{(j,j+1)} = \sigma^{([i,i+1],[j,j+1])}$, abbreviated as $\overline{\sigma}$ in following formula.

$$\begin{bmatrix}
\left\langle AP_{(i,j)} + B_2 Z_{(i,j)} \right\rangle - \dot{P}_{(i,j)} + (\lambda_0 + \overline{\sigma}) P_{(i,j)} & * & B_1 \\
CP_{(i,j)} + D_2 Z_{(i,j)} & -\gamma_{(i,j)} I & D_1 \\
* & * & -\gamma_{(i,j)} I
\end{bmatrix} < 0 \quad (2.121)$$

$$\begin{bmatrix}
\langle AP_{(i+1,j)} + B_2 Z_{(i+1,j)} \rangle - \dot{P}_{(i+1,j)} + (\lambda_0 + \overline{\sigma}) P_{(i+1,j)} & * & B_1 \\
CP_{(i+1,j)} + D_2 Z_{(i+1,j)} & -\gamma_{(i+1,j)} I & D_1 \\
* & * & -\gamma_{(i+1,j)} I
\end{bmatrix} < 0$$
(2.122)

$$\begin{bmatrix}
\left\langle AP_{(i,j+1)} + B_2Z_{(i,j+1)} \right\rangle - \dot{P}_{(i,j+1)} + (\lambda_0 + \overline{\sigma})P_{(i,j+1)} & * & B_1 \\
CP_{(i,j+1)} + D_2Z_{(i,j+1)} & -\gamma_{(i,j+1)}I & D_1 \\
* & * & -\gamma_{(i,j+1)}I
\end{bmatrix} < 0$$
(2.123)

$$\begin{bmatrix}
\left\langle AP_{(i+1,j+1)} + B_2Z_{(i+1,j+1)}\right\rangle - \dot{P}_{(i+1,j+1)} + (\lambda_0 + \overline{\sigma})P_{(i+1,j+1)} & * & B_1 \\
CP_{(i+1,j+1)} + D_2Z_{(i+1,j+1)} & -\gamma_{(i+1,j+1)}I & D_1 \\
* & * & -\gamma_{(i+1,j+1)}I
\end{bmatrix} < 0$$
(2.124)

$$\begin{bmatrix} \langle AP + B_2 Z \rangle - \dot{P} + \lambda_0 P & * & B_1 \\ CP + D_2 Z & -\gamma I & D_1 \\ * & * & -\gamma I \end{bmatrix} < 0$$

$$(2.125)$$

If the PLMI conditions on the subregions $\Theta^{(i,j)}$, $\Theta^{(i+1,j)}$, $\Theta^{(i,j+1)}$, $\Theta^{(i+1,j+1)}$ are proposed in Eqns. (2.121), (2.122), (2.123) and (2.124), then \mathcal{H}_{∞} performance on each individual subregion is guaranteed with associated γ -level. Meanwhile, $\varepsilon_{11} \cdot (2.121) + \varepsilon_{21} \cdot (2.122) + \varepsilon_{12} \cdot (2.123) + \varepsilon_{22} \cdot (2.124)$ yields PLMI (2.125), where

$$\gamma = \varepsilon_{11} \cdot \gamma_{(i,j)} + \varepsilon_{21} \cdot \gamma_{(i+1,j)} + \varepsilon_{12} \cdot \gamma_{(i,j+1)} + \varepsilon_{22} \cdot \gamma_{(i+1,j+1)}
< \max\{\gamma_{(i,j)}, \gamma_{(i+1,j)}, \gamma_{(i,j+1)}, \gamma_{(i+1,j+1)}\},$$
(2.126)

which indicates that \mathcal{H}_{∞} performance on double-overlapped subregion is guaranteed with four adjacent subregions for two-dimensional scheduling parameter cases.

For these single-overlapped subregion, denoted by slash shadows in Figure 2.2, the \mathcal{H}_{∞} performance can also be achieved if Eqns. (2.121), (2.122), (2.123) and (2.124) are satisfied, which can be easily validated by eliminating either θ_1 or θ_2 in Eqn. (2.119) and convert it into Eqn. (2.107) used in one-dimensional scheduling parameter case .

When designing $K_{(i,j)}$ in sequential order, all its four overlapped subregion with adjacent subregions should be considered, in other words, σ -relative stability needs to be satisfied under the

most conservative condition. Hence, we have the largest σ -relative stability index

$$\overline{\sigma}^{(i,j)} = \max{\{\sigma_1^{(i-1,i)}, \sigma_1^{(i,i+1)}\}} + \max{\{\sigma_2^{(j-1,j)}, \sigma_2^{(j,j+1)}\}}.$$

The switching stability condition between any adjacent subregions can be calculated according to the average-dwell-time switching conditions [52, 10, 53]. To ensure switching stability, the minimum average dwell time can be calculated as $\tau_a^* = \frac{\ln \mu^*}{\lambda_0}$,

$$\mu^* = \max \left\{ 1 + \frac{\left[\left(\frac{\lambda(i+1,j) + \lambda(i,j+1)}{\overline{\lambda}(i,j)} \right) e^{\beta} + \frac{\lambda(i+1,j+1)}{\overline{\lambda}(i,j)} - 1 \right]}{(e^{\beta} + 1)^2}, 1 + \frac{2e^{\beta} + 1}{e^{2\beta}} \right\}$$

 $\overline{\lambda}_{(i,j)}$ and $\underline{\lambda}_{(i,j)}$ denote the maximum and minimum eigenvalues of matrix $P_{(i,j)}(\theta)$ over switching surfaces. If the interpolation coefficient β is chosen large enough, $\mu^* \approx 1$ and the minimum dwell time τ_a^* is very close to 0, which indicates that switching signal can be almost arbitrary.

By this point, it's obvious to conclude the following theorem of designing switching state-feedback LPV controller for two-dimensional scheduling parameter system. The proof can be easily proved by the derivation procedure.

Theorem 9. With given λ_0 and given scheduling parameter subregions, if there exist parameter-dependent positive-definite matrices $P_{(i,j)}(\theta)$, parameter-dependent matrices $Z_{(i,j)}(\theta)$, and positive scalars $\gamma_{(i,j)}$, satisfying the PLMIs (2.127) for any $(\theta,\dot{\theta})\in\Theta^{(i,j)}\times\Lambda$, then the switching controller gain $K_{(i,j)}(\theta)=Z_{(i,j)}(\theta)P_{(i,j)}^{-1}(\theta)$ guarantees the closed-loop system \mathcal{H}_{∞} performance $\gamma_{(i,j)}$, and the interpolated controllers with its adjacent controllers by Eqn. (2.119) also guarantees same performance on the overlapped subregions with its adjacent subregions for switching signals with average dwell time τ_a larger than τ_a^* which is close to 0.

$$\begin{bmatrix} \left\langle AP_{(i,j)} + B_2Z_{(i,j)} \right\rangle - \dot{P}_{(i,j)} + (\lambda_0 + \overline{\sigma}^{(i,j)})P_{(i,j)} & * & B_1 \\ CP_{(i,j)} + D_2Z_{(i,j)} & -\gamma_{(i,j)}I & D_1 \\ * & * & -\gamma_{(i,j)}I \end{bmatrix} < 0 \quad (2.127)$$

2.3.2.3 Scheduling parameter of any dimensions

Consider the general scenario that $\theta(t) = \left[\theta_1(t), \theta_2(t), \dots, \theta_q(t)\right]^T$ with M numbers of divided scheduling parameters $[\theta_1, \theta_2, \dots, \theta_m, \dots, \theta_M]$. The overlapped subregion formed by 2^M neighboring subregions is denoted as $\Theta^{([n_1, n_1+1], \dots, [n_M, n_M+1])}$, and the associated Lyapunov matrix $P(\theta)$ and controller variable $Z(\theta)$ are defined as (2.128) by the convex combination of Lyapunov matrices on neighboring overlapping subregions. Note that subregion numbering is abbreviated, for example $P_{(n_1+i_1-1,n_2+i_2-1,\dots,n_M+i_M-1)}$ is abbreviated by $P_{(i_1,i_2,\dots,i_M)}$.

$$P = \sum_{i_{1}=1}^{2} \sum_{i_{2}=1}^{2} \cdots \sum_{i_{M}=1}^{2} \left\{ \varepsilon_{1i_{1}}(\theta_{1}) \varepsilon_{2i_{2}}(\theta_{2}) \dots \varepsilon_{Mi_{M}}(\theta_{M}) P_{(i_{1},i_{2},\dots,i_{M})}(\theta_{1},\theta_{2},\dots,\theta_{q}) \right\}$$

$$= \sum_{i_{1}=1}^{2} \sum_{i_{2}=1}^{2} \cdots \sum_{i_{M}=1}^{2} \left\{ \prod_{m=1}^{M} \varepsilon_{mi_{m}}(\theta_{m}) P_{(i_{1},i_{2},\dots,i_{M})}(\theta_{1},\theta_{2},\dots,\theta_{q}) \right\}$$
(2.128)

where $\varepsilon_{m1}(\theta_m) = \frac{e^{\alpha(\theta_m)}}{e^{\alpha(\theta_m)}+1}, \varepsilon_{m2}(\theta_m) = \frac{1}{e^{\alpha(\theta_m)}+1}, m = 1, 2, \cdots, M.$

Moreover,
$$\alpha(\theta_m) = \frac{\beta_m[2(\theta_m - \underline{\theta}_m^{n_m+1}) - L_m^{(n_m,n_m+1)}]}{L_m^{(n_m,n_m+1)}}$$
, where $L_m^{(n_m,n_m+1)} = \overline{\theta}_m^{n_m} - L_m^{(n_m,n_m+1)}$

 $\underline{\theta}_m^{n_m+1}$ denotes the size of overlapped subregion in θ_m direction, and β_m determines the interpolation rate in θ_m direction. Obviously, we have the equation that summation of all coefficients equals to 1,

$$\sum_{i_1=1}^{2} \sum_{i_2=1}^{2} \cdots \sum_{i_M=1}^{2} \left\{ \varepsilon_{1i_1}(\theta_1) \varepsilon_{2i_2}(\theta_2) \cdots \varepsilon_{Mi_M}(\theta_M) \right\} = 1.$$
 (2.129)

Thus we have the bounds for the derivative of interpolation coefficient as

$$\dot{\varepsilon}_{mim}(\theta_m) = \varepsilon_{mim} (1 - \varepsilon_{mim}) \frac{(-1)^{im+1} 2\beta_m \dot{\theta}_m}{L_m^{(n_m, n_m + 1)}} < \varepsilon_{mim} \frac{2\beta_m \nu_m}{L_m^{(n_m, n_m + 1)}}.$$
 (2.130)

The time derivative of Lyapunov matrix $P(\theta_1, \theta_2, \dots, \theta_q)$ can be derived as,

$$\dot{P} = \sum_{i_{1}=1}^{2} \sum_{i_{2}=1}^{2} \cdots \sum_{i_{M}=1}^{2} \left\{ \varepsilon_{1i_{1}} \varepsilon_{2i_{2}} \dots \varepsilon_{Mi_{M}} \dot{P}_{(i_{1},i_{2},\dots,i_{M})} + \dot{\varepsilon}_{1i_{1}} \varepsilon_{2i_{2}} \dots \varepsilon_{Mi_{M}} P_{(i_{1},i_{2},\dots,i_{M})} \right. \\
+ \varepsilon_{1i_{1}} \dot{\varepsilon}_{2i_{2}} \dots \varepsilon_{Mi_{M}} P_{(i_{1},i_{2},\dots,i_{M})} + \dots + \varepsilon_{1i_{1}} \varepsilon_{2i_{2}} \dots \dot{\varepsilon}_{Mi_{M}} P_{(i_{1},i_{2},\dots,i_{M})} \right\} \\
< \sum_{i_{1}=1}^{2} \sum_{i_{2}=1}^{2} \cdots \sum_{i_{M}=1}^{2} \left\{ \prod_{m=1}^{M} \varepsilon_{mi_{m}} (\theta_{m}) \dot{P}_{(i_{1},i_{2},\dots,i_{M})} \right. \\
+ \prod_{m=1}^{M} \varepsilon_{mi_{m}} (\theta_{m}) \underbrace{\left[\frac{2\beta_{1}\nu_{1}}{L_{1}^{(n_{1},n_{1}+1)}} + \dots + \frac{2\beta_{M}\nu_{M}}{L_{M}^{(n_{M},n_{M}+1)}} \right]}_{E_{i_{1},i_{2},\dots,i_{M}}} P_{(i_{1},i_{2},\dots,i_{M})} \right\} \\
= \sum_{m=1}^{M} \left(\frac{2\beta_{m}\nu_{m}}{L_{m}^{(n_{m},n_{m}+1)}} \right) = \sum_{m=1}^{M} \sigma_{m}^{(n_{m},n_{m}+1)} \\
= \sum_{i_{1}=1}^{2} \sum_{i_{2}=1}^{2} \dots \sum_{i_{M}=1}^{2} \left\{ \prod_{m=1}^{M} \varepsilon_{mi_{m}} \left[\dot{P}_{(i_{1},i_{2},\dots,i_{M})} + \sum_{m=1}^{M} \sigma_{m}^{(n_{m},n_{m}+1)} P_{(i_{1},i_{2},\dots,i_{M})} \right] \right\}$$
(2.131)

For the subregion $\Theta^{(n_1+i_1-1,\cdots,n_M+i_M-1)}\times\Lambda$, PLMI for \mathcal{H}_{∞} performance is formulated as

$$\begin{bmatrix} e_{(i_{1},\cdots,i_{M})} & * & B_{1} \\ CP_{(i_{1},\cdots,i_{M})} + D_{2}Z_{(i_{1},\cdots,i_{M})} & -\gamma_{(i_{1},\cdots,i_{M})}I & D_{1} \\ * & * & -\gamma_{(i_{1},\cdots,i_{M})}I \end{bmatrix} < 0$$
 (2.132)

where $e_{(i_1,\cdots,i_M)}$

$$= \left\langle AP_{(i_1,\dots,i_M)} + B_2 Z_{(i_1,\dots,i_M)} \right\rangle - \dot{P}_{(i_1,\dots,i_M)} + (\lambda_0 + \sum_{m=1}^M \sigma_m^{(n_m,n_m+1)}) P_{(i_1,\dots,i_M)},$$

such that the convex combination of PLMI conditions (2.132) on all 2^M overlapping subregions

$$\sum_{i_1=1}^{2} \sum_{i_2=1}^{2} \cdots \sum_{i_M=1}^{2} \left\{ \prod_{m=1}^{M} \varepsilon_{mi_m} \cdot (2.132) \right\}$$

yields the PLMI condition on M -overlapped subregion $\Theta^{([n_1,n_1+1],\cdots,[n_M,n_M+1])}$

$$\begin{bmatrix} \langle AP + B_2 Z \rangle - \dot{P} + \lambda_0 P & * & B_1 \\ CP + D_2 Z & -\gamma I & D_1 \\ * & * & -\gamma I \end{bmatrix} < 0$$
(2.133)

which indicates that the \mathcal{H}_{∞} performance $\gamma = \sum\limits_{i_1=1}^2\sum\limits_{i_2=1}^2\cdots\sum\limits_{i_M=1}^2\left\{\prod\limits_{m=1}^M\varepsilon_{mi_m}\gamma_{(i_1,i_2,\cdots,i_M)}\right\}$ is achieved by interpolating controller variables, and it's obvious that $\gamma < \max\left\{\gamma_{(i_1,i_2,\cdots,i_M)}\right\}$ for any $i_1,i_2,\cdots i_M=1,2$.

The \mathcal{H}_{∞} performance on the rest less than M-overlapped subregion can also be achieved, if Eqn. (2.132) is satisfied on each individual subregion, which can be easily validated by eliminating terms related to the un-overlapped scheduling parameter. When designing $K_{(n_1,\cdots,n_M)}$ on $\Theta^{(n_1,\cdots,n_M)}$ in a sequential order, all overlapped subregions produced by this subregion with its adjacent subregions should be considered, in other words, σ -relative stability index needs to be replaced by

$$\overline{\sigma}^{(n_1, \dots, n_m)} = \sum_{m=1}^{M} \max \{ \sigma_m^{(n_m - 1, n_m)}, \sigma_m^{(n_m, n_m + 1)} \}.$$

To ensure switching stability, the minimum average dwell time can be calculated by the eigenvalues of $P(\theta)$ over switching surfaces. If the interpolation coefficient β is chosen large enough, the minimum dwell time is very close to 0, which indicates that switching signal can be almost arbitrary.

By this point, it's obvious to provide the following theorem of designing switching state-feedback LPV controller for two-dimensional scheduling parameter system. The proof is provided by the above derivation procedures.

Theorem 10. With given λ_0 and given scheduling parameter subregions, if there exist parameter-dependent positive-definite matrices $P(\theta)$, parameter-dependent matrices $Z(\theta)$, and positive scalars $\gamma_{(n_1,\cdots,n_M)}$, satisfying the PLMIs (2.134) for any $(\theta,\dot{\theta})\in\Theta^{(n_1,\cdots,n_M)}\times\Lambda$, then the switching controller gain $K_{(n_1,\cdots,n_M)}(\theta)=Z(\theta)P^{-1}(\theta)$ guarantees the closed-loop system \mathcal{H}_{∞} performance $\gamma_{(n_1,\cdots,n_M)}$, and the interpolated controllers with its adjacent controllers by E-qn. (2.119) also guarantee same performance on the overlapped subregions with its adjacent

subregions for switching signals with average dwell time τ_a larger than τ_a^* which is close to 0..

$$\begin{bmatrix} \langle AP + B_2 Z \rangle - \dot{P} + \overline{\sigma}^{(n_1, \dots, n_m)} P & * & B_1 \\ CP + D_2 Z & -\gamma_{(n_1, \dots, n_M)} I & D_1 \\ * & * & -\gamma_{(n_1, \dots, n_M)} I \end{bmatrix} < 0 \qquad (2.134)$$

2.4 PLMI Relaxation Method

2.4.1 Modeling scheduling parameters

The scheduling parameter vector considered in the open-loop system (2.1) is defined in an affine manifold, so we first need to map that into a multi-simplex manifold for subsequent convex analysis. Following the aprocedure presented in Lacerda et al.[82] and Oliveira et al.[70], the original parameter domain can be converted into a convex multi-simplex domain. Note that a multi-simplex domain is defined as the Cartesian product of multiple unit-simplexes. Thus, the scheduling parameter $\theta_i(t)$ can be converted into the unit-simplex variable $\alpha_i(t)$ using the following formula,

$$\alpha_{i,1} = \frac{\theta_i(t) - \underline{\theta}_i}{\overline{\theta}_i - \underline{\theta}_i}, \quad \alpha_{i,2} = 1 - \alpha_{i,1} = \frac{\overline{\theta}_i - \theta_i(t)}{\overline{\theta}_i - \underline{\theta}_i}, \quad i = 1, 2, \dots, q.$$
 (2.135)

As a result, we have $\alpha_i = (\alpha_{i,1}, \alpha_{i,2}) \in \Lambda_{i,2}$, where the two dimensional unit-simplex $\Lambda_{i,2}$ for α_i is defined as

$$\Lambda_{i,2} := \{ \alpha_i \in \mathbb{R}^2 : \sum_{k=1}^2 \alpha_{i,k} = 1, \alpha_{i,k} \ge 0 \}.$$

Hence, the unit-simplex variable $\alpha_i \in \Lambda_{i,2}$ is created. Similarly, the time derivative of the scheduling parameter can also be converted into a unit-simplex variable by utilizing the following condition,

$$\dot{\alpha}_{i,1}(t) + \dot{\alpha}_{i,2}(t) = 0. {(2.136)}$$

Hence, the rates of convex parameters are bounded as follows,

$$\frac{-\nu_{\theta_i}}{\bar{\theta_i} - \underline{\theta}_i} \le \dot{\alpha}_{i,k} \le \frac{\nu_{\theta_i}}{\bar{\theta_i} - \underline{\theta}_i}, \quad i = 1, 2, \dots, q; \ k = 1, 2. \tag{2.137}$$

Note that the time derivative of parameter α_i lies in the space modeled by the convex combination of the columns of the matrix $H_i \in \mathbb{R}^{2 \times 2}$ given by

$$H_{i} = \begin{bmatrix} -\frac{\nu_{\theta_{i}}}{\overline{\theta_{i}} - \underline{\theta_{i}}}, & \frac{\nu_{\theta_{i}}}{\overline{\theta_{i}} - \underline{\theta_{i}}} \\ \frac{\nu_{\theta_{i}}}{\overline{\theta_{i}} - \underline{\theta_{i}}}, & -\frac{\nu_{\theta_{i}}}{\overline{\theta_{i}} - \underline{\theta_{i}}} \end{bmatrix}, i = 1, 2, \dots, q,$$

$$(2.138)$$

and $\dot{\alpha}_i$ can be established using a unit-simplex of dimension 2 as

$$\Omega_{i,2} := \{ \phi_i \in \mathbf{R}^2 : \phi_i = \sum_{k=1}^2 \eta_{i,k} H_i^k, \eta_i \in \Lambda_{i,2} \}, \quad i = 1, 2, \dots, q,$$
(2.139)

where $\eta_i=(\eta_{i,1},\eta_{i,2})$ and H_i^k denotes the k^{th} column of matrix H_i . Therefore, the unit-simplex variable $\dot{\alpha}_i\in\Omega_{i,2}$ is created. Furthermore, the scheduling parameters $(\theta,\dot{\theta})$ with given bounds can then be converted into multi-simplex domain from Cartesian product of multiple unit-simplexes as follows,

$$(\alpha, \dot{\alpha}) \in \Lambda \times \Omega := \prod_{i=1}^{q} \Lambda_{i,2} \times \prod_{i=1}^{q} \Omega_{i,2}.$$

By utilizing the scheduling parameter transformation presented above, the LPV system $\Sigma(\theta)$ described in (2.1), which is an affine function of parameter θ , can now be transformed into an LPV system representation $\Sigma(\alpha)$ that is a function of α in multi-simplex domain. For simplicity, we assume that $\Sigma(\alpha)$ takes the same form as $\Sigma(\theta)$ in that all the system matrices are now functions of α . Subsequently, the LPV controller design, to be presented in the next section, will be based on the convex scheduling parameter α . However, in actual control implementation, the designed LPV controller in multi-simplex α domain will need to be mapped back to the controller in the affine θ domain [70].

2.4.2 PLMIs relaxation

The PLMIs formulated in Theorem 5, 7, 8, 9, and 10 renders an optimization problem of infinite dimensions and un-defined decision variable structures. To numerically tackle this optimization problem, affine decision variable structure is assumed, for example, $\hat{A}_K^j(\theta)$ is expressed as $\hat{A}_K^j(\theta) = \hat{A}_{K0}^j + \sum_{i=1}^q \hat{A}_{Ki}^j \theta_i$. Coefficient check in multi-simplex domain [19, 70, 71] has been adopted to

successfully obtain a finite set of LMIs but with introduced conservativeness. Other options [72, 73] can also be applied, for instance, sum-of-square relaxation [74] and enforcing multi-convexity method [75].

Therefore, controller decision variables can be iteratively searched to optimize the cost function. The operation of PLMIs and optimization problem are solved by using the parser YALMIP [76] jointly with optimization algorithm SeDuMi [77].

CHAPTER 3

APPLICATION EXAMPLES

3.1 Active Magnetic Bearing (AMB) Model

An active magnetic bearing (AMB) system borrowed from Lu and Wu [1, 83, 84, 85] is revisited to demonstrate the effectiveness of the proposed smooth-switching LPV control design. In [1], states and control inputs experience sharp jump over switching surfaces, and these sharp jumps will be effectively smoothened by applying the proposed method.

The AMB system is formulated into an LPV model with rotor speed as the scheduling parameter θ . In the automatic balancing design, the measured rotor displacements are assumed to be exposed to sensor noises, and the gain-scheduling controller is desired to suppress the displacements of rotor centerlines. While \mathcal{H}_{∞} channels are kept the same as these in [1] for attaining guaranteed robust stability, the outputs of \mathcal{H}_2 channels are chosen to be $[x_1,x_2]^T=[l\theta,l\psi]^T$, the displacements of rotor centerline. In this way, the smooth-switching mixed ICC/ \mathcal{H}_{∞} LPV controller will be designed to suppress rotor displacements subject to measurement noise, with constrained control inputs and bounded modeling uncertainty. The main benefits of the proposed method over [1] are three-fold. First, ϵ -balanced optimal \mathcal{H}_2 performance is achieved with smooth responses over switching surfaces. Second, the control input constraint is enforced during the control design. Last, the trade-off among system \mathcal{H}_2 performance, ICC condition, and switching smoothness is established and provides insights as to how to tune the controllers to attain a balanced system performance.

The weighting functions used in this study are the same as those in [1, 86]. That is, $W_z=\frac{10(s+8)}{s+0.001}I_2$, $W_u=\frac{0.01(s+100)}{s+100000}I_2$, and $W_n=0.001I_2$. The rotor speed is assumed to vary within the range $\theta\in[315,1100]$ rad/s and variational rate $\dot{\theta}\in[-100,100]$ rad/s^2 . The scheduling parameter is divided into two overlapping subregions; namely, $\theta\in[315,720]$ and $\theta\in[700,1100]$, and its trajectory is defined in Figure 3.1. Switching events happen when $\theta=720$ rad/s (at

 $t_1 = 2.9s$) and $\theta = 700 \ rad/s$ (at $t_2 = 6.5s$). Same as [1], the two dimensional measurement noises are chosen as step inputs with the same magnitude of 0.001m but with the opposite sign.

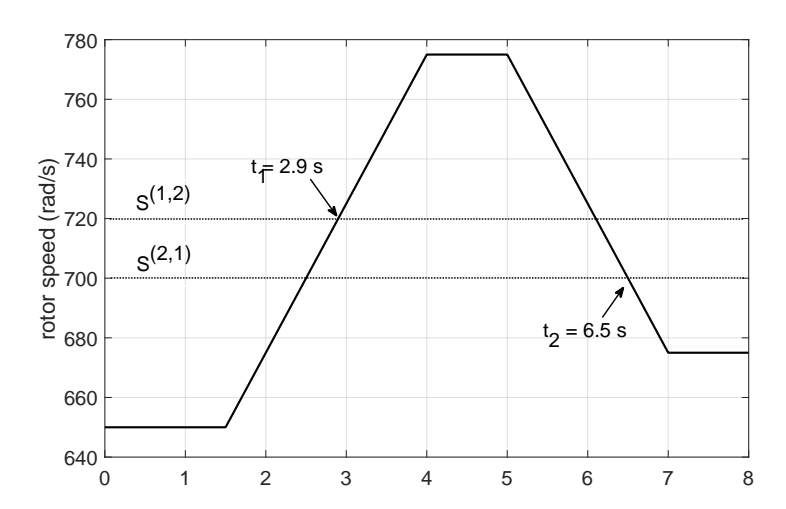


Figure 3.1: Trajectory of scheduling parameter, rotor speed

3.1.1 Trade-off between trace(W) and ICC conditions

To study the influence of ICC conditions when optimizing the \mathcal{H}_2 performance, different upper bounds of control inputs are considered in PLMIs. When the cost function (2.81) without smoothness index is minimized to obtain the optimal \mathcal{H}_2 performance, the trade-off relationship of ICC conditions \overline{U} and \mathcal{H}_2 performance upper bound trace(W) can be found in Figure 3.2. It can be observed that increasing ICC bound \overline{U} leads to decreasing trace(W), indicating that larger control authority will result in improved system performance. Moreover, when \overline{U} is greater than 10^8 , further reducing trace(W) requires much larger control authority. Hence, $\overline{U}=10^8$ is selected as the *optimal* trade-off point, considering both control effort and achievable performance.

The displacement and control input responses under different \overline{U} and fixed $\gamma=36$ are investigated. As shown in Figures 3.3 and 3.4, with larger control authority, the displacements are suppressed to a much smaller level. In the case of infinite ICC condition, the gray solid curve provides the best performance, and $\overline{U}=10^8$ produces slightly better responses than the duplicated results following the procedure in [1]. Furthermore, the responses experience smaller jumps, because of the lack of

feed-forward term D_K in the mixed ICC/ \mathcal{H}_{∞} control. In Figures 3.5-3.7, larger control constraint leads to larger control effort in order to achieve better performance. Infinitely large \overline{U} will produce control input magnitude larger than 6000 N, in order to achieve the best \mathcal{H}_2 performance as shown in Figures 3.3 and 3.4. From the time-domain simulation results, considering both control effort \overline{U} and achievable system \mathcal{H}_2 performance, the selection of *optimal* trade-off ICC constraint $\overline{U}=10^8$ can be cross-validated with Figure 3.2.

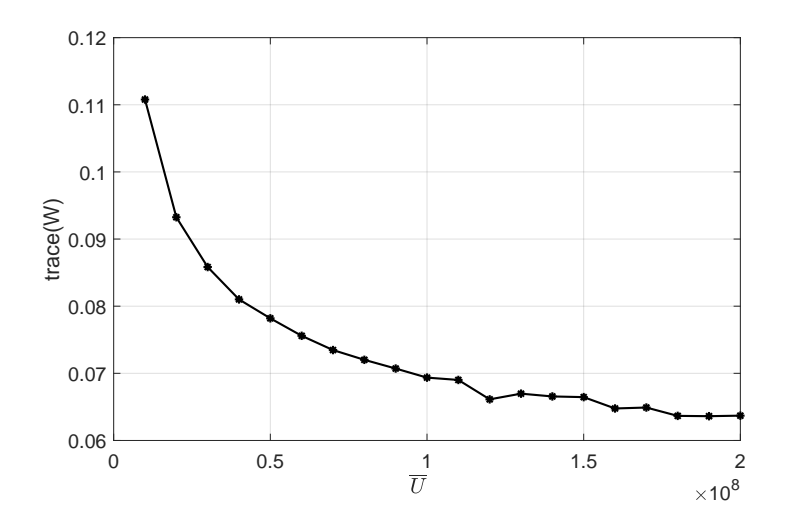


Figure 3.2: Trade-off relationship between \overline{U} and trace(W)

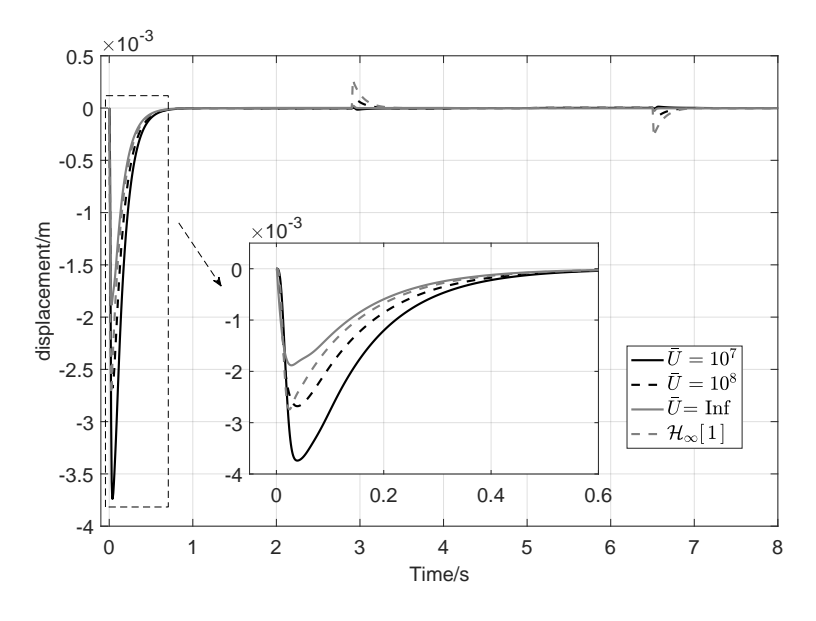


Figure 3.3: x_1 response under different ICC conditions

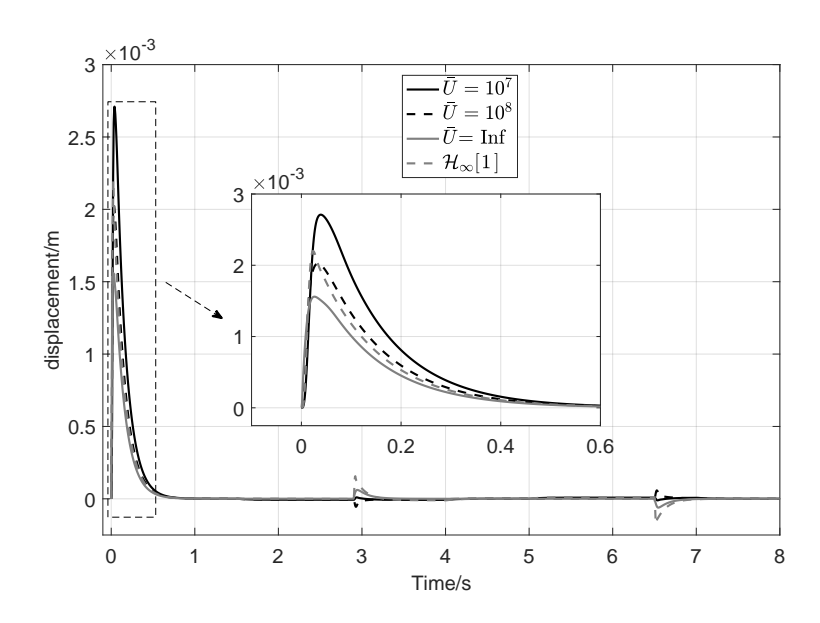


Figure 3.4: x_2 response under different ICC conditions

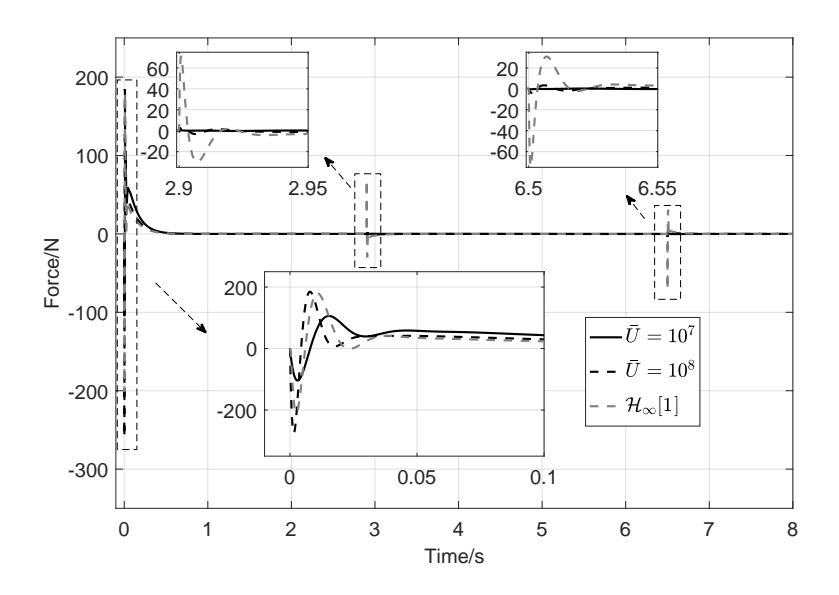


Figure 3.5: u_1 response under different ICC conditions

3.1.2 Smooth switching LPV control by simultaneous design

3.1.2.1 Trade-off between trace(W) and switching smoothness

In this subsection, the smoothness index is considered in the cost function in order to attain an optimal trade-off relationship between system performance and switching smoothness. With the fixed robustness level $\gamma=36$, weighting factor ϵ is tuned to balance the system performance and

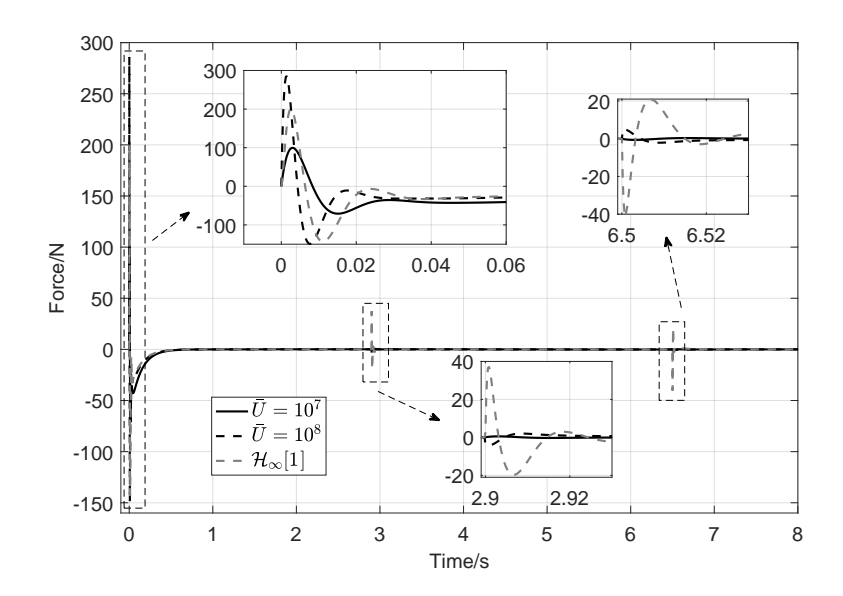


Figure 3.6: u_2 response under different ICC conditions

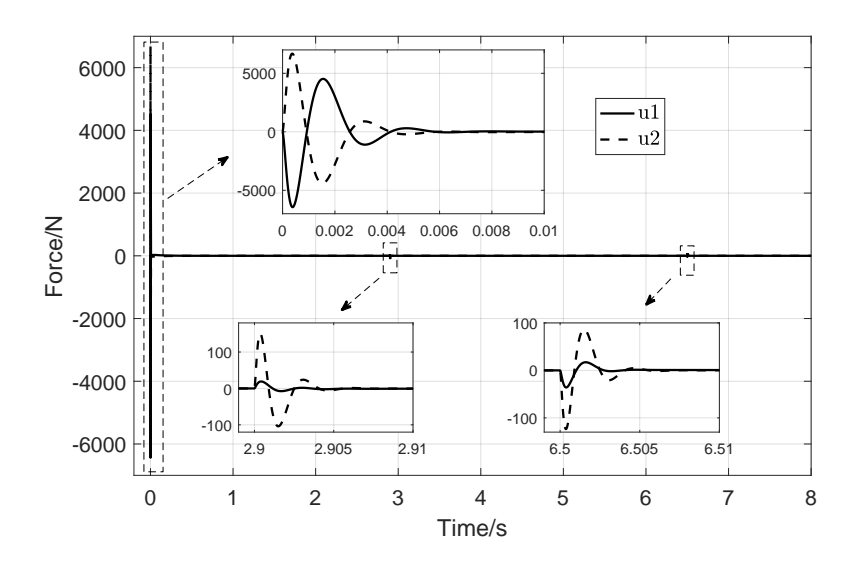


Figure 3.7: Control inputs under infinite ICC conditions

switching smoothness on $S^{(1,2)}$ and $S^{(2,1)}$. Two different ICC conditions $\overline{U}_1=10^7$ and $\overline{U}_2=10^8$ are considered in this study. From Figures 3.8 and 3.9, one can see that increased weighting factor ϵ leads to decreased trace(W) or improved output performance. Note that increased I_{sm} leads to decreased controller switching performance. These results clearly show the trade-off relationship between performance and switching smoothness. One choice of *optimal* trade-off point is that magnitude trace(W) is small, and the smoothness index is not yet increased significantly, such

that system performance is close to the best achievable level while the switching smoothness is acceptable. The chosen weighting factor for two cases are: $(\epsilon_1, \epsilon_2) = (10, 1)$.

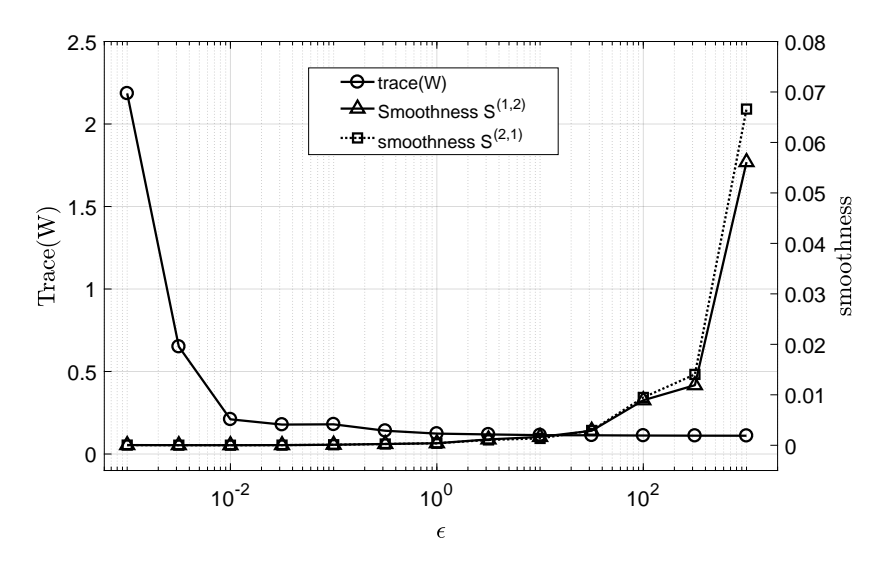


Figure 3.8: Trade-off relationship between switching smoothness and trace(W) under \overline{U}_1 =10 7

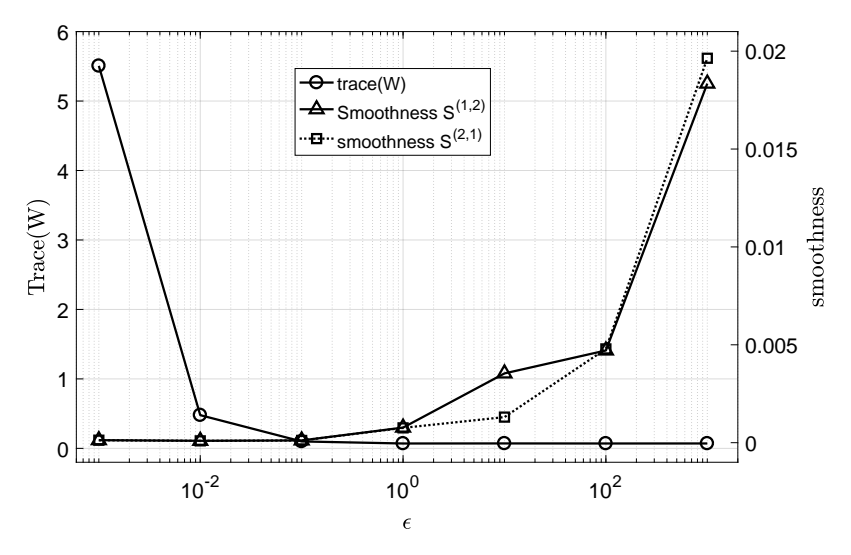


Figure 3.9: Trade-off relationship between switching smoothness and trace(W) under \overline{U}_2 =10 8

3.1.2.2 Simulation results and discussions

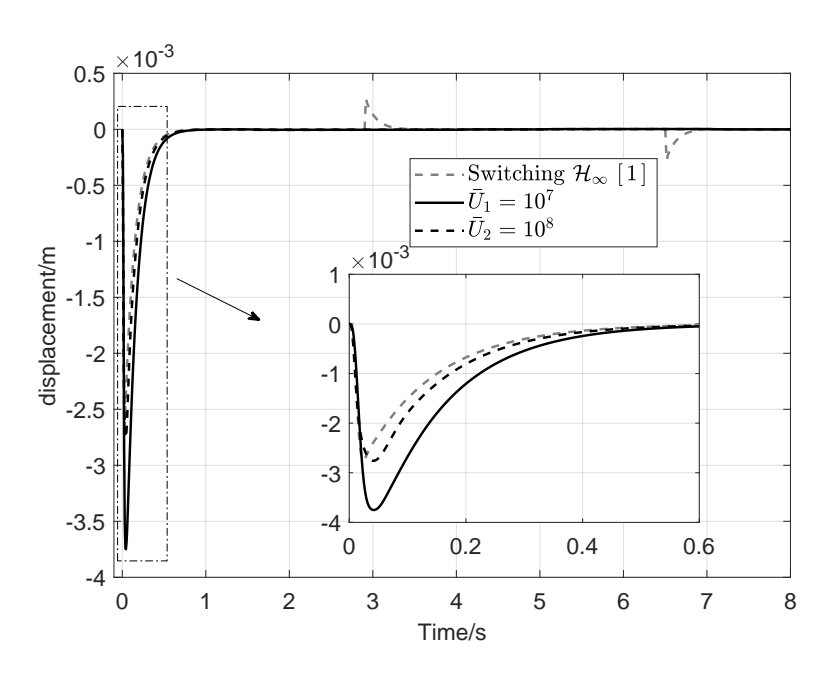


Figure 3.10: State x_1 response by [1] and proposed method

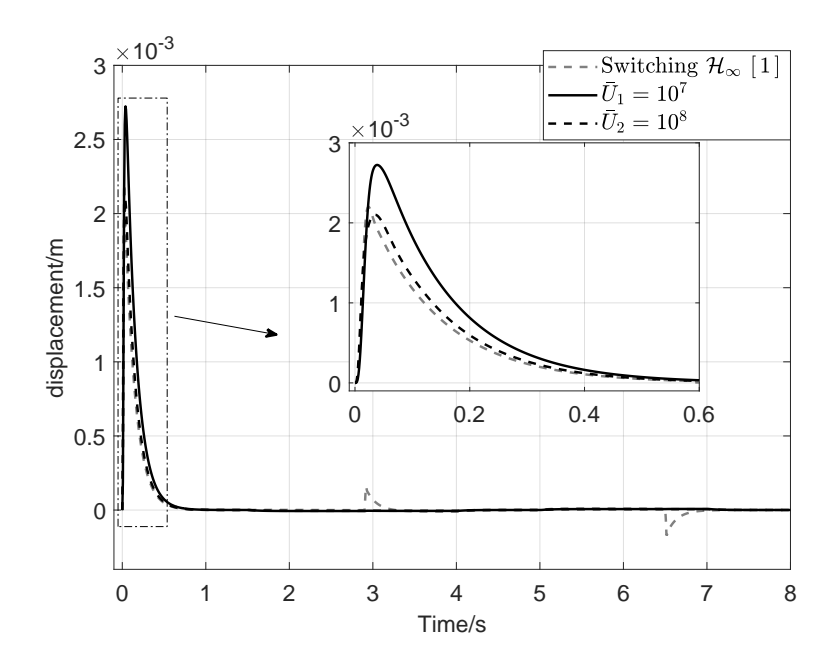


Figure 3.11: State x_2 response by [1] and proposed method

After an optimal trade-off point is chosen, the time-domain simulations under different ICC

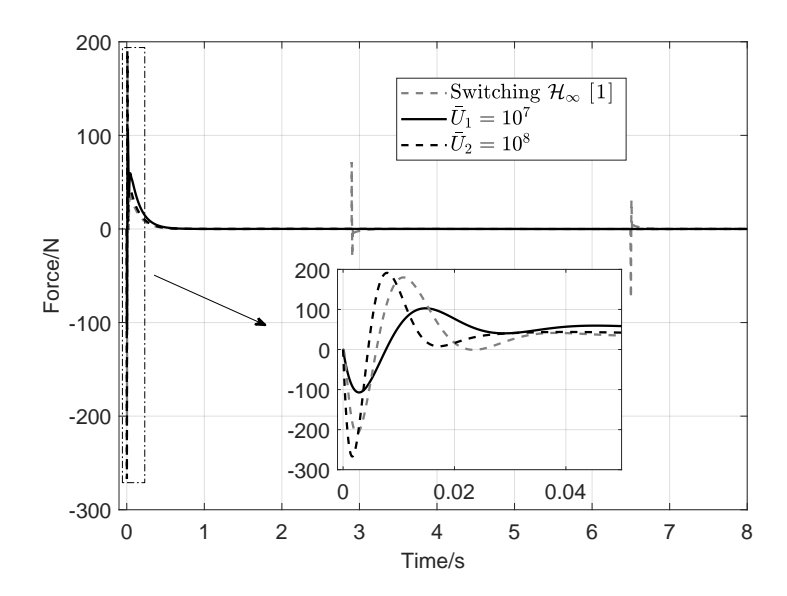


Figure 3.12: Control input u_1 response by [1] and proposed method

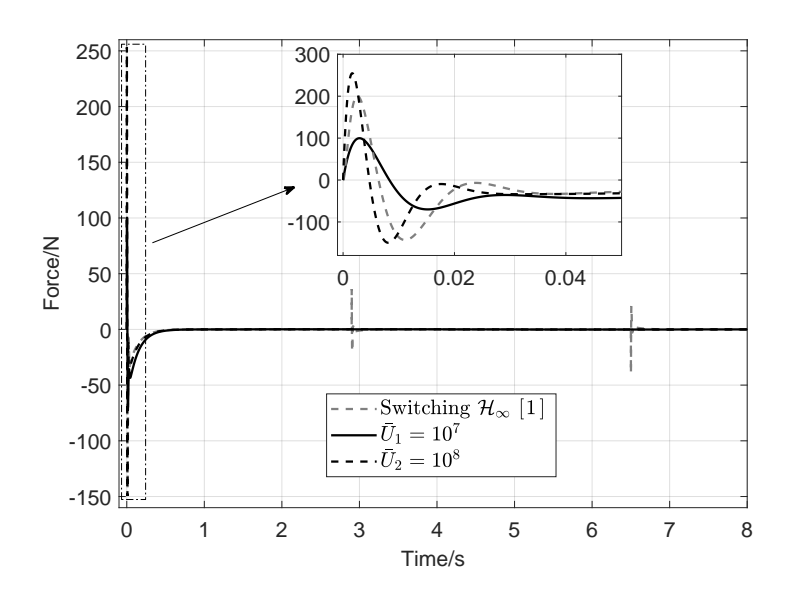


Figure 3.13: Control input u_2 response by [1] and proposed method

conditions are conducted with designed controllers¹. As shown in Figures 3.10 and 3.11, dashed-lines are the un-smooth state responses duplicated using the method in [1], while solid- and dotted-lines represent these responses obtained by the proposed method under two different ICC conditions.

¹The designed switching controller matrices are available online, https://github.com/hetianyi1992/smooth_switching_LPV.

The unsmooth state responses from [1] experience sharp jumps on switching surfaces at $t_1 = 2.9s$ and $t_2 = 6.5s$. However, with the proposed method, the sharp jumps of state responses are successfully smoothened by minimizing the ϵ -balanced cost function (2.81), which demonstrates the effectiveness of the proposed smooth-switching control design.

By comparing state responses under different ICC conditions, it is easy to find that rotor displacements can be further suppressed when larger control authority is made available. With tuned $\overline{U}_2=10^8, \epsilon_2=1$, the proposed method not only leads to a smooth-switching controller, but also reduces the peak magnitude of rotor displacements over the un-smooth responses duplicated by following the procedure in [1]. That is, the well-tuned ICC conditions and smoothness weighting coefficient lead to significantly improved switching smoothness, while system performance is not degraded compared to conventional LPV control .

Figures 3.12 and 3.13 show the unsmooth control responses duplicated from [1] and smooth control inputs under different ICC conditions. Unsmooth control inputs experience sharp jumps at switching instants, while control inputs are smoothened using the proposed smooth-switching controllers. By comparing control input responses, it can be found that ICC conditions influence the peak magnitudes of control inputs. With determined ICC conditions, a well-tuned weighting coefficient enforces smooth switching without sacrificing system performance.

Besides the demonstrated switching smoothness, this study also provides valuable insights regarding how to tune the model-based controller gain. Note that tuning control gain plays an essential role in implementing model-based controllers for practical applications. Due to system modeling error, high gain controllers often lead to instability or degraded system performance, while low gain controllers might not improve system performance much. Therefore, the ability to design a controller with an adequate gain is essential in practice, and the proposed method makes it possible to design controllers with different gains by modifying ICC conditions. The ICC condition tuning along with the line search of smoothness weighting coefficient makes it possible to balanced switching smoothness and system performance in practice, which is very beneficial for practical applications.

3.2 Blended-Wing-Body (BWB) Airplane Flexible Wing

3.2.1 LPV modeling of BWB airplane flexible wing

Before the smooth switching LPV control design is applied to the BWB airplane flexible wing model, in this section, we consider the LPV modeling of BWB flexible wing; see Figure 3.14 for a schematic illustration. Assume that the BWB airplane is flying at a fixed altitude but with varying flight speed. The main body of BWB is gridded into six beam elements, and each wing is gridded into four beam elements. The inner three elements at each wing are selected as control surfaces, labeled as U1-U6 in Figure 3.14, and wing bending displacements are to be suppressed by activating the control surfaces. In order to modulate the vibrational behaviors of entire airplane wings, a total of 18 bending displacements are selected as system outputs. For example, outputs 1 and 9 are the nodal displacements at the right-wing root and right wing tip in Figure 3.14.

The LPV modeling procedure can be described as follows:

- A bundle of LTI full-order models (FOMs) are derived by linearizing nonlinear aero-elastic model at each gridded flight speed [87];
- FOMs are then transformed into modal coordinates and all system modes are properly aligned to track mode variations from one flight speed to the next;
- Model-reduction is conducted to keep the most significant modes over the entire gridded flight envelop [88];
- Linear interpolation over the aligned reduced-order models to attain the affine LPV model. The interpolation of aligned modes is able to capture the variation of system's coupled aerodynamic mode with varying flight speed, which cannot be achieved by direct interpolation of LTI system matrices [88].

In this study, the scheduling parameter is chosen to be the airplane flight speed, and it ranges from 110 to 130 m/s. A bundle of reduced-order LTI models are derived at varying flight speeds

Table 3.1: Mode description in reduced-order model

Mode ID	Rigid-body component	Flexible component	Note
M1	Plunging and pitching	First symmetric out-of-plane bending	Bending/torsion coupling
M2	Plunging and pitching	Second symmetric out-of-plane bending	Bending/torsion coupling
M3	Plunging and pitching	First symmetric in-plane bending	Bending/torsion coupling
M4	Roll	Second anti-symmetric out-of-plane bending	Bending/torsion coupling
M5	-	First anti-symmetric in-plane bending	Bending/torsion coupling
M6	-	-	Aerodynamic dominant mode

and at an increment of 0.5 m/s to capture model variation. Six dominant modes are kept in the reduced-order LTI models, as marked by M1-M6 in Figure 3.15. Physical meanings of these modes are summarized in Table 3.1. Note that all the bending/torsion coupling effects come from the backswept of the wing, and the wing structural rigidity itself has no inherent bending/torsion coupling. The vibration modes stay stable when flight speed is below 115 m/s, and mode M1 becomes unstable beyond 115 m/s as shown in Figure 3.15.

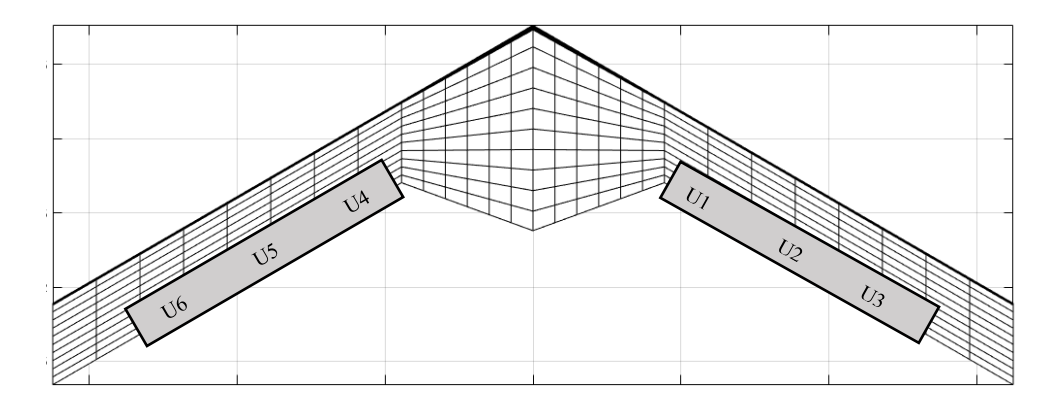


Figure 3.14: Schematic layout of BWB airplane configuration

The affine LPV model is obtained by linearly interpolating the first and last eigenvalues of each mode. As shown in the close-up view of Figure 3.15, the solid line shows the linear interpolation of the eigenvalues, where crosses denote the loci of actual eigenvalues as function of flight speed. As a result, in the interpolated affine LPV model, system damping coefficient is approximated while system stability remains unchanged over the entire flight envelope. Similarly, all other system matrices are also obtained by following the same linear interpolation process. The resulted affine LPV model consists of 12 states (6 modes), 6 control inputs (control surfaces deflection angles) and 18 performance outputs (wing bending displacements).

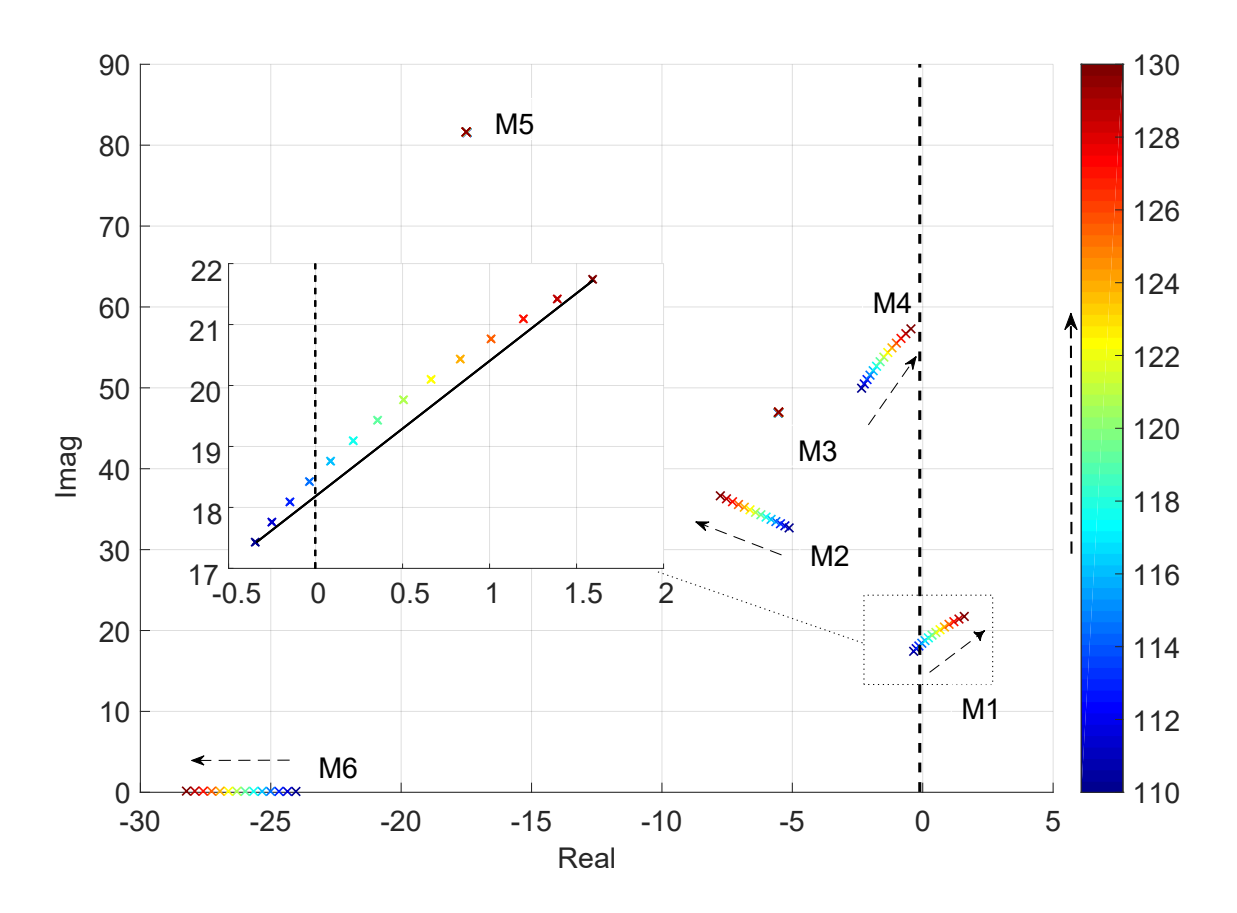


Figure 3.15: Root loci of open-loop system with varying flight speed

There are two main control design goals. One is to robustly stabilize the closed-loop system under bounded modeling error and the other is to suppress wing bending displacements, excited by the gust disturbance, using control surfaces on the wing. As a result, two independent \mathcal{H}_{∞} and \mathcal{H}_2 input channels are used along with two independent \mathcal{H}_{∞} and \mathcal{H}_2 output channels for the system described in Eqn. (2.1), where modeling error is modeled as system disturbance input w_{∞} excited by the system output z_{∞} through uncertainty Δ and the closed-loop robust stability is achieved by satisfying the desired \mathcal{H}_{∞} performance; the gust disturbance is treated as disturbance input w_2 with associated \mathcal{H}_2 performance output z_2 to be optimized for suppressing bending displacement z_2 caused by the gust disturbance. In addition, ICC constraints are imposed on control inputs or deflection angles of control surfaces, so that they are hard-constrained to operate within their limits. In order to apply switching LPV control, the switching LPV model is developed by dividing

the scheduling parameter range into multiple overlapping subregions, as shown in Figure 3.16. In the next subsection, a generic LPV model with \mathcal{H}_{∞} and \mathcal{H}_2 channels will be considered and the associated system performances defined.

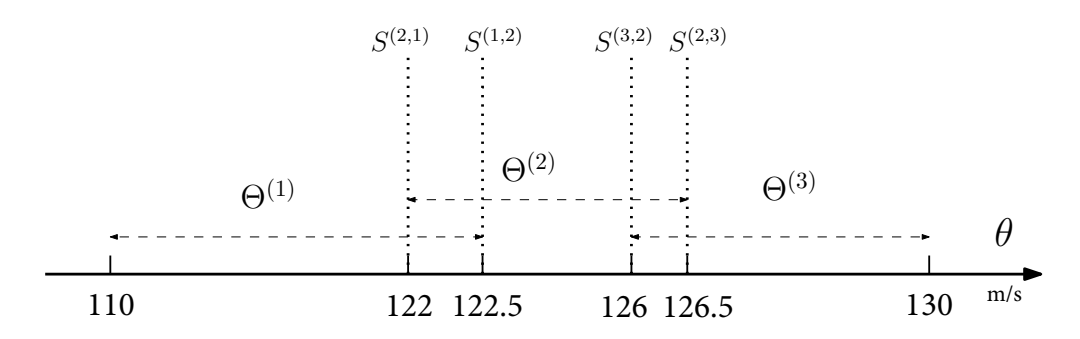


Figure 3.16: Three-subregion partition for scheduling parameter

3.2.2 Mixed ICC/ \mathcal{H}_{∞} LPV control

The \mathcal{H}_2 outputs of interest are bending displacements, while the \mathcal{H}_∞ outputs include bending displacements and control inputs. The weighting matrix Q is chosen to be identity matrix, that is, all outputs are weighted equally. The scheduling parameter is chosen as a biased sinusoidal function, $\theta(t) = 110 + 20\sin(t/20)$ m/s, as shown in Figure 3.17. Therefore, within the time interval of $[0, 20\pi]$ second, the scheduling parameter is bounded as $110 \text{ m/s} \leq \theta \leq 130 \text{ m/s}$, and its rate bounded as $-1 \text{ m/s}^2 \leq \dot{\theta} \leq 1 \text{ m/s}^2$. In general, the scheduling parameter trajectory should satisfy the boundary conditions for both θ and $\dot{\theta}$, and be at least piece-wise differentiable. It is commonly accepted that the variation of the scheduling parameters must be "slow" compared to the system dynamics, because designing an LPV controller for fast-varying scheduling parameters is a challenge [89].

3.2.2.1 Constraints and performance trade-off

In the mixed ICC and \mathcal{H}_{∞} (or robust ICC) LPV control problem, both control input constraints and robustness requirement would significantly impact the optimal solution to the PLMIs. Hence, a trade-off study is conducted to better understand the characteristics of LPV models. Figure 3.18

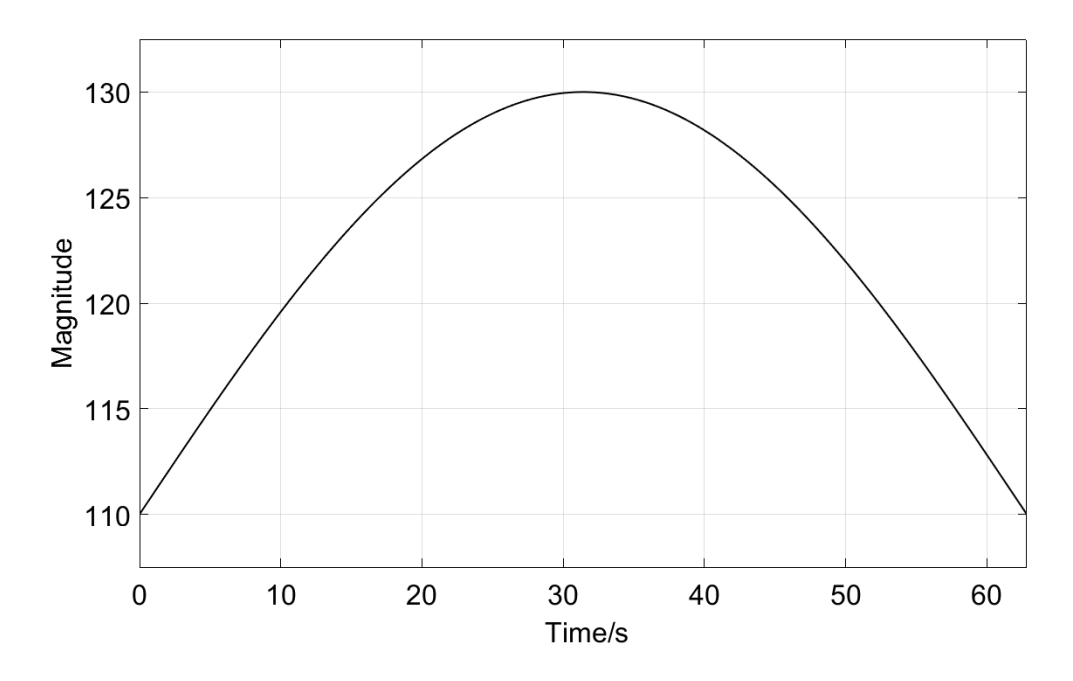


Figure 3.17: Scheduling parameter (flight speed) trajectory

shows the complete trade-off between the control effort \bar{U} , the robustness levels γ_{∞} , and the output performance trace(W). For a given robustness level, the trade-off contour illustrates that larger control input constraint leads to smaller output covariance, hence better \mathcal{H}_2 performance for the closed-loop system. In addition, with small control effort, output performance will be degraded, resulting in a large output covariance. An increase in control effort leads to notable improvement on system \mathcal{H}_2 performance with wider range of admissible robustness levels. This demonstrates that larger control input can effectively compensate for the robustness constraints.

Furthermore, based on the Small Gain Theorem [33], the closed-loop system satisfying the condition $||T_{\infty}||_{\infty} \leq \gamma_{\infty}$ is well-posed and internally stable for all uncertainty satisfying $||\Delta||_{\infty} < 1/\gamma_{\infty}$, where Δ can be considered as an interconnection from z_{∞} to w_{∞} , as shown in Figure 1.3. In Figure 3.18, with a fixed \bar{U} , it is obvious that with more stringent requirement on robust performance, i.e. smaller γ_{∞} , the output performance degrades with increase in trace(W), leading to worsen \mathcal{H}_2 performance. Note that, while γ_{∞} decreases incrementally, trace(W) increases or \mathcal{H}_2 performance degrades much drastically. This can be explained by the reciprocal relation between uncertainty Δ and γ_{∞} .

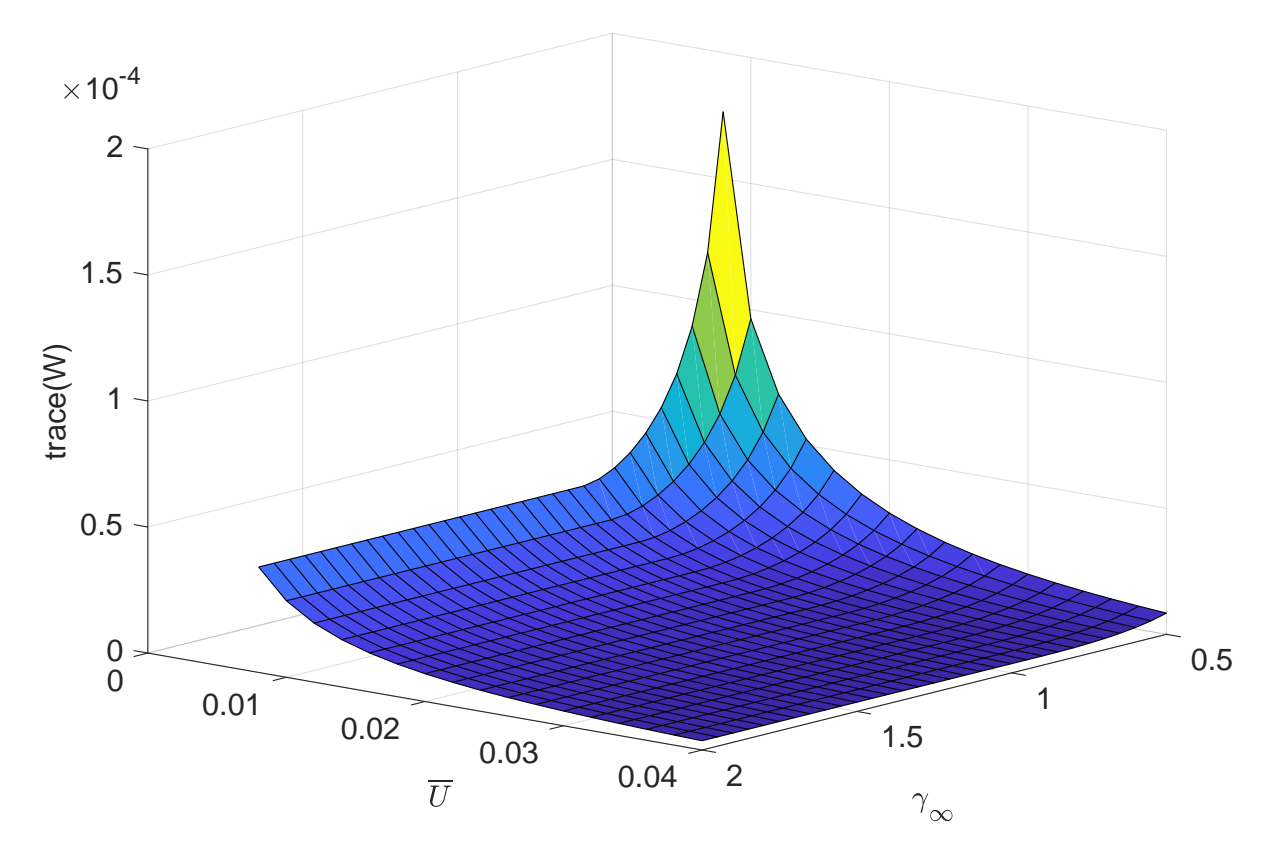


Figure 3.18: Trade-off between control limit \bar{U} and trace(W) at different robustness conditions

The trend at higher or lower robustness level reveals an important implication for controller design. At lower robustness level, for instance $\gamma_{\infty}=2$, the achievable \mathcal{H}_2 performance remains almost unchanged when $\bar{U}>0.01$. This indicates that the robust \mathcal{H}_{∞} performance requirement is not the dominant factor for control design and the \mathcal{H}_2 performance can be achieved with a relatively small control effort. However, at higher robustness level, for instance $\gamma_{\infty}=0.5$, the \mathcal{H}_{∞} performance becomes critical for control design. As a result, in order to achieve a specific \mathcal{H}_2 performance, more control effort is required. It is also observed that the achievable \mathcal{H}_2 performance degrades with increased robustness level. Based on the above-mentioned trade-offs, the constraints for the control design are chosen to be $\bar{U}=0.02$ and $\gamma_{\infty}=1$, which ensure a good robustness margin to handle modeling error with good balance between \mathcal{H}_2 performance and control effort.

3.2.2.2 Mixed ICC and \mathcal{H}_{∞} Control Problem

The mixed ICC and \mathcal{H}_{∞} control problem is to find a state-feedback gain-scheduling controller (2.52) for the LPV system (2.1), while minimizing the upper bound of \mathcal{H}_2 performance cost [90, 35]

$$\min_{K(\theta)} trace(W) , \qquad (3.1)$$

such that:

- the closed-loop system (2.5) is exponentially stable,
- the following constraints of robustness level and control input covariance are satisfied,

$$||T_{\infty}(K(\theta), s)||_{\infty} \le \gamma_{\infty}, \tag{3.2}$$

$$Cov(u_k(t)) \le \bar{U}_k, k = 1, 2, \dots, n_u,$$
 (3.3)

where $\gamma_{\infty} > 0$ is the given \mathcal{H}_{∞} -norm bound on system robustness, and \bar{U}_k the given bound on the control covariance $Cov(u_k(t))$ for the k^{th} control input $u_k(t)$ defined below,

$$Cov(u_k(t)) = \left[\frac{1}{2\pi} \int_{-\infty}^{\infty} T_u^*(K(\theta), j\omega) T_u(K(\theta), j\omega) d\omega \right], \tag{3.4}$$

and $T_u(K(\theta), s) := T_{w_2 \to u}(K(\theta), s)$ denotes the transfer function from $w_2(t)$ to u(t) for the LPV system (2.5). Note that, for deterministic signal, covariance is defined in terms of time correlation [51, 91, 7, 92].

As a result, the proposed mixed ICC and \mathcal{H}_{∞} control problem has interesting interpretations in stochastic and deterministic perspectives. The stochastic interpretation assumes that the exogenous input $w_2(t)$ is an uncorrelated zero-mean white noise with unit intensity. Then, the mixed ICC and \mathcal{H}_{∞} control problem is to minimize the output covariance (or RMS-value) while satisfying multiple control input covariance constraints and \mathcal{H}_{∞} robust performance criterion. The control input covariance constraints can be considered as constraints on the variances of the control actuation. In other words, the proposed control provides the best output \mathcal{H}_2 performance with the given control

 \mathcal{H}_2 performance and robust \mathcal{H}_∞ constraints. On the other hand, the deterministic interpretation assumes that the exogenous input $w_2(t)$ is an unknown disturbance that belongs to a bounded \mathcal{L}_2 set. Then, the mixed ICC and \mathcal{H}_∞ control problem is to minimize the square summation of \mathcal{L}_2 to \mathcal{L}_∞ gains from $w_2(t)$ to individual output channel $z_{2,k}(t)$ for $k=1,2,\ldots,n_{z2}$, subject to the \mathcal{L}_2 to \mathcal{L}_∞ gain constraints (3.3) on $u_k(t)$ for $k=1,2,\ldots,n_u$ and the \mathcal{H}_∞ constraint (3.2). In other words, the proposed control problem is to minimize the weighted sum of the worst case peak values of performance output subject to the constraints on worst-case peak values of control inputs and the \mathcal{H}_∞ constraint. It should be noted that the \mathcal{L}_2 - \mathcal{L}_∞ gain from $w_2(t)$ to $z_2(t)$ is defined in White et al. [91] as follows,

$$\overline{\sigma} \left[\frac{1}{2\pi} \int_{-\infty}^{\infty} T_2^*(K(\theta), j\omega) T_2(K(\theta), j\omega) d\omega \right] = \sup_{w_2 \in \mathcal{L}_2, z_2 \in \mathcal{L}_\infty, ||w_2||_2 \neq 0} \frac{||z_2(t)||_\infty^2}{||w_2(t)||_2^2}$$
(3.5)

where $\overline{\sigma}\left[\cdot\right]$ denotes the maximum singular value operator.

3.2.2.3 Time-domain simulation results

Given the range of θ and $\dot{\theta}$, the control input constraints, and the robustness level, the LPV model of the BWB airplane is simulated when it is subjected to a sharp-edged gust disturbance for 5 seconds. Figures 3.19 and 3.20 show the wing root (output 1) and wing tip (output 12) bending displacement of the right wing for open-loop case, and as can be seen the results are unstable. Therefore, a state-feedback LPV controller in the form of Eqn. (2.52) is designed to stabilize wing elements and suppress the bending displacement.

Using Theorem 3, a state-feedback LPV controller can be design with scheduled control gain matrix of dimension 6×12 , mapping 12 states to 6 control inputs. Note that the LPV model is developed in the modal coordinate, the measured or observed states in original coordinate need to be transformed to the modal coordinate. In practical implementation, scheduling parameter (flight speed) will be online measured in each sampling time, and control inputs of altering flap angles can be calculated from corresponding controller gain matrix and measured or observed states.

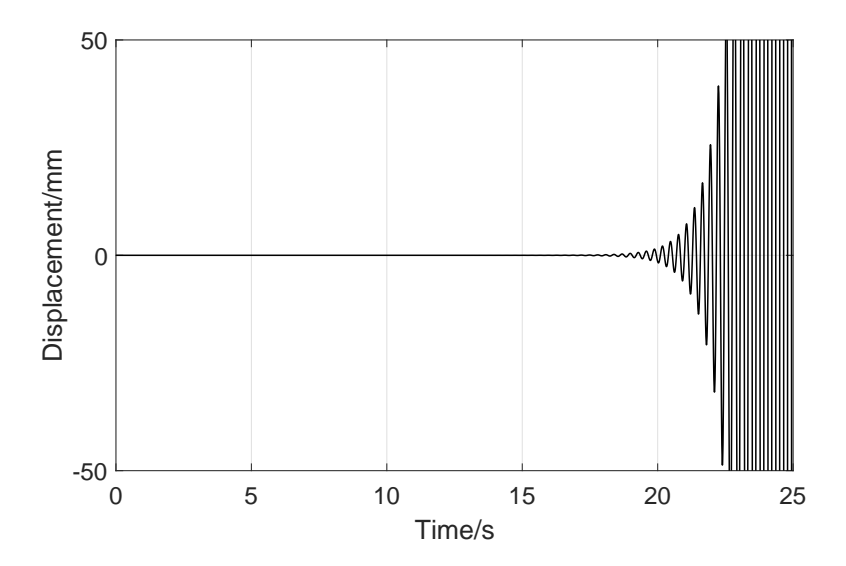


Figure 3.19: Bending displacement at wing root

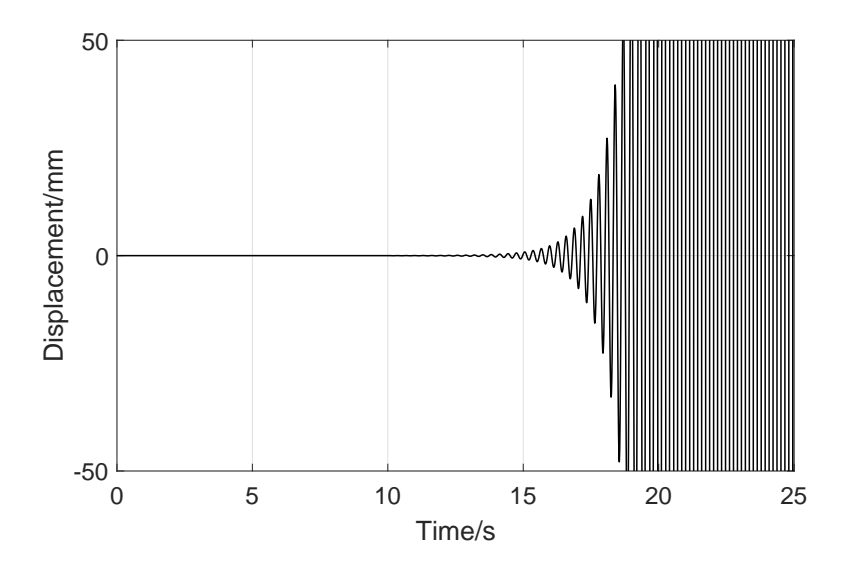


Figure 3.20: Bending displacement at wing tip

To demonstrate the effect of control input constraints and robustness levels to \mathcal{H}_2 performance, multiple simulations are performed for comparison. When robustness level $\gamma_{\infty}=1$ is fixed, each control input is identically constrained by various upper bounds \bar{U} . Figures 3.21 and 3.22 show the bending displacement at wing root and wing tip for $\bar{U}=0.01,0.02,0.04$. As can be seen, during the gust disturbance, the outputs are converged and bounded. In addition, with larger control inputs, the output responses have smaller overshoot and faster convergent rate, indicating that \mathcal{H}_2

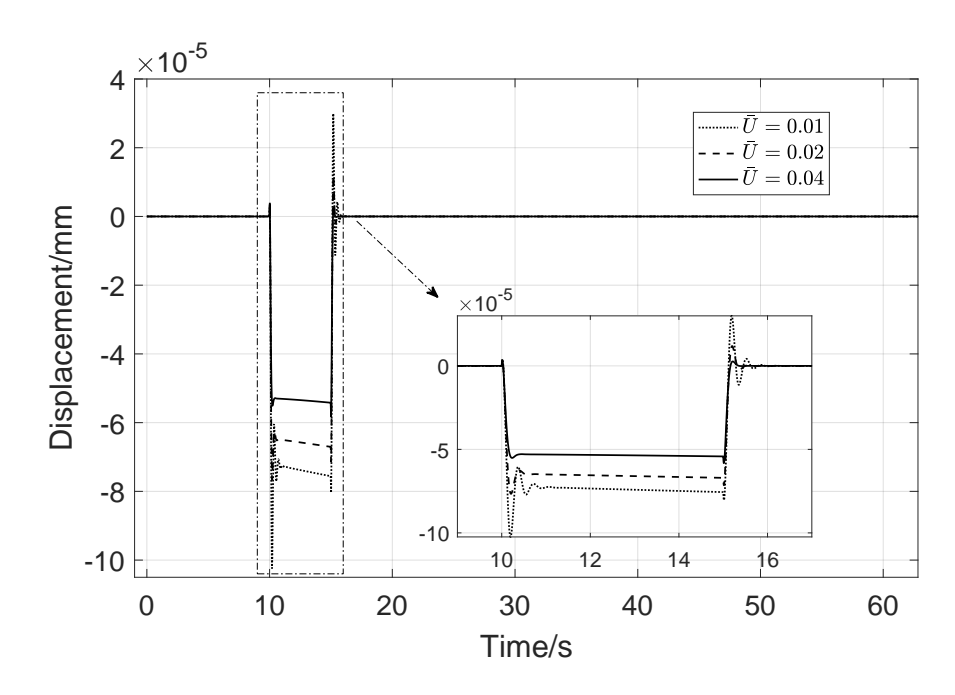


Figure 3.21: Wing root bending under different \bar{U}

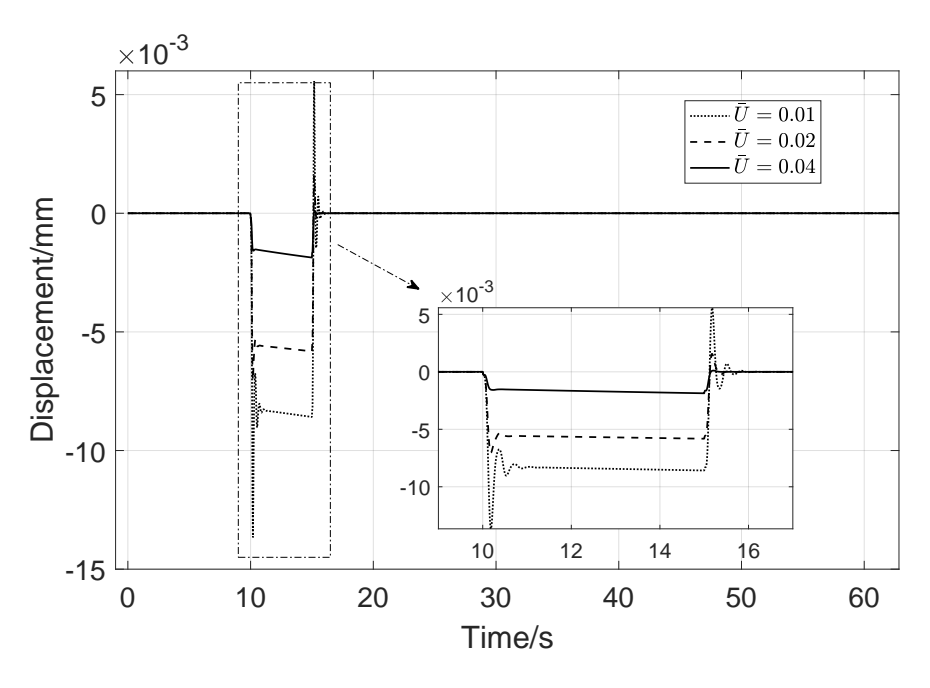


Figure 3.22: Wing tip bending under different \bar{U}

output performance are improved. As shown in Figures 3.23 - 3.28, the control inputs U1-U6 are increased by more than twice when upper bounds become doubled. This comparison indicates that the selection of $\bar{U}=0.02$ offers a good balance between the performance and the control effort, which produces an upper bound of u=0.14 rad $\approx 8^{\circ}$.

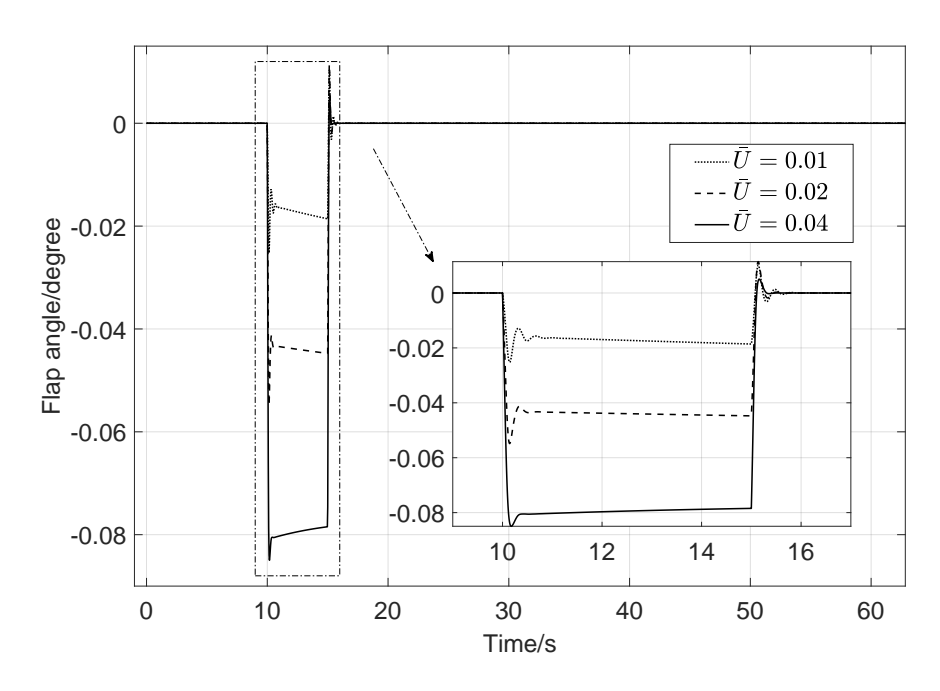


Figure 3.23: Control input 1 under different \bar{U}

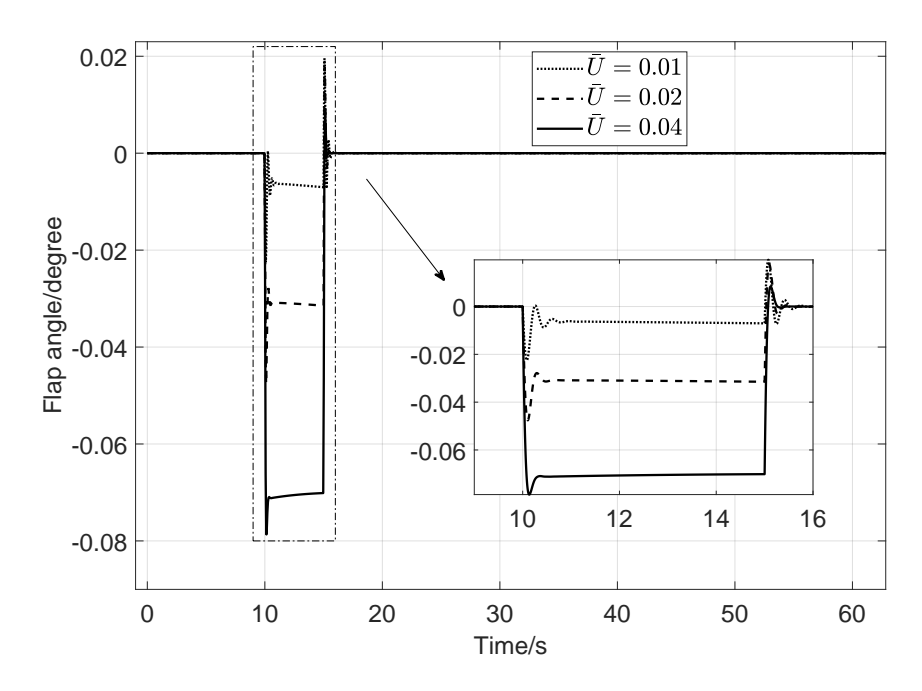


Figure 3.24: Control input 2 under different \bar{U}

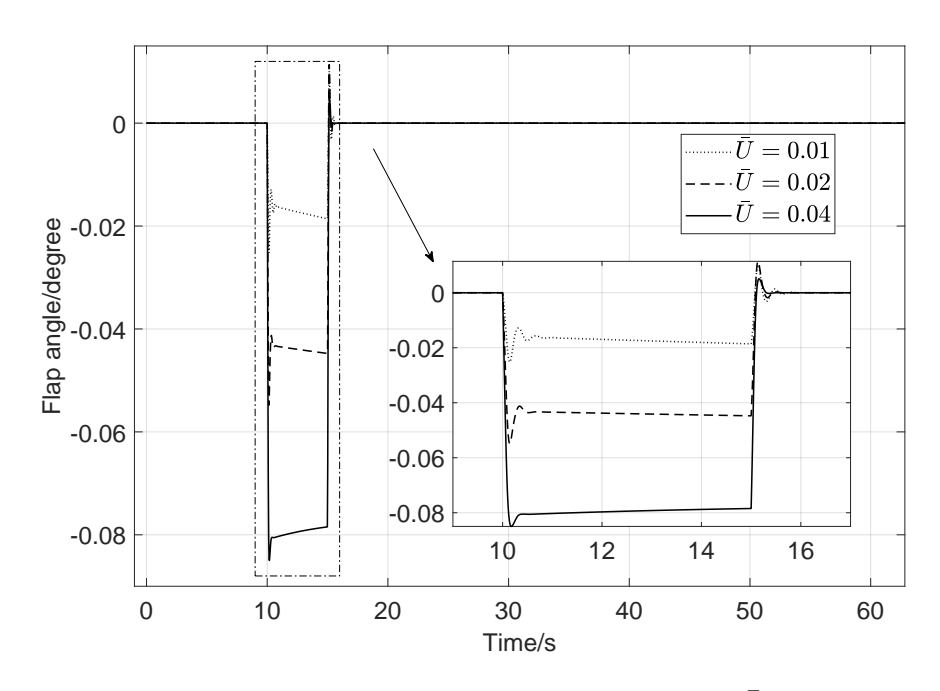


Figure 3.25: Control input 3 under different \bar{U}

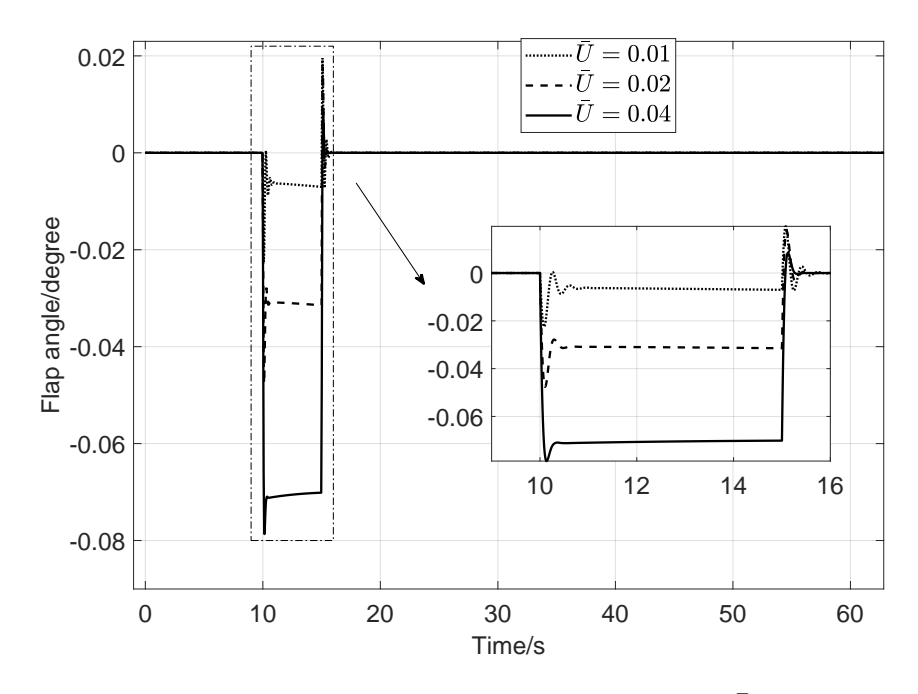


Figure 3.26: Control input 4 under different \bar{U}

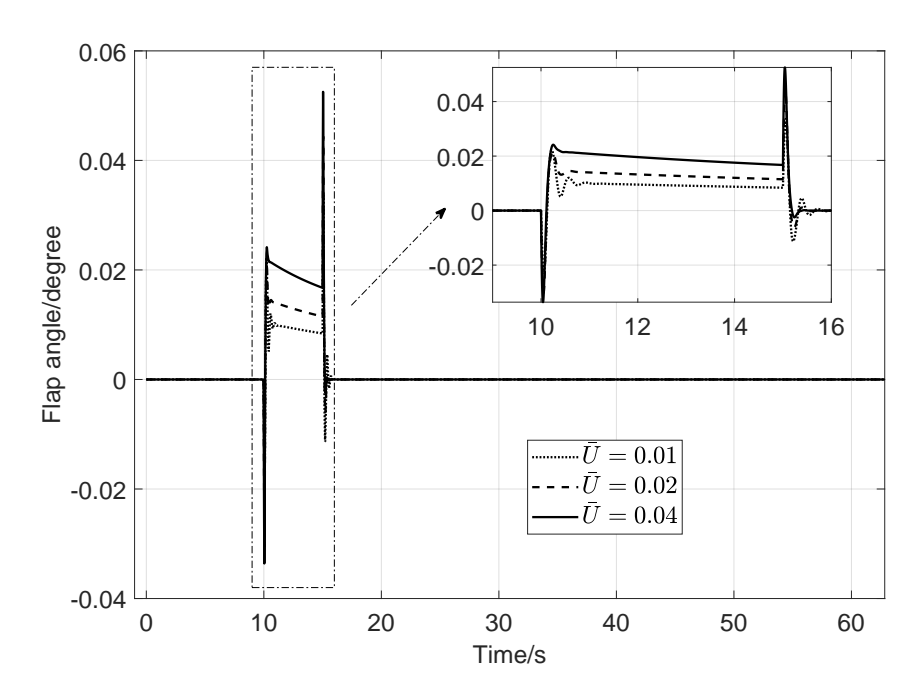


Figure 3.27: Control input 5 under different \bar{U}

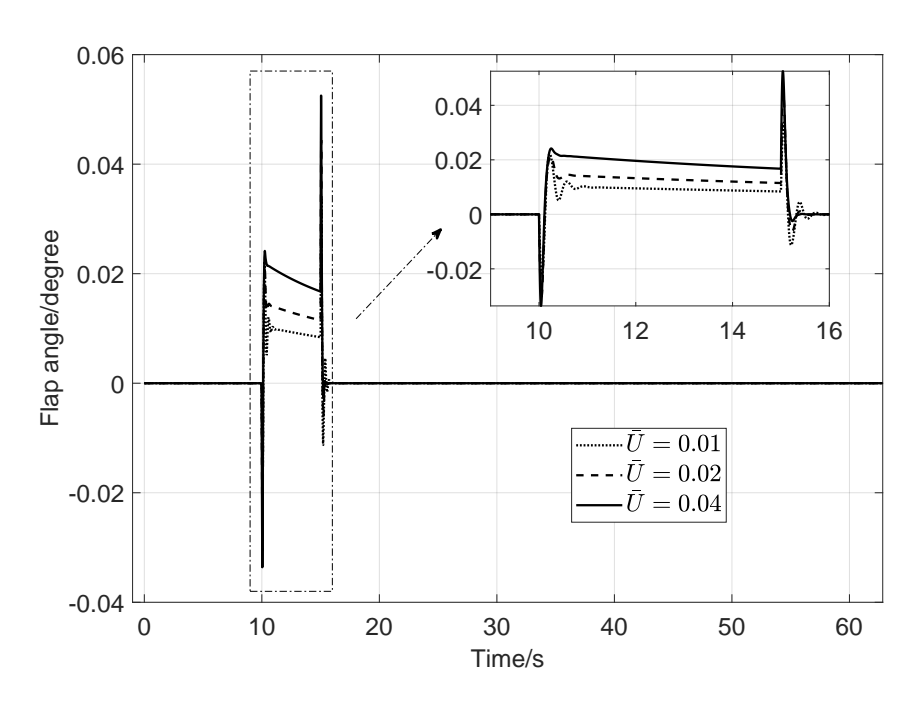


Figure 3.28: Control input 6 under different \bar{U}

All 6 inputs are compared to show how the control law allocates 6 independent inputs to suppress airplane wing displacements. It can be observed that inputs 1 and 3 are distributed by similar control authority. The equal distribution of control authority also happens on control inputs 2 and 4, control inputs 5 and 6.

When $\bar{U}=0.02$ is fixed, the robustness level γ_{∞} is varied to study its influence on output performance. As shown in Figures 3.29 and 3.30, the bending displacement at wing root and wing tip are improved when γ_{∞} increases from 0.5 to 1. However, the responses remain almost unchanged when γ_{∞} increases from 1 to 2. This phenomenon matches well with the earlier trade-off study shown in Figure 3.18. Figures 3.31 and 3.32 show the control inputs when the robustness level is greater than 1, as can be seen that γ_{∞} is no longer the dominant factor for output performance.

After \bar{U} is chosen, the LPV controller is designed and applied to actual gridded LTI models to validate its feasibility. Figure 3.37 shows the root loci of the closed-loop system with varying flight speed. As shown, the proposed LPV controller stabilizes the gridded LTI models subject to input constraints, while minimizing the output \mathcal{H}_2 performance. However, in an effort to reduce control energy, some modes are kept unchanged by the proposed controller. Comparing Figures 3.15 and 3.37, the modes (M1, M2, M4), which dominate in z-directional bending motion, have been significantly shifted, while other modes (M3, M5, M6) are kept unchanged. In addition, Figure 3.38 shows the ICC cost or \mathcal{H}_2 norm of the closed-loop system with the LPV controller applied to the interpolated LPV system and actual gridded LTI models, respectively. Their magnitudes are very close and upper bounded by trace(W). When combining with Figure 3.37, Figure 3.38 effectively validates that the proposed interpolation of LTI models and LPV controller design is feasible for vibration control of the BWB airplane.

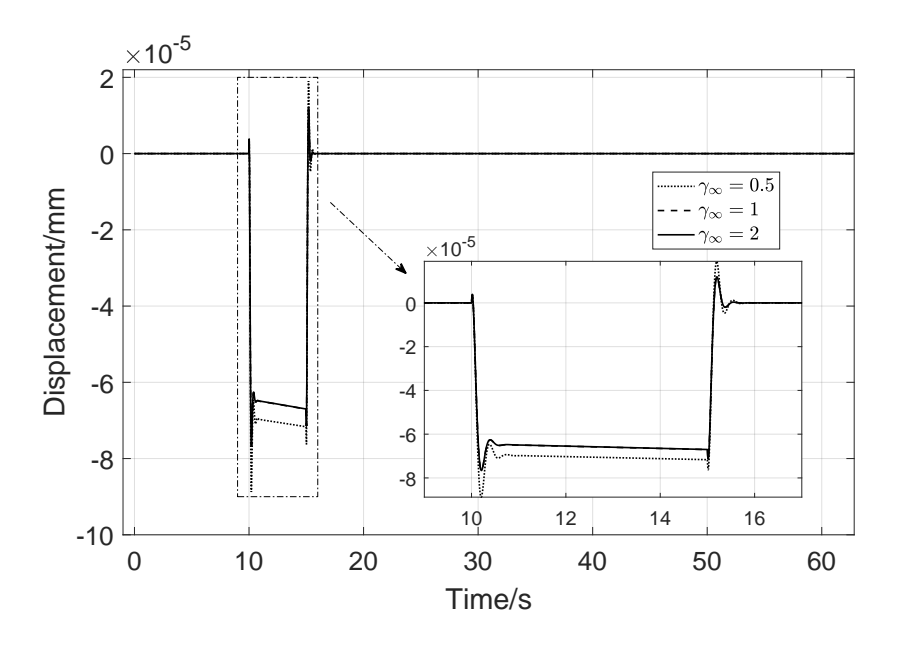


Figure 3.29: Wing root bending under different γ_{∞}

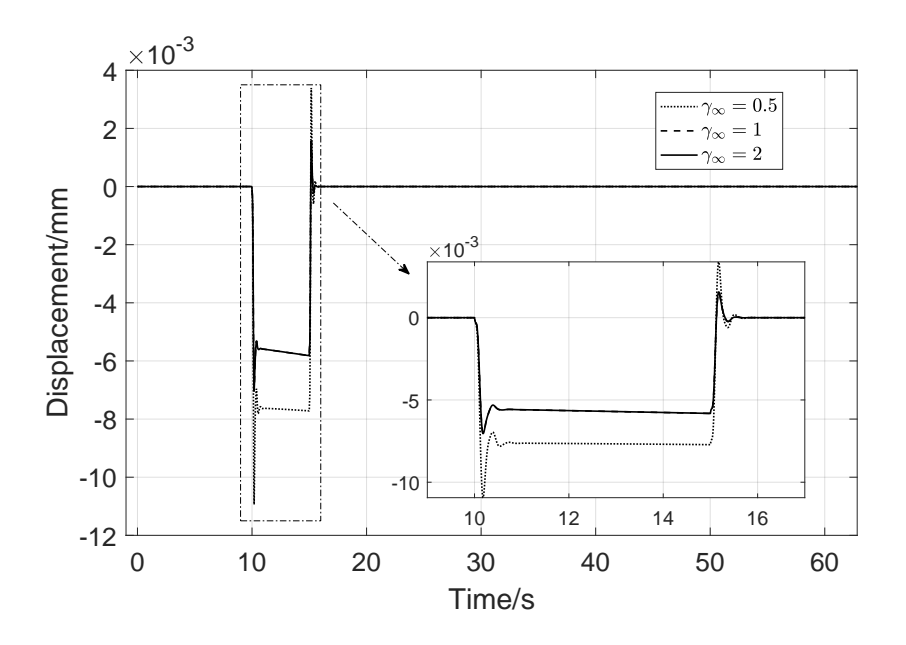


Figure 3.30: Wing tip bending under different γ_{∞}

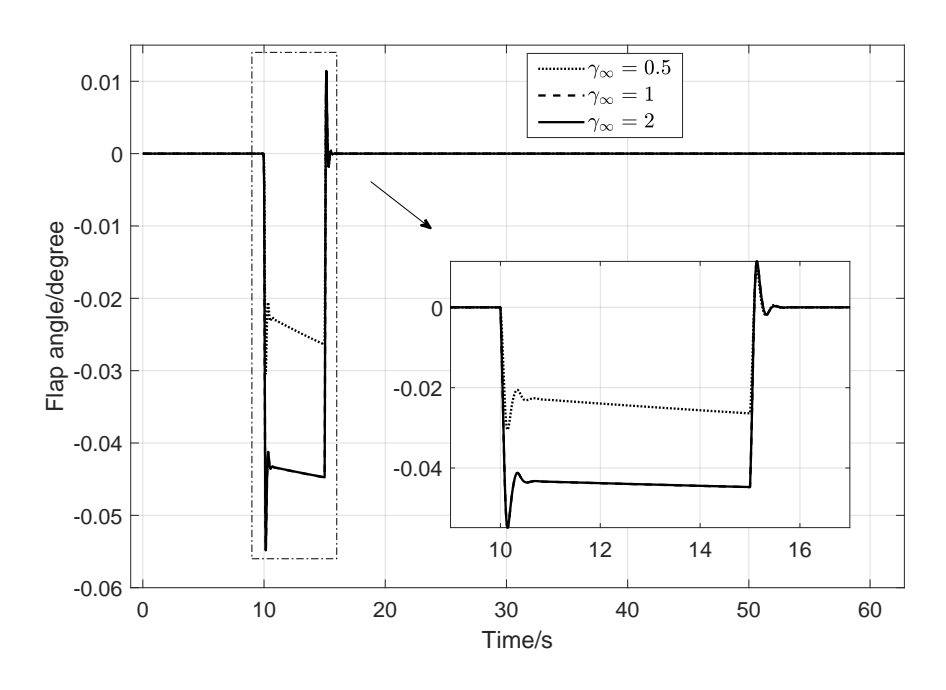


Figure 3.31: Control input 1 under different γ_{∞}

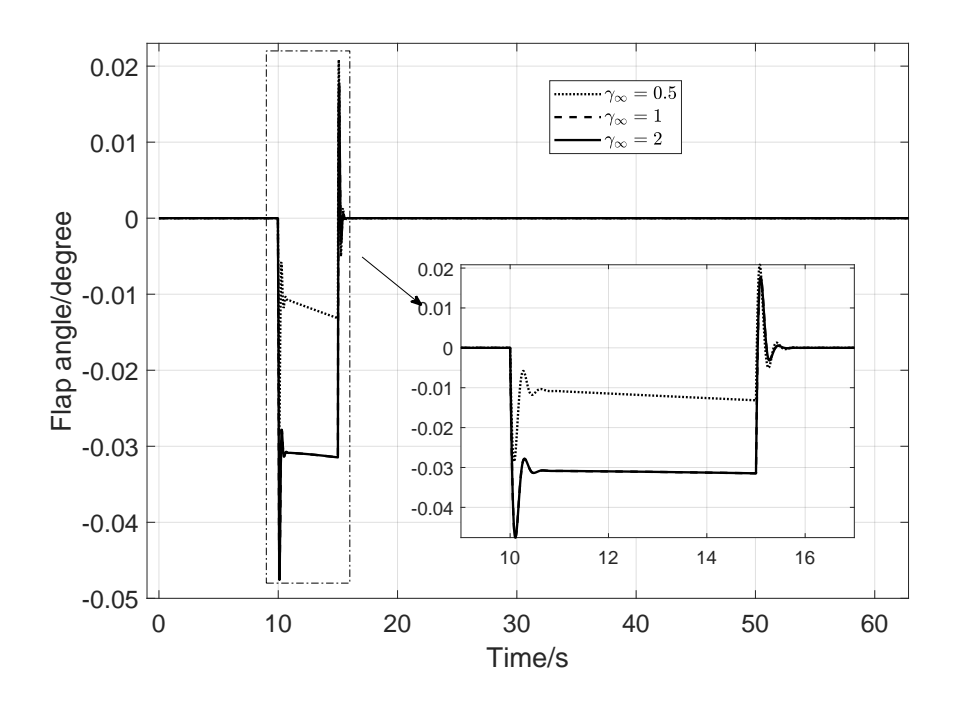


Figure 3.32: Control input 2 under different γ_{∞}

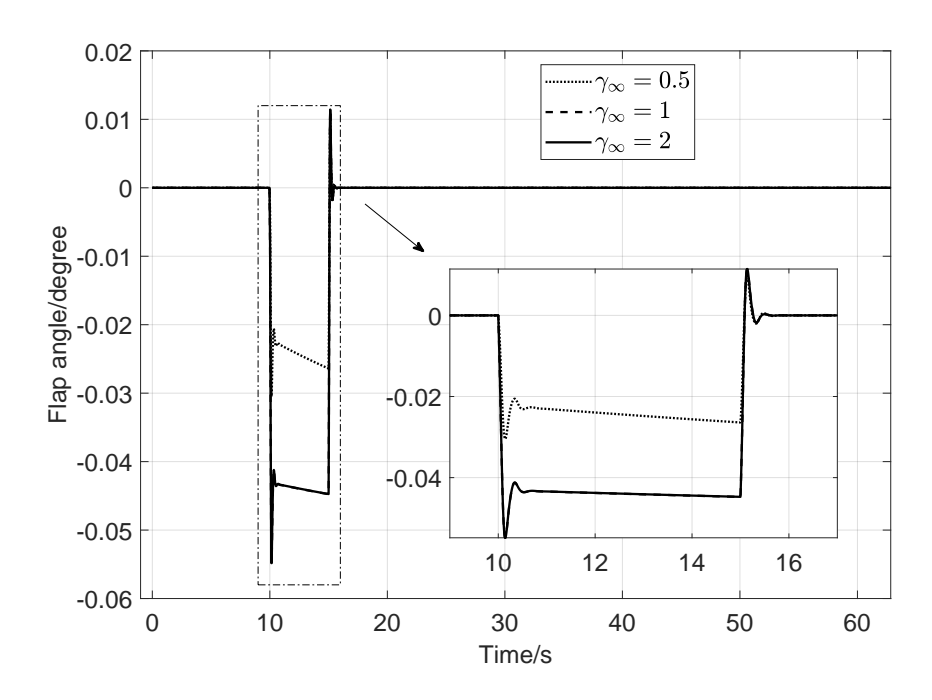


Figure 3.33: Control input 1 under different γ_{∞}

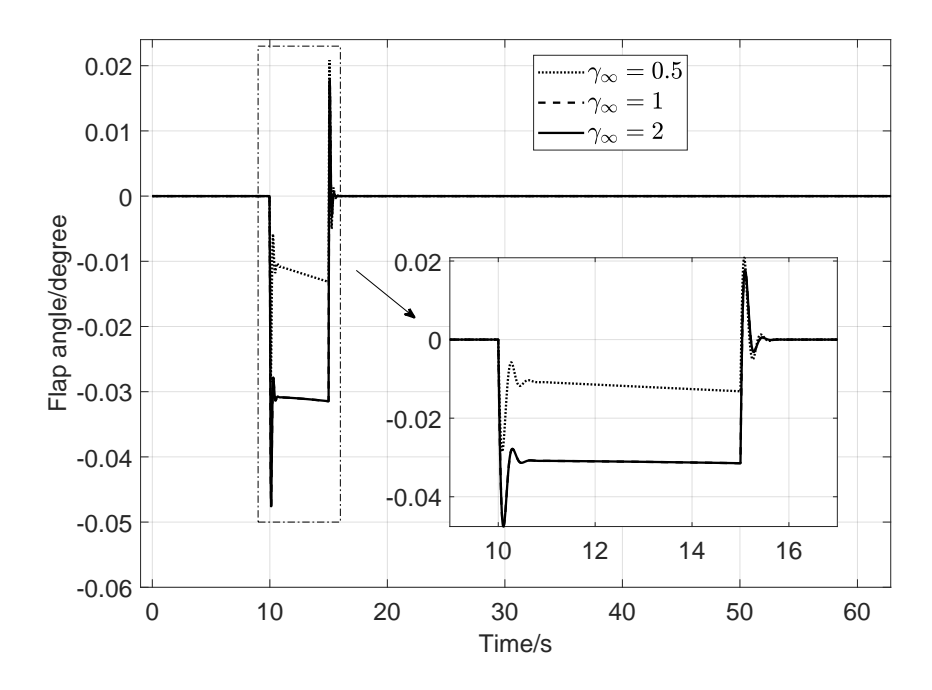


Figure 3.34: Control input 2 under different γ_{∞}

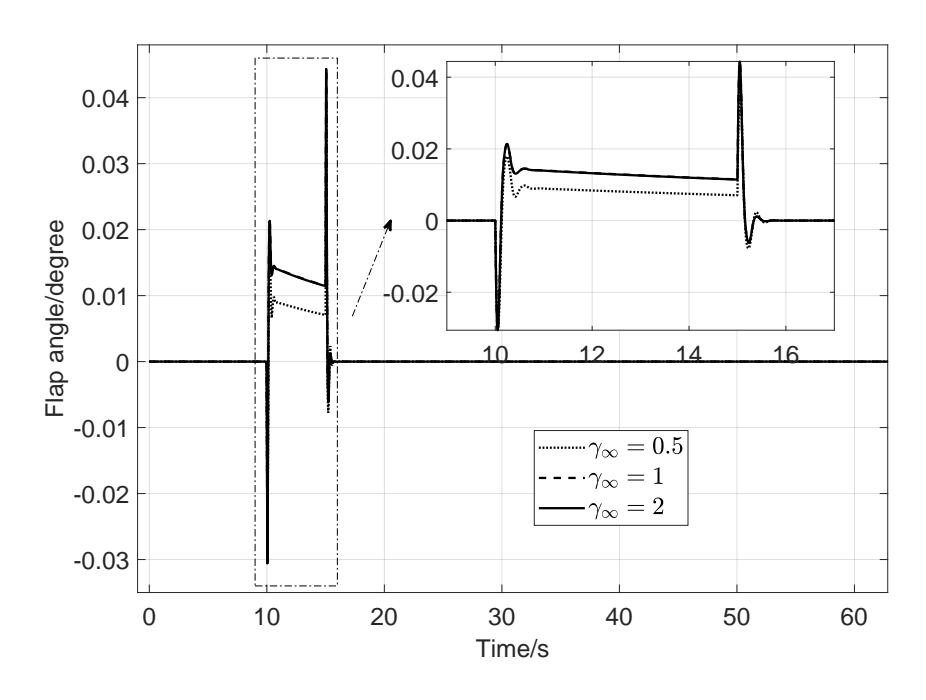


Figure 3.35: Control input 1 under different γ_{∞}

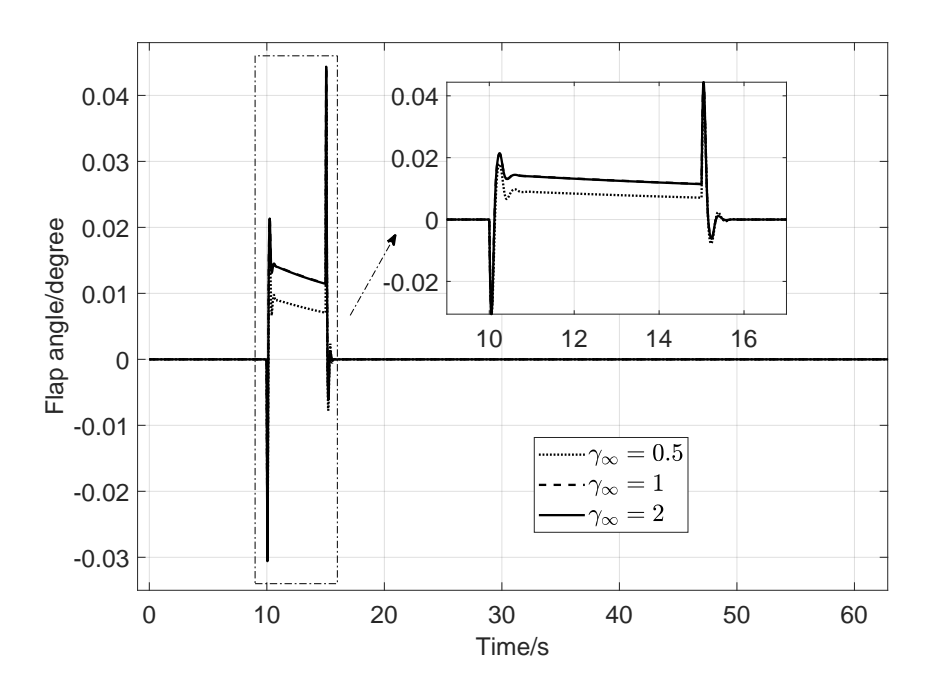


Figure 3.36: Control input 2 under different γ_{∞}

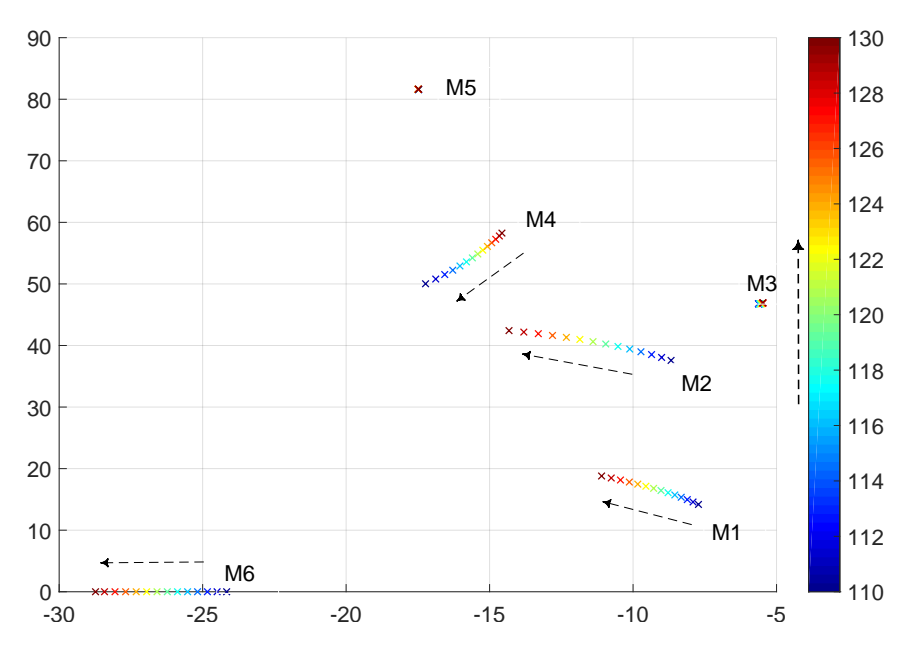


Figure 3.37: Root loci of closed-loop system

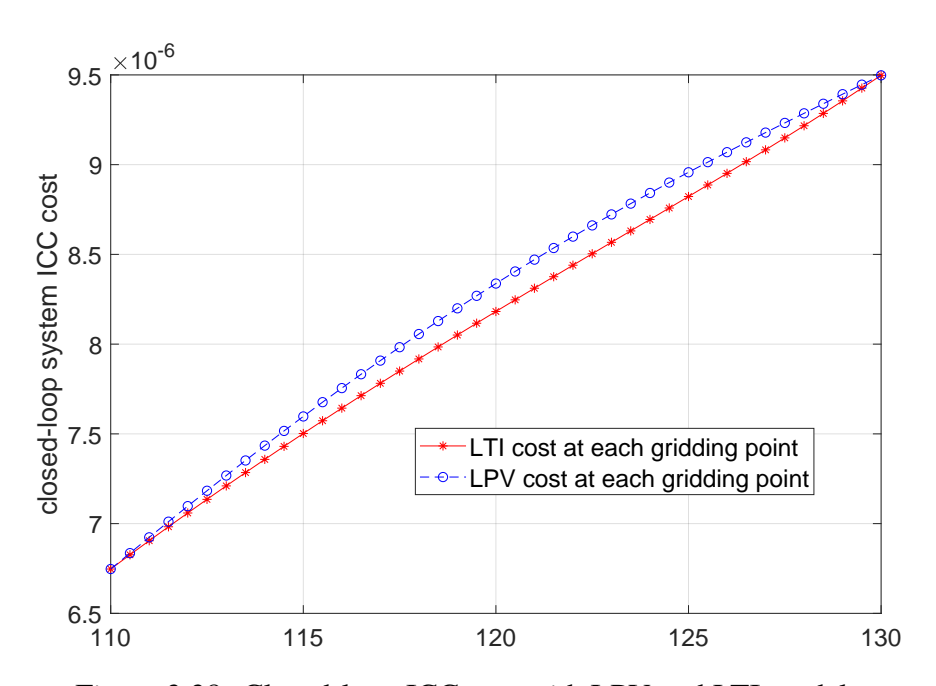


Figure 3.38: Closed-loop ICC cost with LPV and LTI models

3.2.3 Smooth switching LPV control by simultaneous design

3.2.3.1 Time-domain simulation results

The scenario that a BWB airplane experiences a sharp gust disturbance is considered in this study. The gust disturbance is assumed to induce a constant shift angle w_2 on all control surfaces for $t \in [0,9]$ second, and we assume that $w_2 = 0.005$ rad $\approx 0.28^\circ$. As shown in Figure 3.39, two switching events happen at $t = T_1 = 3s$ and $t = T_2 = 8s$. Therefore, within the time interval of [0,10] second, the scheduling parameter is bounded by $110 \text{ m/s} \le \theta \le 130 \text{ m/s}$, and its rate bounded by $-1 \text{ m/s}^2 \le \dot{\theta} \le 1 \text{ m/s}^2$. Note that when the open-loop system is subject to gust disturbance, bending displacements are unstable, as shown in Figure 3.40. A family of smooth-switching mixed ICC/ \mathcal{H}_{∞} LPV DOF controllers are to be designed using Theorem 7 for stability as well as achieving a balanced \mathcal{H}_2 performance and switching smoothness, with guaranteed \mathcal{H}_{∞} robust performance (at $\gamma = 10$).

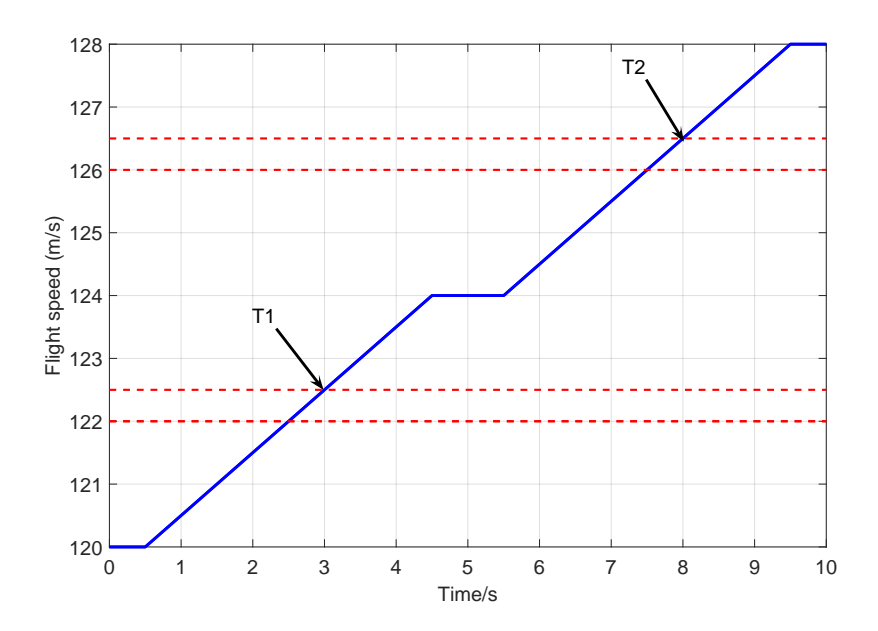


Figure 3.39: Scheduling parameter with switching events

The trade-off relationship is explored by line search of weighting coefficients ϵ under different ICC constraints: $\bar{U}_1=8,\ \bar{U}_2=12$ and $\bar{U}_3=20$. As shown in Figure 3.41, the switching smoothness index can be reduced by decreasing the weighting coefficient ϵ , which results in an

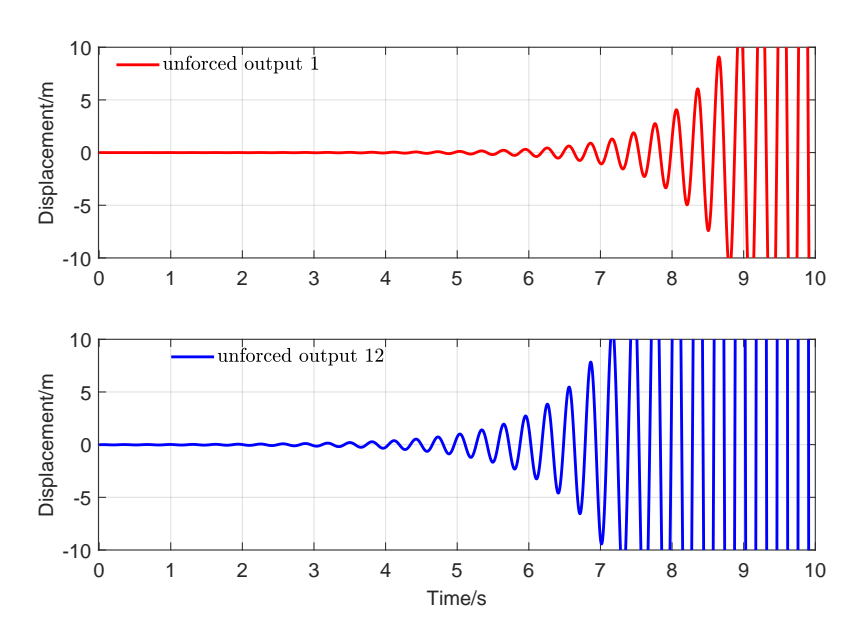


Figure 3.40: Unforced bending displacements at wing root (upper) and wing tip (lower)

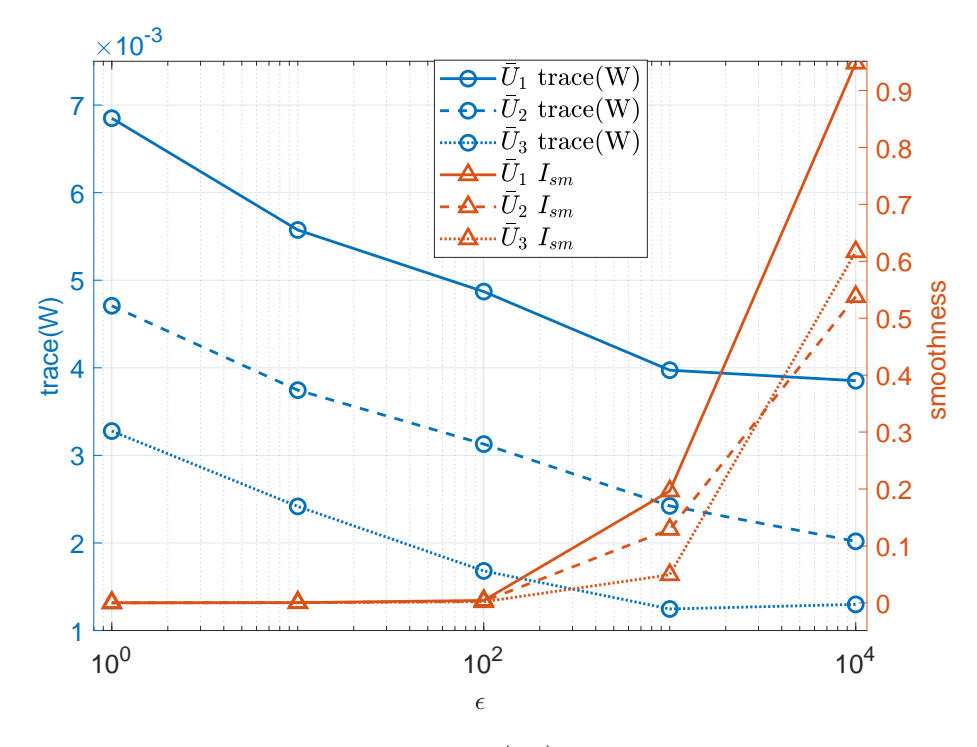


Figure 3.41: Trade-off between trace(W) and smoothness index I_{sm}

increased \mathcal{H}_2 performance index trace(W) or degraded \mathcal{H}_2 performance. This illustrates that system performance is sacrificed in order to enforce switching smoothness. Especially, when $\epsilon < 10^2$, the system performance index increases significantly for all three ICC constraints, indicating that

system performance is degrading much drastically in order to achieve smoother responses. Thus, an optimal weighting coefficient is chosen to be $\epsilon=10^2$ to attain smooth switching with acceptable system performance. To demonstrate the effectiveness of the proposed method, extensive simulations are conducted by considering three different controllers: 1) non-switching LPV controller, 2) un-smooth switching LPV controller, and 3) the proposed smooth-switching LPV controller. And these controllers are applied to the BWB flexible wing model for vibration suppression.

Figures 3.42 and 3.43 show the bending displacement at wing root (output 1) and wing tip (output 12), respectively, while Figures 3.44-3.49 show the control allocation of deflection angles of six flaps according to three different control strategies.

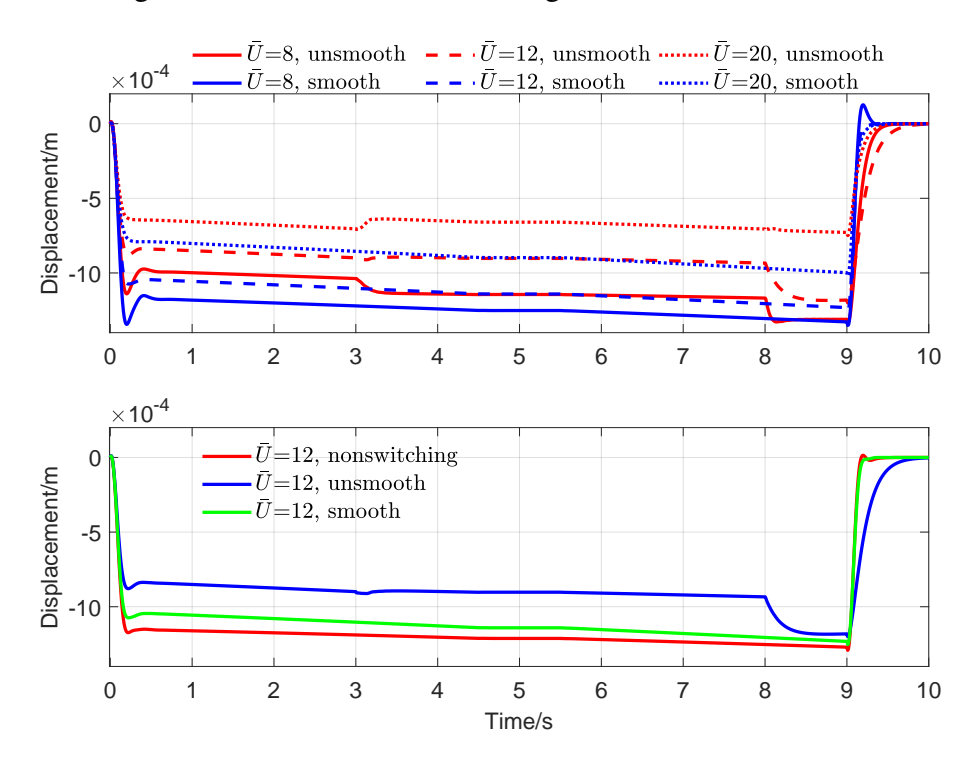


Figure 3.42: Upper: comparison at wing root with smooth/un-smooth switching controller; Lower: comparison at wing root with three control methods

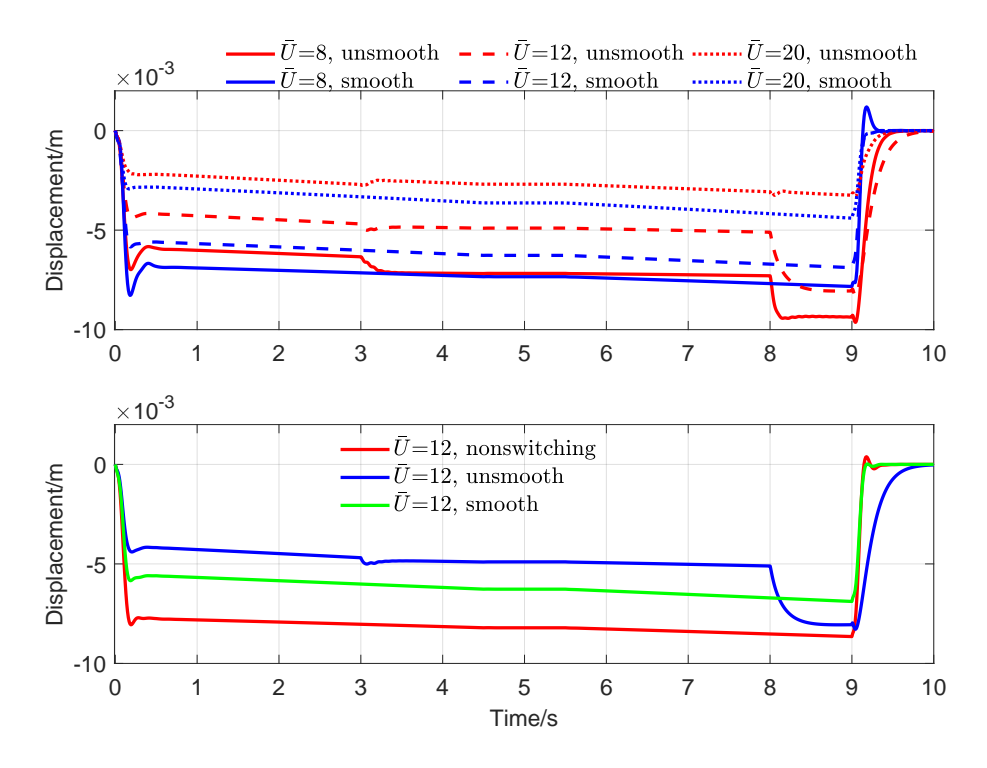


Figure 3.43: Upper: comparison at wing tip with smooth/un-smooth switching controller; Lower: comparison at wing tip with three control methods

In the upper sub-figure of Figure 3.43, smooth (blue) and un-smooth (red) responses of bending displacement at wing root are shown. At switching event $T_1=3s$, controller 1 is switched to controller 2, and the sudden changes of un-smooth controllers cause abrupt jumps for all three different ICC conditions. On the other hand, the smooth-switching LPV controllers enforce smooth output responses, with slightly increased bending displacement as a minor penalty on system performance. Similar behaviors can be observed at the switching event $T_2=8s$. Another trade-off relationship can be observed from output responses. Different ICC constraints will influence the optimal achievable system performance. With larger control input, the bending displacements can be suppressed even further, however, when $\bar{U}>12$, much more control effort will be consumed to further improve system performance, as seen from control responses in Figures 3.44-3.49. Therefore, the hard constraint on control input is chosen as $\bar{U}=12$, in order to achieve acceptable performance and energy saving.

The lower sub-figure of Figure 3.43 shows the comparison of wing tip responses with three different controllers. As shown, all three control methods are able to stabilize and suppress bending

displacements for the entire flight speed envelope. It can be further observed that both smooth and un-smooth switching LPV controllers produce a smaller magnitude of bending displacements than the non-switching LPV controller, and this is achieved by relaxing the PLMI conservativeness and enforcing the optimal performance on each subregion. However, un-smooth switching LPV leads to undesirable jump on the bending displacement at wing tip, which is effectively smoothened by the proposed smooth-switching LPV controller.

The responses of control input also demonstrate the effectiveness of the proposed control method. In the upper sub-figures of Figures 3.44-3.49, the un-smooth control design results in control inputs exhibiting sharp jump at the switching events, but the proposed smooth-switching LPV controllers effectively remove these jumps. Especially at switching event $T_2 = 8s$, un-smooth switching controller commands the control surfaces to deflect in opposite directions within a very short time, which imposes a severe capacity burden on the actuator. Smooth-switching controller, on the other hand, allocates the deflection angles of control surfaces with smooth control commands when switching occurs. In the lower sub-figures, control commands of three control methods are compared. Unlike switching LPV control, non-switching LPV control results in a conservative control input of a very small magnitude due to the conservativeness introduced in PLMIs. Un-smooth switching LPV control is able to relax conservativeness and assign slightly larger control energy, leading to improved vibration suppression of bending displacements. However, by minimizing control gain differences in the optimization cost function, smooth-switching LPV control can result in much smoother responses with slight degradation on system performance, which is still better than the performance of the un-smooth switching LPV control.

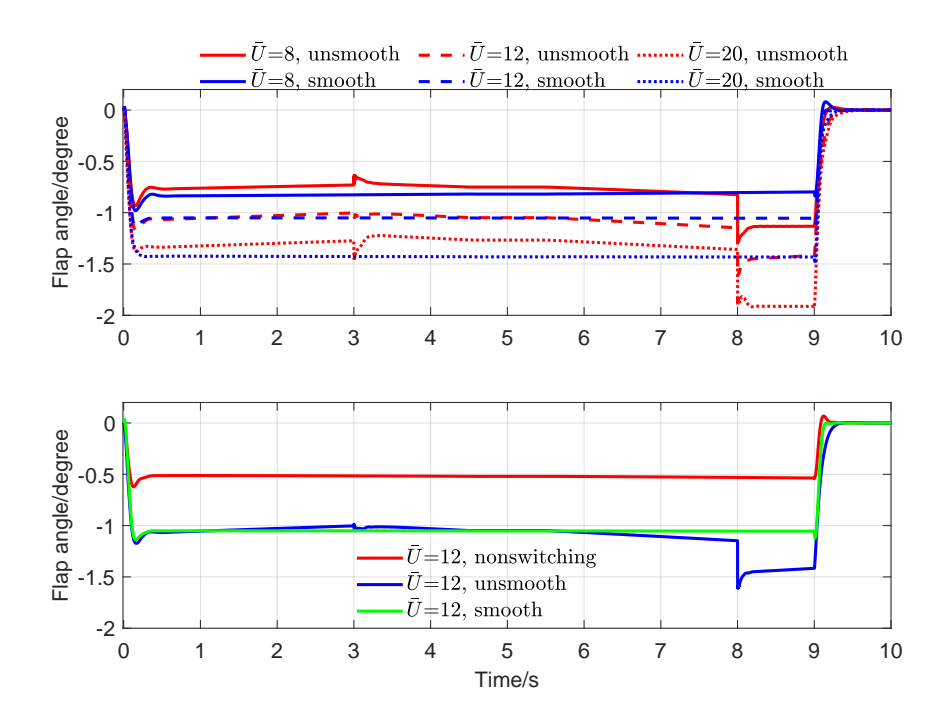


Figure 3.44: Upper: control 1 responses comparison with smooth/un-smooth switching controller; Lower: control 1 responses comparison with three control methods

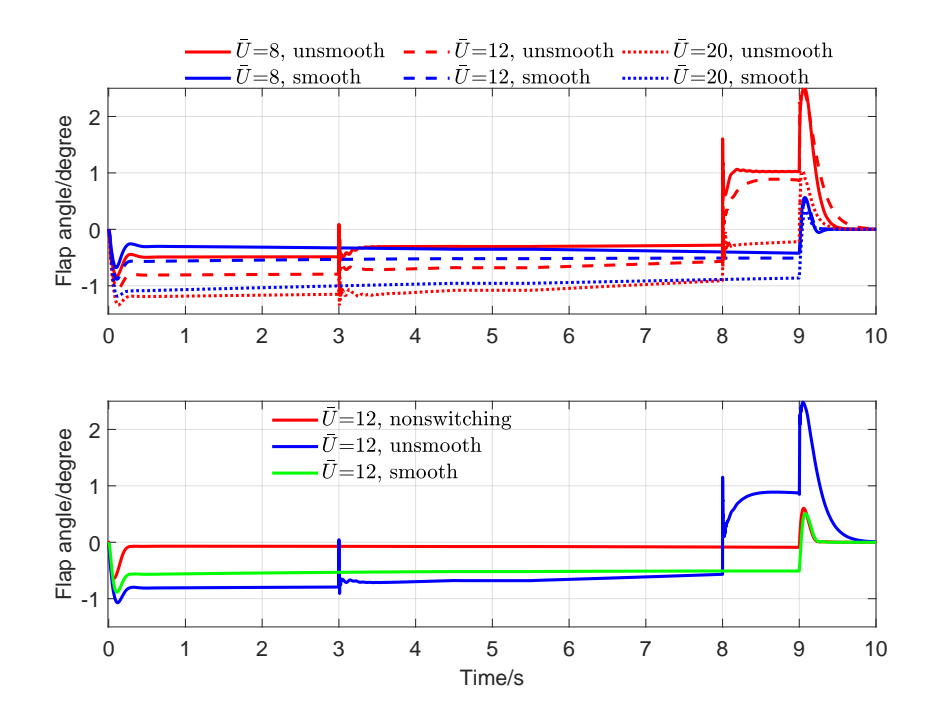


Figure 3.45: Upper: control 2 responses comparison with smooth/un-smooth switching controller; Lower: control 2 responses comparison with three control methods

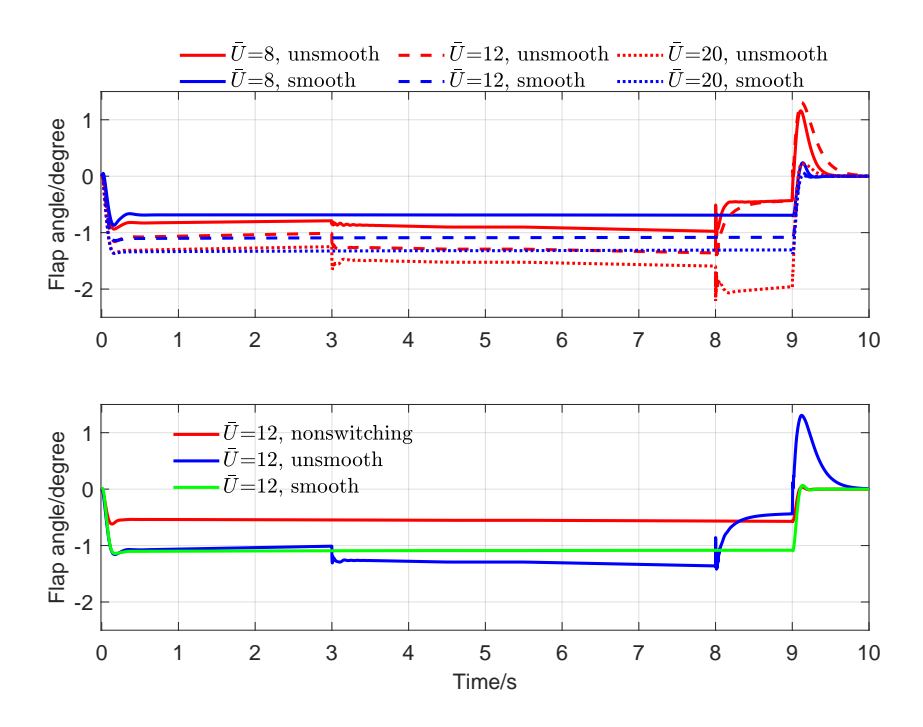


Figure 3.46: Upper: control 3 responses comparison with smooth/un-smooth switching controller; Lower: control 3 responses comparison with three control methods

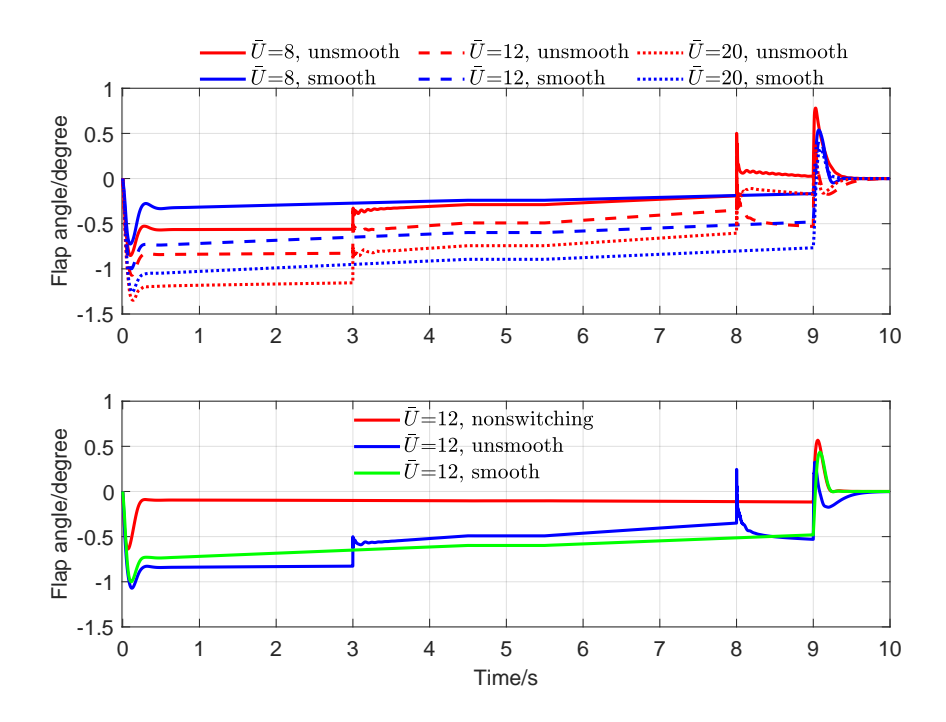


Figure 3.47: Upper: control 4 responses comparison with smooth/un-smooth switching controller; Lower: control 4 responses comparison with three control methods

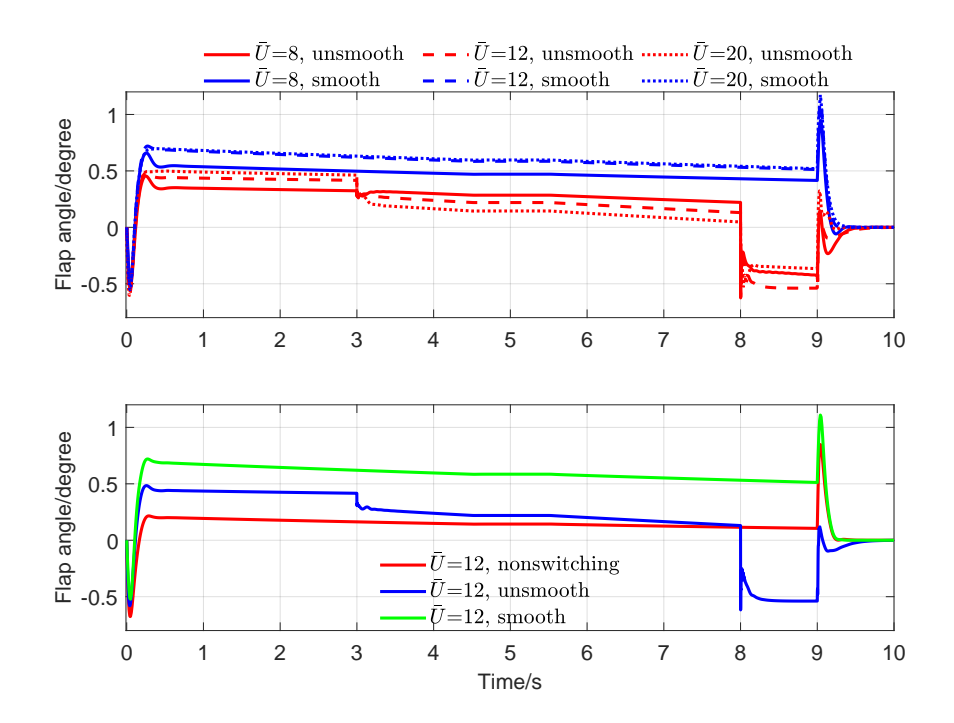


Figure 3.48: Upper: control 5 responses comparison with smooth/un-smooth switching controller; Lower: control 5 responses comparison with three control methods

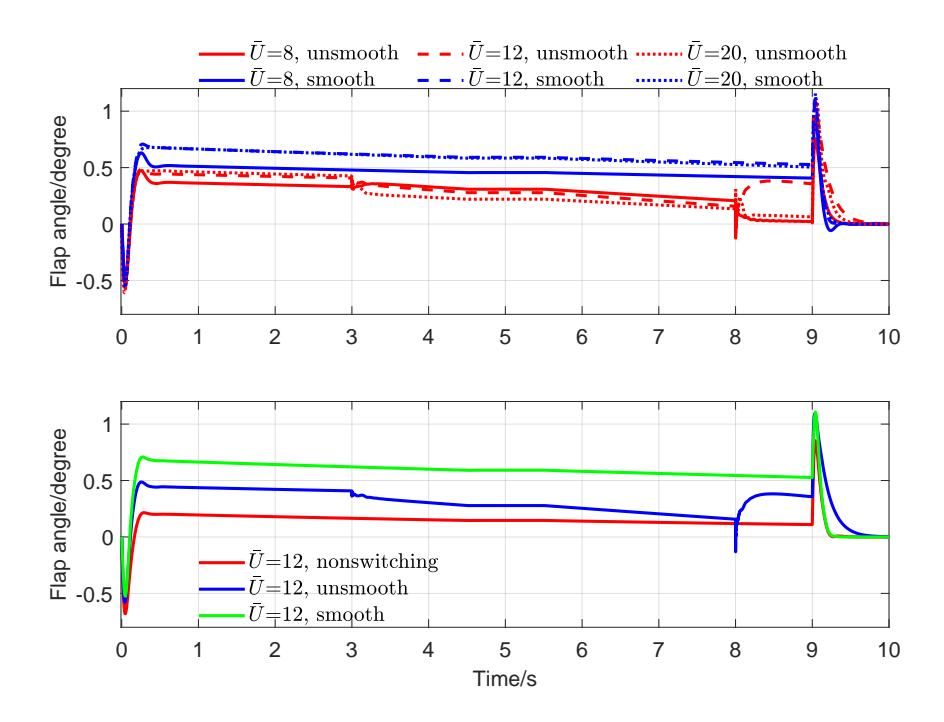


Figure 3.49: Upper: control 6 responses comparison with smooth/un-smooth switching controller; Lower: control 6 responses comparison with three control methods

3.3 Numerical Examples for Sequential Design

In order to demonstrate the feasibility of the proposed method, two examples will be given and results will be compared with simultaneous design, as well as non-switching LPV design. Furthermore, the interpolation rate β and scheduling parameter variational rate are varied to study their ultimate influence to closed-loop \mathcal{H}_{∞} performance γ .

The formulated PLMIs are of infinite-dimension, and they can be transformed into finite-dimensional by means of various relaxation methods. To numerically tackle this optimization problem, coefficient check in multi-simplex domain by Polya theorem [19] is applied. Gridding technique [68] or other relaxation methods [73] can also be potentially used to tackle this problem. Some software is available to manipulate the PLMIs and handle the convex optimization. In this study, The PLMIs are solved by using the parser ROLMIP [93] and YALMIP [76], which work jointly with optimization tool SEDUMI [77]. Computation is operated using a computer with Intel core i7-4770T CPU @2.50 GHz and 16 G RAM, and computation times of three design approaches are obtained by running *tic* and *toc* commands in MATLAB, and they are compared to show computational efforts.

3.3.1 Example 1

The LPV model in reference [94] is revisited to illustrate the feasibility of the proposed sequential design approach of smooth switching LPV controllers. Consider the LPV model with affine dependency of one-dimensional scheduling parameter θ ,

$$A(\theta) = \begin{bmatrix} 25.9 - 60\theta & 1 \\ 20 - 40\theta & 34 - 64\theta \end{bmatrix}, B_u = \begin{bmatrix} 3 \\ 2 \end{bmatrix},$$

$$B_w = \begin{bmatrix} -0.03 \\ -0.47 \end{bmatrix}, C = \begin{bmatrix} 1 & 1 \\ 0 & 0 \end{bmatrix}, D_w = \begin{bmatrix} 0 \\ 0 \end{bmatrix}, D_u = \begin{bmatrix} 0 \\ 1 \end{bmatrix}.$$

The time-varying scheduling parameter $\theta(t)$ is bounded as $0 \le \theta(t) \le 1$, and its variational rate is bounded as $-v \le \dot{\theta}(t) \le v$. The domain of Θ is assumed to be partitioned as three

Table 3.2: Comparison of three different design methods in each design iteration

	non-switching	sequential	simultaneous	
No. LMIs 8		8	27	
No. variables	14	14	42	
tic/toc time (s)	0.23	0.21	0.39	

overlapping subregions of θ range, [0,0.4], [0.3,0.7], [0.6,1], and variational rate bound is kept as not divided. Controller decision variables $P(\theta)$ and $Z(\theta)$ are assumed to be in the affine form as $P(\theta) = P_0 + P_1\theta$, and $Z(\theta) = Z_0 + Z_1\theta$. Controller decision variables P_0, P_1, Z_0, Z_1 are sought to minimize the \mathcal{H}_{∞} performance index γ , while PLMIs formulated by different design approaches are satisfied. In the non-switching LPV control design, a single γ on entire scheduling parameter region is minimized. In the simultaneous design approach, γ_1, γ_2 and γ_3 are associated with three subregions, and $\max\{\gamma_1, \gamma_2, \gamma_3\}$ is minimized in objective function. However, γ_1, γ_2 and γ_3 are minimized sequentially on each subregion by sequential design approach.

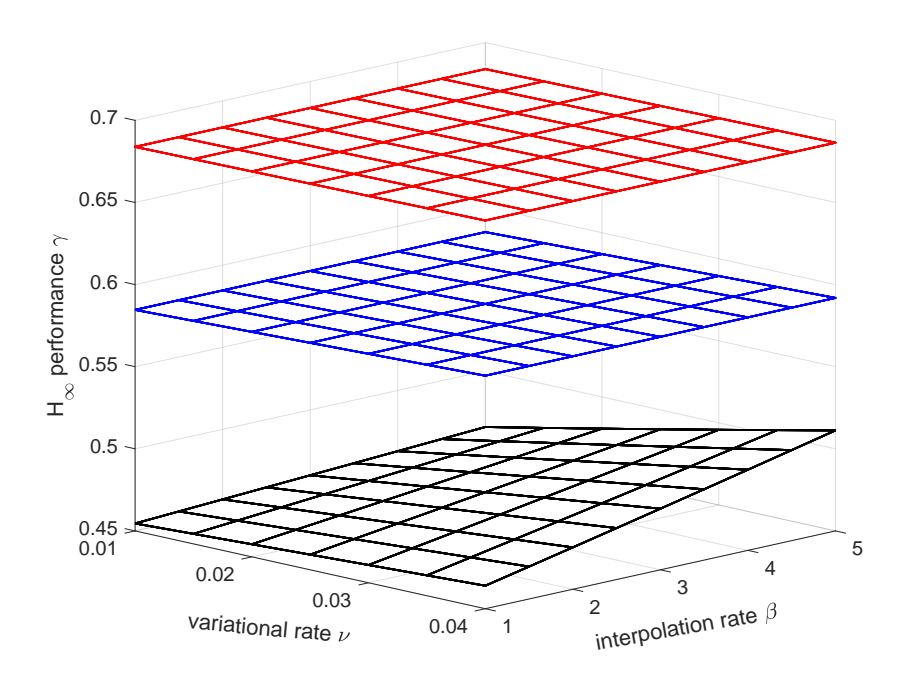


Figure 3.50: γ_1 obtained by sequential (black), simultaneous(blue) and non-switching(red) design approach

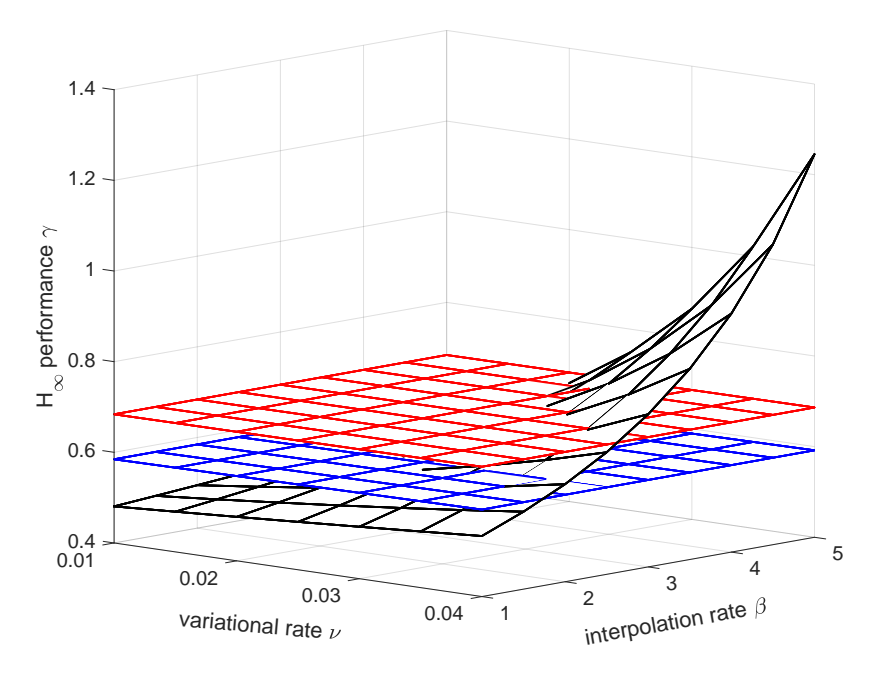


Figure 3.51: γ_2 obtained by sequential (black), simultaneous(blue) and non-switching(red) design approach

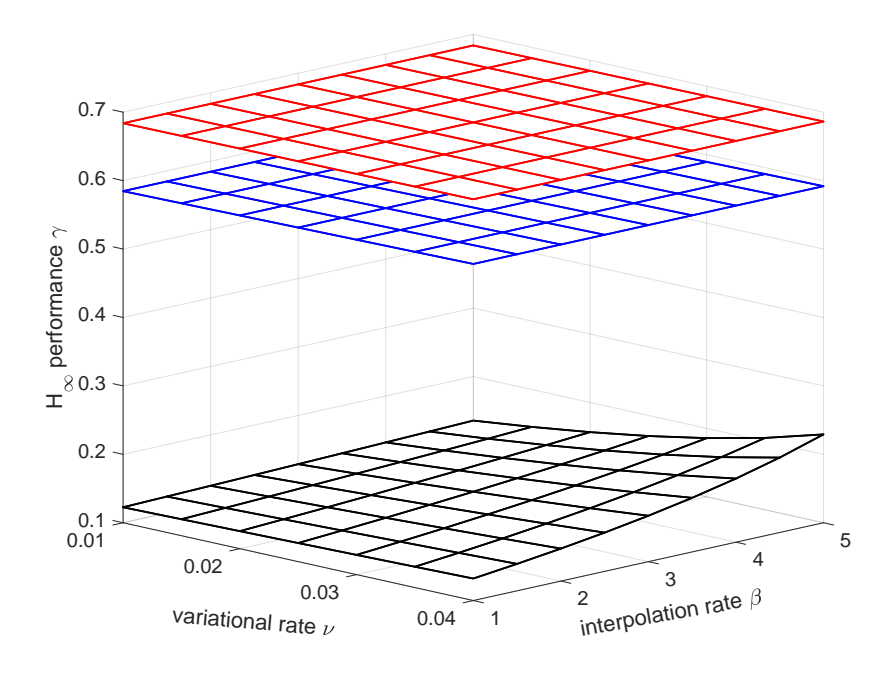


Figure 3.52: γ_3 obtained by sequential (black), simultaneous(blue) and non-switching(red) design approach

With given $\lambda_0=2$, interpolation rate β and variational rate ν are varied to get insight of how they influence the \mathcal{H}_{∞} performance γ_1, γ_2 and γ_3 plotted in Figures. 3.50-3.52. The non-switching design result is plotted as red surface, while γ_1, γ_2 and γ_3 obtained by simultaneous and sequential designs are plotted in blue and black surfaces, respectively.

It can be observed that, both switching design methods lead to an improved closed-loop system \mathcal{H}_{∞} performance over non-switching LPV control. In most area of shown region, sequential design approach results in a smaller γ in magnitude than simultaneous design approach on three subregions, indicating design conservativeness can be relaxed in these cases. In the situation that large variational rate ν and aggressive interpolation rate β , switching smoothness between adjacent controllers will be improved, but conservative constraints of additional relative σ -stability will be introduced. As a consequence, \mathcal{H}_{∞} performance by sequential design is worse than that of simultaneous design. Thus, there exists a trade-off relationship between system performance and switching smoothness represented by interpolation coefficient. Performance degradation is a sacrifice to guarantee the robust performance by interpolated controller variables. In other words, the limitation of this method is that tuning work may be needed if optimizing system performance is the objective rather than reducing design complexity.

The time-domain responses of three different design approaches have been simulated and compared in Figure 3.53. System disturbance is set as w(t)=0.5 for $t\in[0,4.5]$ second and w(t)=0 for t>4.5 second. Scheduling parameter trajectory is set as $\theta(t)=0.3+0.1t$. In the sequential design approach, interpolation rate and variational rate are chosen as $\beta=2$ and $\nu=0.02$, respectively. It is easy to observe that switching controllers by the sequential design lead to state responses with smaller signal norms than these from simultaneous design approach and nonswitching control. This conclusion matches well with these results in Figures 3.50-3.52 that sequentially designed switching controller leads to smaller \mathcal{H}_{∞} norm. Moreover, simultaneous design results in jumps at switching instants of t=1 and t=4 second, whereas the proposed sequential design leads to smooth responses because controller gains are interpolated over overlapped subregions. After t=4.5 second when system disturbance disappears, states are regulated to 0 by all three

controllers.

Table 3.2 summarizes the number of relaxed LMIs and controller decision variables and computation time by three different design approach. Non-switching design approach deals with fewer LMIs and search for minima in a smaller space of variables, thus less computational time is utilized in the optimization. However, the optimized \mathcal{H}_{∞} performance is worse than both switching LPV control design approaches. Sequential design iterates the optimization on each individual subregion sequentially, thus in each design iteration, sequential design deals with same amounts of LMIs and variables with non-switching design, but within smaller size of subregion. The simultaneous design approach is imposed with all LMIs and variables, thus has the largest computational complexity. Note that in this example, total solving time of sequential design is slightly larger than simultaneous design approach, and it can be possibly reasoned that optimization problem formulated by low-order system can still be well handled by the simultaneous design approach.

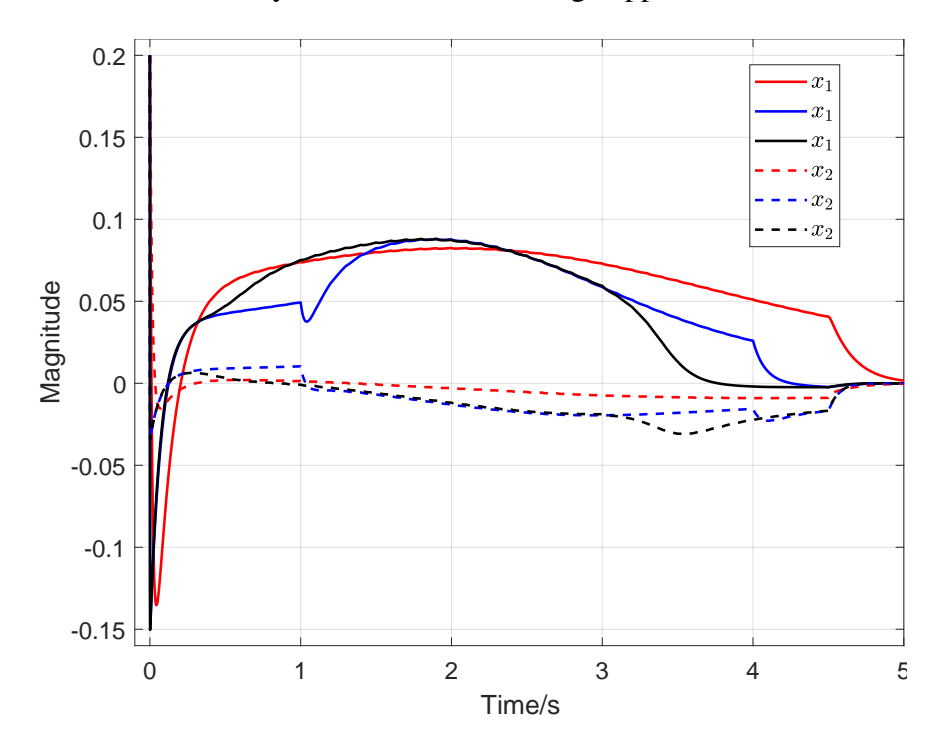


Figure 3.53: Closed-loop system states responses by sequential (black), simultaneous(blue) and non-switching(red) design approaches

3.3.2 Example 2

The $A(\theta)$ matrix in Example 1 is modified into two-dimensional affine dependency of θ_1 and θ_2 , while other system matrices are unchanged. The domains of two scheduling parameters are $\Theta_1 = [0, 10]$, $\Theta_2 = [0, 7]$, and they are respectively divided into [0, 7], [5, 10] and [0, 5], [3, 7]. With given $\lambda_0 = 0.1$ and division of scheduling parameter domain, three different design approaches are conducted again to compare optimized \mathcal{H}_{∞} performance and computational efforts.

$$A(\theta) = \begin{bmatrix} 20 - 2\theta_1 & 16\\ 12 & 8 - 6\theta_2 \end{bmatrix}$$

Similar to Example 1, controller decision variables $P(\theta)$ and $Z(\theta)$ are assumed to be in the affine form as $P(\theta) = P_0 + P_1\theta_1 + P_2\theta_2$, and $Z(\theta) = Z_0 + Z_1\theta_1 + Z_2\theta_2$. On each subregion, controller decision variables $P_0, P_1, P_2, Z_0, Z_1, Z_2$ are sought to minimize the \mathcal{H}_{∞} performance index γ , while PLMIs formulated by different design approaches are satisfied.

The optimized system performance indexes on subregions by sequential design, simultaneous design and non-switching design are plotted by black, blue and red surfaces in Figures. 3.54-3.57. Non-switching control design minimizes \mathcal{H}_{∞} performance γ over entire subregion. In the simultaneous design approach, $\gamma_{11}, \gamma_{12}, \gamma_{21}$ and γ_{22} are associated with four subregions, and $\max\{\gamma_{11}, \gamma_{12}, \gamma_{21}, \gamma_{22}\}$ is minimized in objective function. However, they are minimized sequentially on each subregion by sequential design approach. It can be seen that in most cases, sequential design approach obtains smaller γ magnitudes, in other words, better system performance than simultaneous design and non-switching LPV control design.

From simulation results, the conservativeness of high-dimensional optimization in simultaneous design can be relaxed by iterating low-dimensional optimization in the sequential design approach. However, in the scenario of aggressive interpolation rate β and large variational rate ν , sequential design provides very conservative σ -stability and hence worse system performance is obtained by sequential design approach. This surface gives insight of how σ -stability will trade-off with \mathcal{H}_{∞} performance in switching LPV control, and gives hint on how to further tune subregion division

and interpolation rate.

Table 3.3 summarizes the number of LMIs and controller matrices variables and computational time by three different design approach. Both switching LPV control design approaches sacrifice more solving time to obtain better system performances. In the simultaneous design, much more constraints than sequential design are imposed, thus more solving time are taken to obtain an optimal solution. However, the resulting system performance is contrarily worse than that of sequential design approach if interpolation coefficient is properly chosen. In this example with 4 subregions formed by two-dimensional scheduling parameters, sequential design approach exceeds simultaneous design approach in terms of computational efforts and achieved system performance.

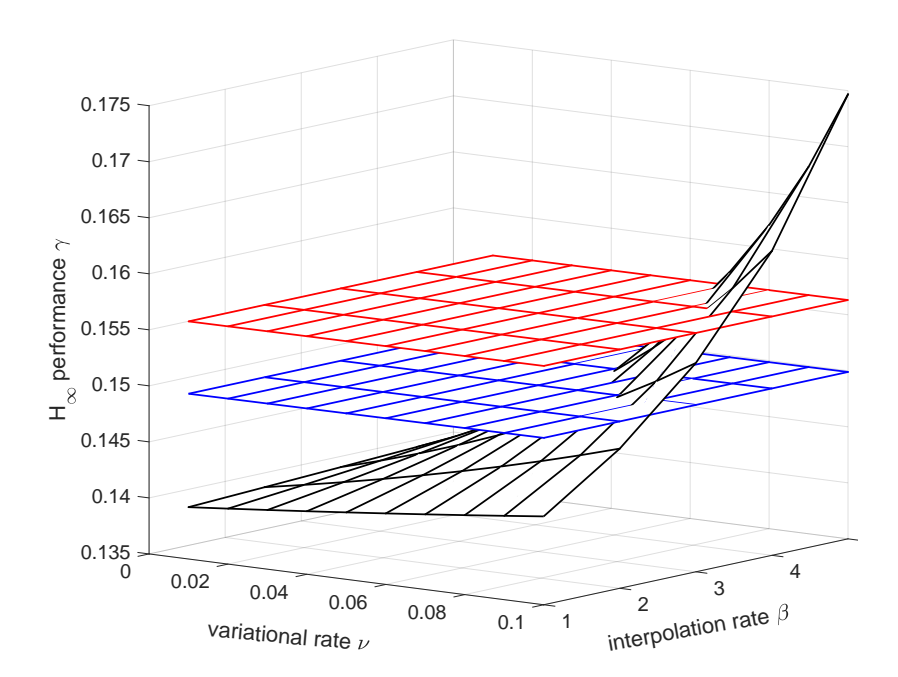


Figure 3.54: γ_{11} obtained by sequential(black), simultaneous(blue) and non-switching(red) design approach

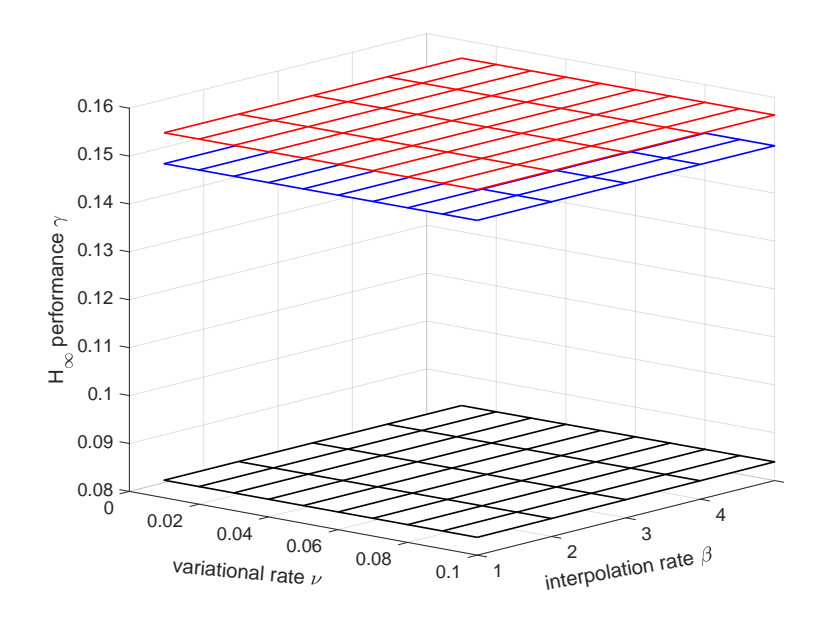


Figure 3.55: γ_{12} obtained by sequential(black), simultaneous(blue) and non-switching(red) design approach

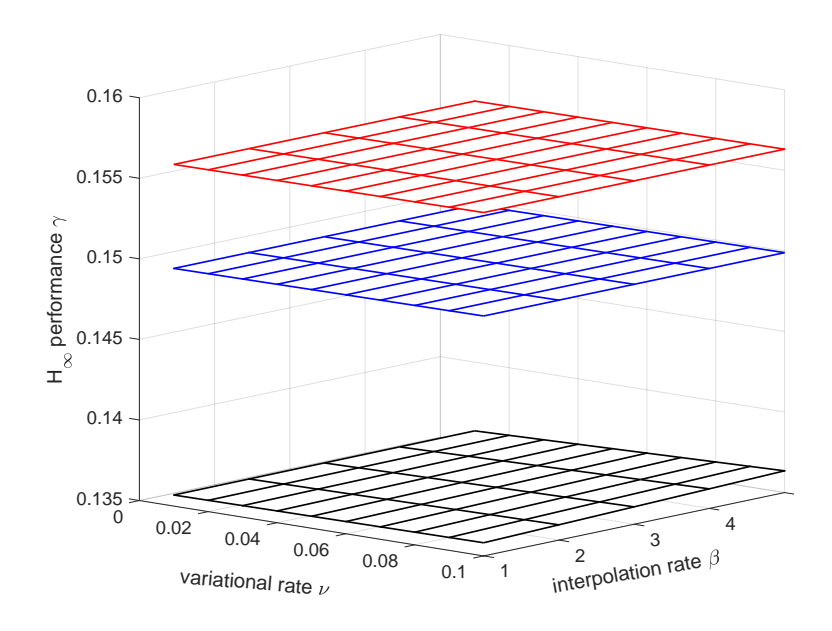


Figure 3.56: γ_{21} obtained by sequential(black), simultaneous(blue) and non-switching(red) design approach

Table 3.3: Comparison of three different design methods in each design iteration

	non-switching	sequential	simultaneous	
No. LMIs	40	40	192	
No. variables	o. variables 21		84	
tic/toc time(s)	0.40	0.47	3.48	

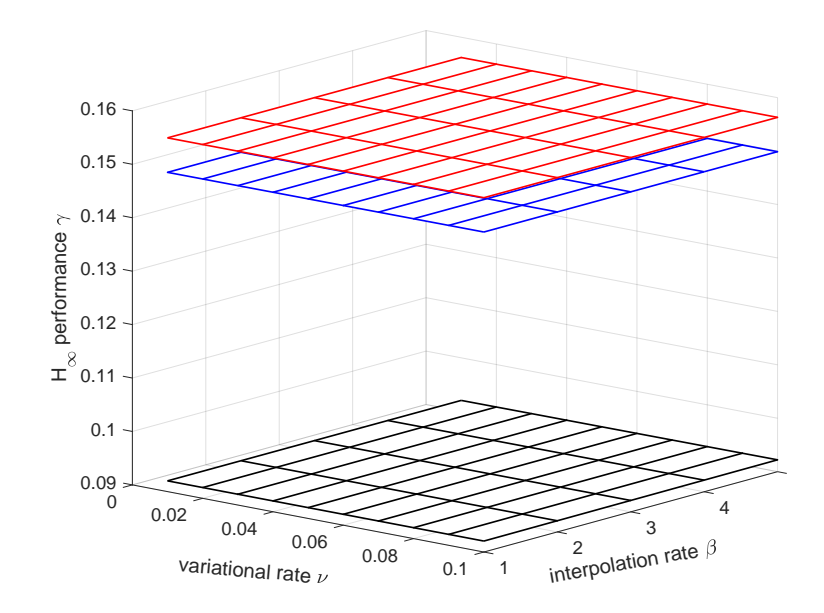


Figure 3.57: γ_{22} obtained by sequential(black), simultaneous(blue) and non-switching(red) design approach

CHAPTER 4

OPTIMAL SENSOR PLACEMENT

4.1 Introduction

A light and flexible airplane wing is benefited from structure flexibility, and it features with high aerodynamic and fuel efficiency. However, the structure flexibility poses a great challenge to control system design for active vibration suppression. Structural control community has made various attempts on developing effective control techniques in order to suppress vibration, avoid structural failure and enlarge flight stability margin. Among control system components, positioning and selection of sensors play a role of great importance but have not been paid enough attention. Sensor placement needs to be integrated into both modeling and control design, and will ultimately influence state observability, as well as the achievable closed-loop system performance.

As a large-scale structural system, a flexible wing exhibits coupled aero-structure dynamics at various flight conditions [87, 88]. Multiple nodal points along the wing span are often selected to get insight on overall structural behavior. Moreover, multiple sensors are needed to be installed at different locations to provide feedback information for active vibration control. Sensor positioning on a large-scale flexible wing structure is even more complex. Sparse density of measured locations cannot capture all vibrational modes and very likely lead to no feasible solution for an output feedback-based controller. On the contrary, too dense of sensor placement will increase both model and controller dimensions, which dramatically increases computational complexity and potentially limits achievable system performance. These practical demands call for a systematic method to compute, evaluate and determine optimal number of sensors and their placement.

In this dissertation, we investigate the problem that with a given range of varying flight speed, how to determine sensor position within a limited number of feasible locations to achieve optimal vibration suppression [95]. Known as part of input/output selection problem, sensor positioning together with actuator positioning have been widely studied in flexible structures [96, 97, 98].

Readers are suggested to the reference [97] for more detailed survey. These methods are mostly based on quantitative measures for state controllability, observability or efficiency of manipulation, estimation. These measures can be connected well with the energy stored by structural system, supplied by actuators or being supplied to sensors. However, these methods are mostly established for linear time-invariant (LTI) systems, which have static vibration frequency and damping, and hence static vibration nodes. For a BWB airplane flexible wing, it has been demonstrated that flexible modes will vary under different flight conditions. Hence, the LTI framework is not capable of capturing the mode dynamics, thus a new framework that is able to handle varying modes is needed.

Linear parameter-varying (LPV) modeling and control have been demonstrated as an effective alternative for active vibration suppression for a BWB airplane flexible wings [88, 87, 62, 35, 99]. The LPV model is able to capture mode dynamics with varying flight condition and depict varying input-output characteristics between flap deflection angles (control surfaces) and wing bending displacements (controlled outputs). The LPV controller then schedules the control gains according to the measured real-time flight condition to achieve specific system performance. By this way, the controller synthesis is well defined as an optimization problem, with performance-associated index as objective function and a set of PLMIs (Parametric Linear Matrix Inequalities) derived from specific system performance requirements.

The LPV framework is adopted in this study to numerically analyze how a sensor selection and its location influence the closed-loop system performance. To the best knowledge of authors, such an attempt has never been made in structural control literature. With \mathcal{H}_2 LPV controllers, different combinations of sensor locations are evaluated in terms of the guaranteed closed-loop system performance. Because the control input, e.g. flap angle, is physically limited, ICC (Input Covariance Constraint) is applied to controller synthesis conditions. Under this constraint, the worst-case \mathcal{H}_2 performance within given range of flight speed is treated as the evaluation index for achievable system performance, which guarantees the performance under any possible flight condition within the flight envelope.

4.2 Problem formulation of sensor placement

Revisit the LPV model of the BWB airplane flexible wing. for simplicity, we consider the \mathcal{H}_2 performance of sensor placement, thus only \mathcal{H}_2 performance of signal pair (w, z) is considered.

$$\dot{x}_p(t) = A(\theta(t))x_p(t) + B_1(\theta(t))w(t) + B_2(\theta(t))u(t)$$

$$z(t) = C(\theta(t))x_p(t)$$

$$\bar{y}(t) = C_{\bar{y}}(\theta(t))x_p(t) + v(t)$$
(4.1)

where the external disturbance w(t) and measurement noise v(t) are assumed to be zero-mean, Gaussian white noise, but not necessarily stationary. They are also assumed as independent as

$$E\left\{w(s)w^{T}(t)\right\} = W(t)\delta(t-s), \quad E\left\{v(s)v^{T}(t)\right\} = V(t)\delta(t-s) \tag{4.2}$$

As shown in Figure. 4.1, the sensor location candidates are marked by triangles in red. It is assumed that bending displacements in z-direction can be measured by available sensors. All of these equally spaced locations together are selected as performance outputs to evaluate closed-loop \mathcal{H}_2 system performance. Some or all these candidate locations may be selected to install bending displacement sensors. For the given flight speed range, the question that how many candidates and what candidates group will lead to the optimal system performance, arises as the objective of this study.

Note that $\bar{y}(t) = [\bar{y}_1(t), \bar{y}_2(t), \cdots, \bar{y}_m(t), \cdots, \bar{y}_M(t)]$, where M = 9 is the total number of sensor location candidates. All available measurement output $\bar{y}(t)$ can be derived from $C_y(\theta)x_p$, where

$$C_{ar{y}}(heta) = \left[egin{array}{c} C_1(heta) \\ dots \\ C_m(heta) \\ dots \\ C_M(heta) \end{array}
ight].$$

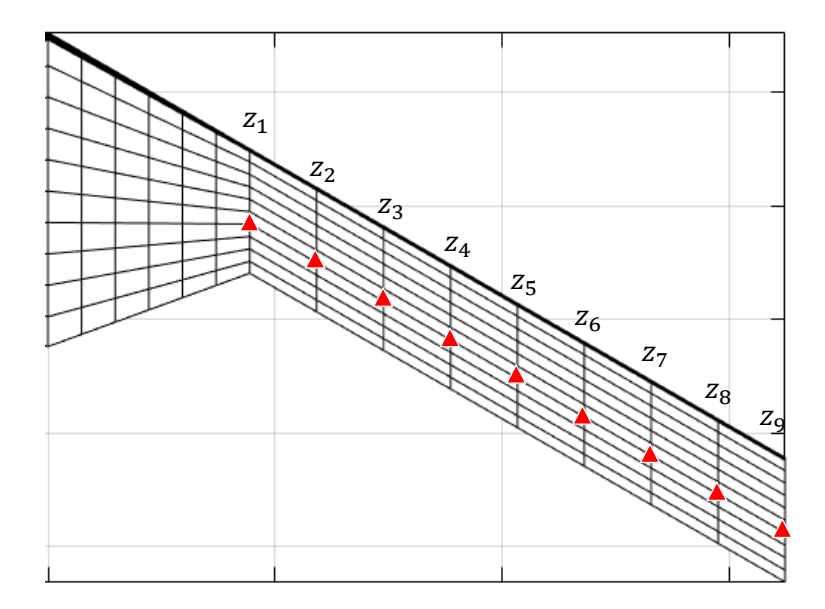


Figure 4.1: Sensor location candidates

The selected subset of measured output y(t) is obtained by stacking the chosen measurement y_m , then $N \leq M$ measured outputs are obtained by C_y as

$$C_y = \left[\begin{array}{c} C_{y1}(\theta) \\ \vdots \\ C_{yN}(\theta) \end{array} \right].$$

Therefore, there is a total of $C_M^N = \frac{M!}{N!(M-N)!}$ combinations to choose N sensor locations from M candidate locations.

Suppose the projection operator $P_N \in R^{N \times M}$ maps the selected sensor subset from the entire set of available sensors, where the m^{th} column is 1 for the selected m^{th} sensor and the column is 0 if associate sensor is not chosen. Then the selected sensor output can be expressed by

$$y = P_N C_{\bar{y}}(\theta) x_p(t) + P_N v(t). \tag{4.3}$$

The projected measurement noise has the variance as

$$E\left\{ \left[P_N v(s)\right] \left[P_N v(t)\right]^T \right\} = P_N V(t) P_N^T \delta(t-s)$$

Using the selected sensor measurement, the dynamic output-feedback (DOF) LPV controller $K(\theta)$ is expressed as

$$K(\theta) : \begin{cases} \dot{x}_K = A_K(\theta)x_K + B_K(\theta)y \\ u = C_K(\theta)x_K + D_K(\theta)y \end{cases}$$

$$(4.4)$$

Recall the definition of \mathcal{H}_2 performance of LPV system, defined from $\bar{w}=[w(t);v(t)]$ to z(t), is utilized to assess the closed-loop performance against external disturbance. Let $T_2(\theta,s):=T_{z\bar{w}}(\theta,s)$ be the parameter-dependent transfer function from $\bar{w}(t)$ to z(t), and if the system pair $(A_{cl},B_{cl},C_{cl},0)$ is stable, the \mathcal{H}_2 norm $||T_2||_2^2$ can be obtained by minimizing traceW while subject to the following PLMIs over the region $(\theta,\dot{\theta})\in\Theta\times\Lambda$,

$$\begin{bmatrix} -\dot{P}_2 + A_{cl}P_2 + (*) & B_{cl} \\ * & -I \end{bmatrix} < 0, \tag{4.5}$$

$$\begin{bmatrix} W & C_{cl,2}P_2 \\ * & P_2 \end{bmatrix} > 0, \tag{4.6}$$

The optimal sensor placement by selecting from available sensor set is actually deciding the projection operator. By this step, we are ready to give the problem formulation of optimal sensor placement. The \mathcal{H}_2 performance of closed-loop LPV system minimized by the projection operator P_N in dynamic output-feedback LPV control.

$$\min_{P_N} \min trace(W) \tag{4.7}$$

subject to (4.5) and (4.6).

This optimization problem is well-known as an NP hard problem [100, 101], which involves hybrid optimization of integer variable (binary optimization) and real matrix variables(control design).

4.3 Simulation results by global search

4.3.1 Simulation results

Following the same \mathcal{H}_2 LPV control design procedure, different combinations of sensor location candidates are explored to calculate the achievable guaranteed system performance. The observability of system pair $(A(\theta), C_y(\theta))$ is firstly checked at gridded points over the scheduling parameter range. Those sensor combinations which cannot be observed at all gridded points are considered as unobservable, and hence they are removed from controller synthesis.

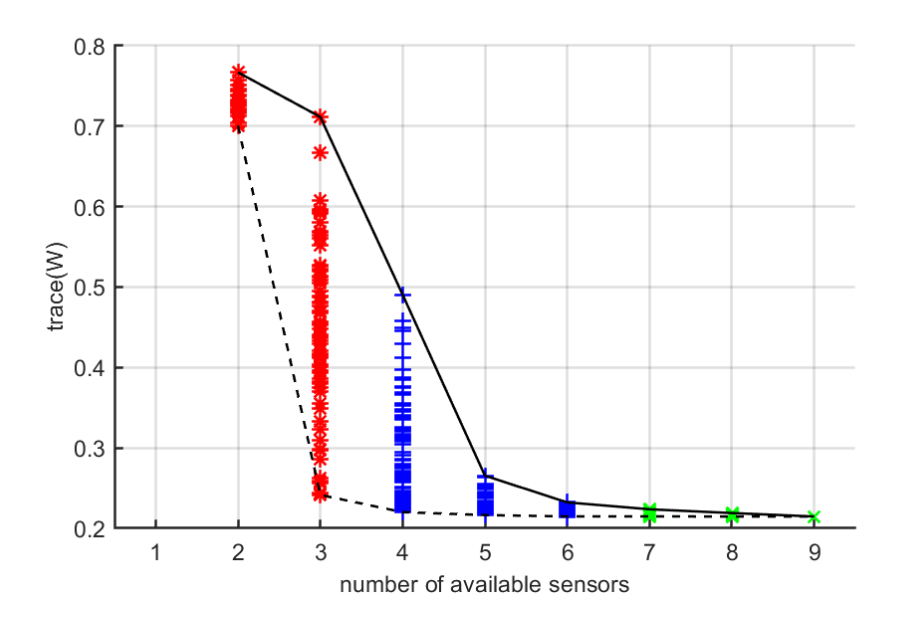


Figure 4.2: trace(W) versus the number of available sensors, U=6

Figures. 4.2 and 4.3 show the \mathcal{H}_2 system performance trace(W) (y-axis) when limited number of sensors (x-axis) are used. Using one sensor and some combinations of two sensors are determined unobservable, thus feasible \mathcal{H}_2 LPV DOF controller cannot be designed. When $N \geq 3$ number of sensor locations are available, the system matrices pairs are checked as observable for entire flight speed range. As a result, there is no data points shown at N=1, and only a few data points can be seen at N=2, whereas $\frac{M!}{N!(M-N)!}$ data points are obtained for other cases.

Note that weighting matrix Q is chosen as $100 \times \mathbf{I}$ for evaluating all bending displacements equally. Figures 4.2 and 4.3 are corresponding to two different ICC conditions for all control

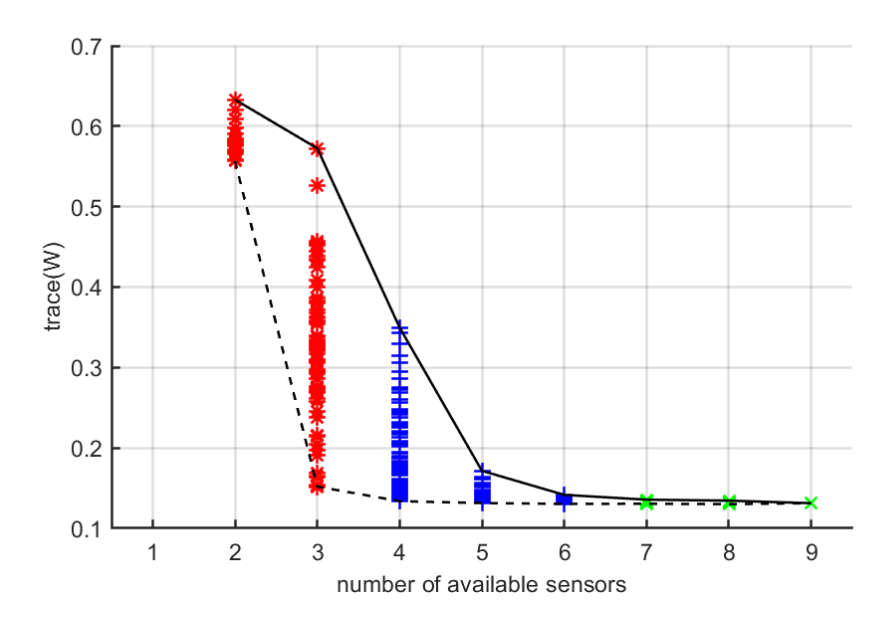


Figure 4.3: trace(W) versus the number of available sensors, U=8

surfaces U=6,8. It is apparent that, when bending displacement sensors are installed at more candidate locations, the upper bound of achievable system performance trace(W) becomes smaller, which indicates that improved system performance can be achieved. Moreover, the solid line and dash line are plotted by connecting the best and worst performance of each combination group with available sensor number. The variance trace of system performance is shrinking and converging as available sensor number increases. When sensor number is plenty enough, system states can be well recovered and vibration behaviors within entire flight envelop can be well handled. This is simply due to that with more sensors more useful information can be accessible for feedback control.

Furthermore, when large control authority is allowed, the achievable system performance trace(W) is suppressed further, indicating better system performance can be achieved. The combination candidates with the best system performance for any N number of sensor candidates group are summarized in Table 4.1. Note that, if only one sensor is used, there is no feasible sensor due to the unobservability.

4.3.2 Discussion

As shown in Figures. 4.4 and 4.5, LTI \mathcal{H}_2 controllers with ICC condition U=8 are also designed at gridded flight speed $\theta=115,125$ m/s, and a set of sensor location combinations are globally searched to find optimal sensor placement. The optimal group of sensor locations is found varying with different flight speed. Thus, sensor positioning determined by following conventional LTI approach cannot produce optimal system performance within the flight speed range. For example, when N=7 number of sensors are used at $\theta=115$ m/s, the optimal sensor group is found as $\{1,2,4,5,6,7,8\}$. However, when flexible wing is flying at $\theta=125$ m/s, the optimal sensor location combination is found as $\{2,3,4,5,6,7,9\}$. This validates the fact that the optimal sensor combinations obtained under different specific flying conditions can vary, and hence may not be optimal for the entire flight envelope. On the contrary, the LPV approach considers the optimal sensor combination over the entire flight envelope, and looking for the optimal sensor positioning in terms of the best guaranteed system performance. This is the main advantage of the proposed LPV approach over the conventional LTI approach.

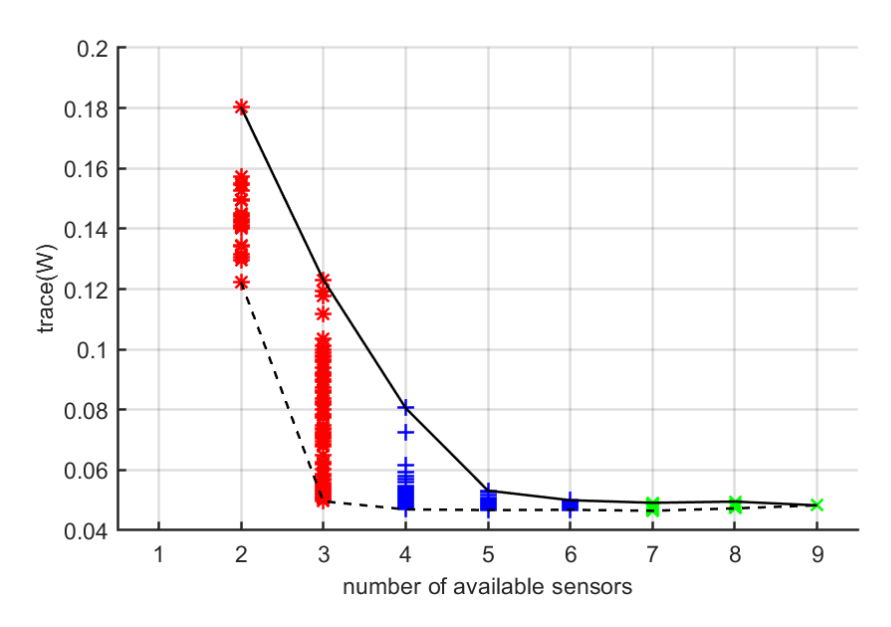


Figure 4.4: trace(W) versus number of available sensors, at flight speed 115 m/s

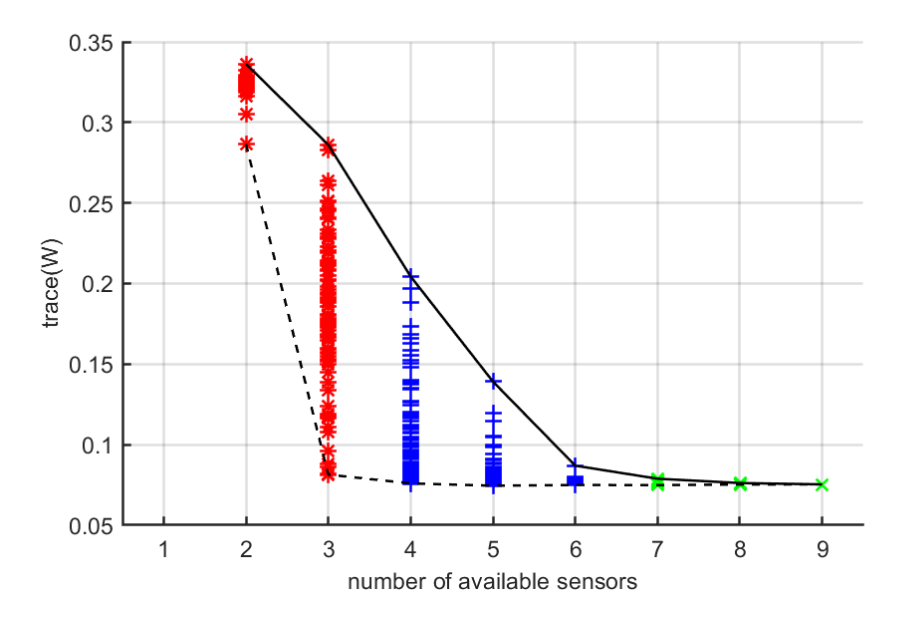


Figure 4.5: trace(W) versus number of available sensors, at flight speed 125 m/s

Table 4.1: Summary of optimal sensor candidate combinations

	LPV approach				LTI approach			
	U=6		U=8		$U = 8, \theta = 115$		$U = 8, \theta = 125$	
\overline{N}	sensor	trace(W)	sensor	trace(W)	sensor	trace(W)	sensor	trace(W)
1	_	_	_	_	_	_	_	_
2	{3,9}	0.7009	{3,8}	0.5569	$\{4, 5\}$	0.1223	{2,3}	0.2866
3	${3,4,5}$	0.2416	${3,7,9}$	0.1519	$\{2, 4, 5\}$	0.0496	$\{6, 7, 9\}$	0.0814
4	${3,5,7,9}$	0.2202	${3,4,7,8}$	0.1338	${3,5,7,9}$	0.0470	$\{5, 7, 8, 9\}$	0.0760
5	$\{1, 3, 4, 6, 8\}$	0.2165	$\{1, 2, 3, 4, 6\}$	0.1314	$\{1, 3, 5, 6, 9\}$	0.0467	${4,5,7,8,9}$	0.0745
6	$\{1, 2, 3, 4, 6, 9\}$	0.2148	{1,2,3,4,6,8}	0.1604	$\{1,4,5,6,7,9\}$	0.0468	$\{1, 2, 3, 6, 7, 9\}$	0.0750
7	$\{1, 2, 3, 4, 5, 7, 8\}$	0.2148	$\{1, 2, 3, 4, 5, 7, 9\}$	0.1306	$\{1, 2, 4, 5, 6, 7, 8\}$	0.0465	${2,3,4,5,6,7,9}$	0.0749
8	$\{1, 2, 3, 4, 6, 7, 8, 9\}$	0.2147	$\{1, 2, 3, 4, 5, 6, 8, 9\}$	0.1301	$\{1, 3, 4, 5, 6, 7, 8, 9\}$	0.0473	$\{1, 2, 4, 5, 6, 7, 8, 9\}$	0.0753
9	$\{1-9\}$	0.2147	$\{1-9\}$	0.1313	$\{1-9\}$	0.0483	$\{1-9\}$	0.0754

4.4 Sub-modular property of sensor placement problem

At different fixed flight condition, the contribution of each sensor to each vibration mode can be calculated based on [102]. The results are shown in the Figures 4.6-4.8.

It is easy to observe that the contribution of sensor to each mode follows an increasing trend, moreover, the contribution of each sensor will vary under different flight conditions. Even though the Gawronski's approximation method [102] can only be applied to stable LTI systems, the results indicate that the sensor placement has the sub-modular property.

In the searching of optimal sensor placement, global search is not an efficient approach, due to the NP hard nature of the hybrid optimization. However, the sub-modular property of the optimal sensor placement problem is uncovered and will be shown in this section.

The sub-modularity will be firstly reviewed and basic greedy algorithm will be introduced [100, 101]

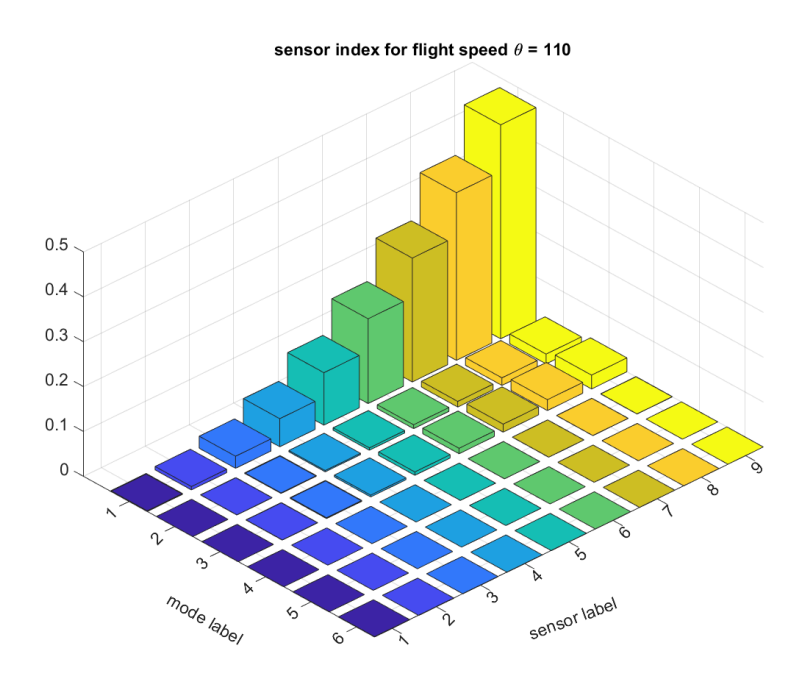


Figure 4.6: Sensor contribution to each vibration mode at flight speed 110 m/s

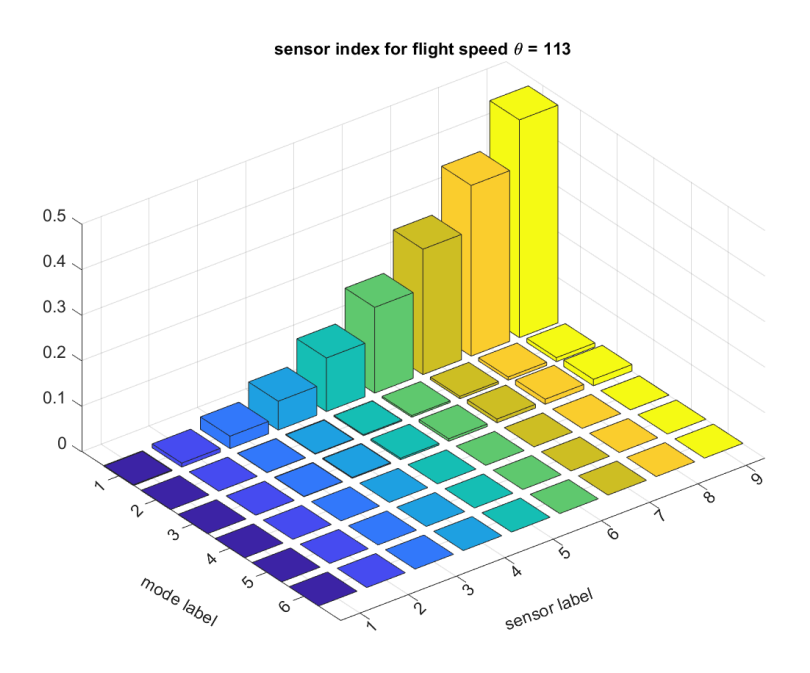


Figure 4.7: Sensor contribution to each vibration mode at flight speed 113 $\ensuremath{m/s}$

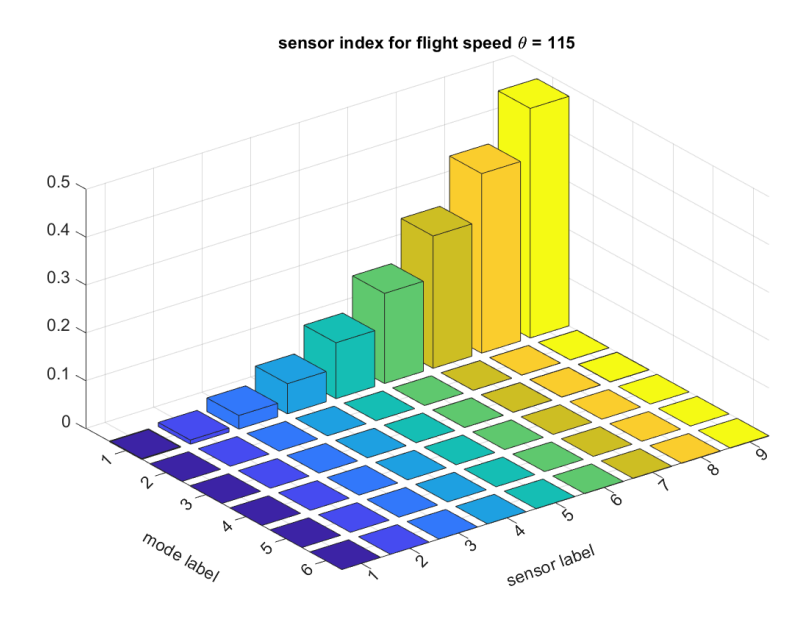


Figure 4.8: Sensor contribution to each vibration mode at flight speed 115 m/s

4.4.1 Set function and sub-modular property

Definition 1 (set function). Let S be a finite set and a set function over S assigns a value to every subset of S, i.e. $f(S): 2^S \to R$.

Definition 2 (submodularity). Let S be a finite set and 2^S denote power set. A set function $f: 2^S \to R$ is said to be submodular if and only if

$$f(A \cup B) + f(A \cap B) \le f(A) + f(B), \qquad \forall A, B \subseteq S. \tag{4.8}$$

For finite set S, this is equivalent to

$$f(A+j) - f(A) \ge f(B+j) - f(B), \quad \forall A \subseteq B \subseteq S, \forall j \in S \backslash B.$$
 (4.9)

In other words, the function f satisfies the diminishing increment property. The submodular function f is monotone if $f(A) \leq f(B), \forall A \subseteq B$. If a set function is submodular, then the contribution of any new element s to the set function value decreases when the set gets bigger.

Based on the definition of submodularity, we can conclude that if the optimal sensor placement problem with LPV DOF control is a submodular function, then performance increment by adding one sensor will decrease with the set size. This indicates that greedy algorithm has the potential to efficiently solve the sensor placement problem.

4.4.2 Greedy algorithm

Greedy algorithm utilizes a series of optimal local steps to conduct the optimization of NP hard problem. Instead of directly searching for a global solution, greedy algorithm searches towards minimum step by step. It has been proved that greedy algorithm has polynomial complexity and achieves to a sub-optimal solution within (1 - [1/e]) of the optimum [103].

$$\max_{|S| \le k} f(S) \tag{4.10}$$

The optimization of the set function f(S) over the set S with the size limit $|S| \le k$ is formulated as (4.10), then the basic greedy algorithm is given as Algorithm 1.

Algorithm 1: Greedy algorithm for set function optimization

Result: K_s

Step 1. Initialization:

$$s = 1, K_s = \{\}, S^s = S$$

while $s \leq k$ do

Step 2. Determine greedily the next element from residual set S^s :

$$k_s = \arg\max_{j \in S^s} f(S)$$

Step 3. Update the residual set S^s and selected set K^s

$$S^{s+1} = S^s \setminus k_s, \quad K^{s+1} = K^s \cup k_s, \quad s \leftarrow s+1$$

end

Optimal set variable K_s is searched within set S to maximize the set function f(S), and the maximum set size is k, residual set S^s and selected set K_s are updated in every step to maximize the updated set function. In this algorithm, Step 2 searches among the residual set for the element to be added into selected set, which will lead to the maximum value of set function f(S).

In the sensor placement problem, Algorithm 1 is customized to Algorithm 2 to select N number of sensors from set S of M number of sensors.

In this modified algorithm, the performance index trace(W) of \mathcal{H}_2 performance with LPV control is minimized by the set variable K_s and LPV controller $K(\theta)$. LPV controller is designed following the design technique discussed in Chapter 1. It is noted that the observability of sensor subset needs to be checked in Step 2, so that there exists a LPV controller stabilizing the flexible wing model.

The greedy algorithm is well-known to have polynomial time efficiency. At each step, the algorithm scans among the residual sensor subset S^s and conduct set function evaluation. After that, the element resulting in maximum set function value is added to selected set, which only needs polynomial number of operations to get local optimal sensor set.

The Figure 4.9 shows the submodular property of sensor placement. When searching only

one single sensor, there is no feasible sensor to achieve observability, thus no value of minimized trace(W) is labeled. In the case of two sensors, the sensor combination of 8,9 leads to the optimal trace(W) of closed-loop system, thus these two sensors are the optimal selection. When more than two sensors are chosen, then it is clear to observe the descending trace(W) value from left to right. This indicates that the sensors close to wing tip lead to better closed-loop system performance. Moreover, the decrement of optimal trace(W), representing improvement of \mathcal{H}_2 performance, decreases with the number of selected sensors, which demonstrates the submodular property of optimal sensor placement on flexible wing.

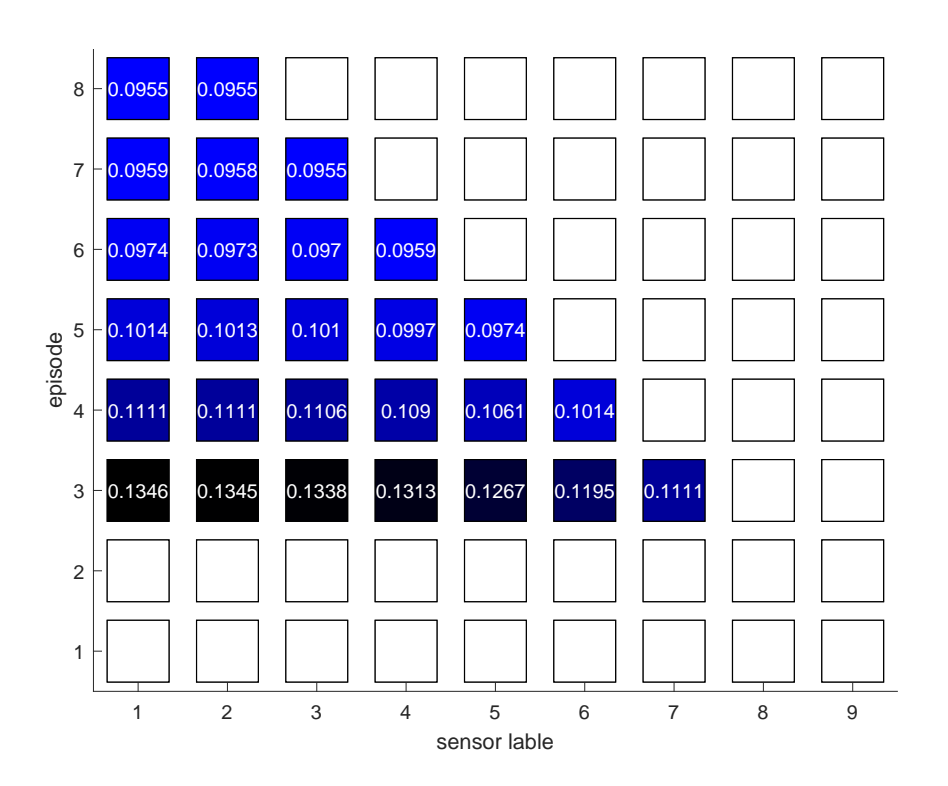


Figure 4.9: Submodular property of sensor placement on flexible wing

Algorithm 2: Greedy algorithm for optimal sensor placement

Result: K_s

Step 1. Initialization of set variable:

$$s = 1, K_s = \{\}, S^s = S$$

while $s \leq N$ do

Step 2. Check observability of sensor subset

$$i = 1$$
;

while $i \leq |S^s|$ do

continue;

if $K_s \cap j$ sensor set is unobservable then $\mid S^s = S^s \backslash j$ else

end

end

Step 3. Determine greedily the next element from residual set S^s :

$$k_s = \arg\min_{K(\theta), j \in S^s} trace(W)$$

Step 4. Update the residual set S^s and selected set K^s

$$S^{s+1} = S^s \setminus k_s, \quad K^{s+1} = K^s \cup k_s, \quad s \leftarrow s+1$$

end

CHAPTER 5

CONCLUSIONS AND RECOMMENDED WORK

5.1 Conclusions

In this dissertation, simultaneous design and sequential design of smooth switching LPV control design have been proposed, and optimal sensor placement on the BWB aircraft flexible wing has been sought in the LPV framework. The main contributions can be grouped into the following items.

- The simultaneous design approach for smooth-switching ICC/\mathcal{H}_{∞} state-feedback and dynamic output-feedback LPV control has been separately explored and PLMIs (Parametric Linear Matrix Inequalities) for controller synthesis have been accordingly derived. To obtain smooth switching, smoothness and system performance indexes were incorporated into the cost function and weighted by a tunable coefficient, introducing another tunable trade-off between system performance and switching smoothness. By tuning the coefficient, optimal balance of switching smoothness and system performance can be attained.
- The sequential design approach designs the LPV controllers independently and uses sigmoid interpolation of adjacent controllers on overlapped subregion. The \mathcal{H}_{∞} LPV state-feedback case is studied and controller synthesis conditions are derived. Furthermore, the effectiveness of sequential design and reduced computational complexity than simultaneous design are demonstrated by two numerical examples.
- The proposed LPV controllers have been applied to an active magnetic bearing system and vibration suppression of a BWB flexible airplane wing. The simulation results demonstrated that the proposed smooth-switching LPV ICC/\mathcal{H}_{∞} controllers are able to balance switching smoothness and system performance subject to constraints on control inputs and system uncertainty. In addition, the results show that the proposed method improves the switching

smoothness significantly compared with the results from the earlier study without considering switching smoothness. Simulation results of BWB airplane wing have showed that the proposed design method is able to significantly reduce the sharp jumps in system controls and responses during switching events. Furthermore, the proposed tunable weighting coefficient provides trade-off between system performance and smoothness of response, and the ICC constraints on control inputs can also be used to tune the achievable performance. These offer great advantages in practical implementation.

• In addition, the LPV approach is utilized to determine optimal sensor position for a BWB airplane flexible wing. A gain-scheduling \mathcal{H}_2 LPV control, subject to ICC hard constraints, is designed for a given scheduling parameter region. The optimal candidate for sensor allocations is obtained by searching for the best guaranteed \mathcal{H}_2 system performance within the flight speed region. By global search and greedy algorithm, the optimal candidate can be obtained for any given number of sensors, and the trade-off between optimal performance and sensor number can also be obtained.

5.2 Recommended work

With the results shown in this dissertation, there are still a few potential directions to work on, in both theory and application parts.

- Potential directions in theory
 - Smooth switching controller synthesis with Youla Parameterization. Recall the Youla Parameterization, let $K(s) = V^{-1}(s)U(s)$ and $G(s) = M^{-1}(s)N(s)$ be the left co-prime factorization of controller K(s) and nominal plant P(s). Then the Youla parameterization of all stabilizable controllers $\hat{K} = (V(s) Q(s)N(s))^{-1}(U(s) + Q(s)M(s))$ for any $Q \in RH_{\infty}$ such that $det(V(\infty) Q(\infty)N(\infty)) \neq 0$. A controller scheme based on Youla parameterization proposed in [104] is shown in Figure 5.1.

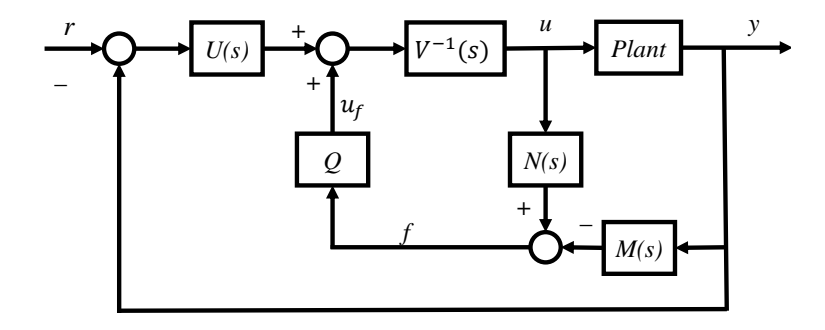


Figure 5.1: A controller scheme with compensating operator Q

Thus the switching controller has the potential to be divided into two parts: nominal controller U(s), $V^{-1}(s)$ and operator Q(s). Then switched controller gain can be included into Q, which will greatly simplify the switching stability conditions, because as long as switching operator $Q \in RH_{\infty}$, the controller \hat{K} is stabilizable for the given plant.

- Exploration of sub-modular property in Kalman Filter design for LTI/LTV/LPV system In conventional Kalman filter design, we utilize the given set of sensors and only focus on the estimator gain to achieve optimal state estimation. The sensor placement usually involves *heuristic* method and will limit estimation performance. However, in engineering practice, the sensor placement is essential and should be decided before Kalman filter design. If these two decision variables can be integrated into one optimization problem, the state estimation can be improved significantly.

Consider a stochastic system

$$\dot{x} = A(t)x + B(t)u + F(t)w$$

$$y = C(t)x + v$$
(5.1)

Assume the disturbance w(t) and noise v(t) are zero-mean, Gaussian white noise, but not necessarily stationary. They are also assumed as independent.

$$E\left\{w(s)w^{T}(t)\right\} = W(t)\delta(t-s), \quad E\left\{v(s)v^{T}(t)\right\} = V(t)\delta(t-s)$$
 (5.2)

The optimal estimation problem is formulated as minimizing the mean square error of $\hat{x}(t)$ with true state value x(t)

$$E\left\{ (x(t) - \hat{x}(t))(x(t) - \hat{x}(t))^{T} \right\}$$
 (5.3)

Theorem 11 (Kalman-Bucy, 1961). The optimal estimator has the form of a linear observer

$$\dot{\hat{x}} = A(t)\hat{x} + B(t)u + L(t)[y - C(t)\hat{x}]$$
(5.4)

where $L(t) = P(t)C^T(t)V^{-1}$ and $P(t) = E\left\{(x(t) - \hat{x}(t))(x(t) - \hat{x}(t))^T\right\}$ satisfies

$$\dot{P} = AP + PA^T - PC^TV^{-1}(t)CP + FW(t)F^T$$

$$P(0) = E\left\{x(0)x^T(0)\right\}$$

Consider a sensor selection problem for Kalman-Bucy filter that, select C_y subset consisting of s row elements in set $C = [C_1^T, C_2^T, \dots, C_m^T]^T$, and estimator gain L(t) such that estimation error is minimized, with given $P(0) = E\left\{x(0)x^T(0)\right\}$ and given $V = diag(V_m)$ and W.

The OSP is formulated as select subset $S \subseteq M$ such that

$$\min_{s \in S \subseteq M} trace(P(t)) \tag{5.5}$$

and P(t) subject to differential equation

$$\dot{P} = AP + PA^{T} - PC_{y}^{T}V_{S}^{-1}(t)C_{y}P + FW(t)F^{T}$$
(5.6)

Suppose the covariance of sensors are known, then selecting properly the sensor set to achieve optimal state estimation by Kalman filter is a very interesting research topic. If the sub-modular property or more mild property can be discovered, then the sensor placement and optimal Kalman filter gain design could be tackled.

• Potential directions in applications

- Applications of sequential design in flight control. The BWB airplane flexible wing model is always of high order, even though model reduction is conducted. This is a promising application filed that could utilize sequential design approach of switching controllers.
- Investigation of sub-modular property of flexible structure elements. In this dissertation, the submodular property is discovered based on the model of one specific flexible wing. It would be very interesting to explore whether the sub-modular property is valid for flexible structures in a general sense. If so, the sensor placement and health monitoring will be easily tackled by greedy algorithm, which has profound influence in civil and mechanical structures.

BIBLIOGRAPHY

BIBLIOGRAPHY

- [1] B. Lu and F. Wu, "Switching LPV control designs using multiple parameter-dependent Lyapunov functions," *Automatica*, vol. 40, no. 11, pp. 1973–1980, 2004.
- [2] G. Becker and A. Packard, "Robust Performance of Linear Parametrically Varying Systems Using Parametrically-Dependent Linear Feedback," *Systems & Control Letters*, vol. 23, no. 3, pp. 205–215, 1994.
- [3] G. Becker, *Quadratic Stability and Performance of Linear Parameter Dependent Systems*. PhD thesis, University of California, Berkeley, 1993.
- [4] S. Lim, *Analysis and Control of Linear Parameter-Varying Systems*. PhD thesis, Stanford University, 1998.
- [5] J. Mohammadpour and C. W. Scherer, *Control of Linear Parameter Varying Systems with Applications*. Springer, 2012.
- [6] W. J. Rugh and J. S. Shamma, "Research on gain scheduling," *Automatica*, vol. 36, no. 10, pp. 1401–1425, 2000.
- [7] A. P. White, G. G. Zhu, and J. Choi, *Linear Parameter-varying Control for Engineering Applications*. Springer, 2013.
- [8] F. Wu, *Control of Linear Parameter Varying Systems*. PhD thesis, University of California, Berkeley, 1995.
- [9] D. Liberzon and A. S. Morse, "Basic problems in stability and design of switched systems," *IEEE Control Systems*, vol. 19, no. 5, pp. 59–70, 1999.
- [10] D. Liberzon, Switching in systems and control. Springer Science & Business Media, 2003.
- [11] J. S. Shamma and M. Athans, "Analysis of gain scheduled control for nonlinear plants," *IEEE Transactions on Automatic Control*, vol. 35, pp. 898–907, Aug. 1990.
- [12] P. Apkarian, P. Gahinet, and G. Becker, "Self-scheduled \mathcal{H}_{∞} control of linear parameter-varying systems: A design example," *Automatica*, vol. 31, no. 9, pp. 1251–1261, 1995.
- [13] P. Gahinet, "A convex characterization of gain-scheduled \mathcal{H}_{∞} controllers," *IEEE Transactions on Automatic Control*, vol. 40, no. 5, pp. 853–864, 1995.
- [14] F. Wu, X. Yang, A. Packard, and G. Becker, "Induced \mathcal{L}_2 -norm control for LPV system with bounded parameter variation rates," *Proceedings of 1995 American Control Conference (ACC)*, vol. 3, pp. 983–998, 1995.
- [15] F. Wu, X. Yang, A. Packard, and B. Greg, "Induced \mathcal{L}_2 -norm control for LPV systems with bounded parameter variation rates," *International Journal of Nonlinear Robust Control*, vol. 6, pp. 983–998, 1996.

- [16] F. Wu and K. Grigoriadis, "LPV systems with parameter-varying time delays," *Automatica*, vol. 2, pp. 221–229, 2001.
- [17] P. Apkarian, H. Tuan, and J. Bernussou, "Continuous-time analysis, eigenstructure assignment, and \mathcal{H}_2 synthesis with enhanced linear matrix inequalities (LMI) characterizations," *IEEE Transactions on Automatic Control*, vol. 46, no. 12, pp. 1941–1946, 2001.
- [18] M. Chilali and P. Gahinet, " \mathcal{H}_{∞} design with pole placement constraints: An LMI approach," *IEEE Transactions on Automatic Control*, vol. 41, no. 3, pp. 358–367, 1996.
- [19] R. C. L. F. Oliveira and P. L. D. Peres, "Parameter-dependent LMIs in robust analysis: Characterization of homogeneous polynomially parameter-dependent solutions via LMI relaxations," *IEEE Transactions on Automatic Control*, vol. 52, pp. 1334–1340, Jul. 2007.
- [20] C. E. de Souza and A. Trofino, "Gain-scheduled \mathcal{H}_2 controller synthesis for linear parameter varying systems via parameter-dependent Lyapunov functions," *International Journal of Robust and Nonlinear Control*, vol. 16, no. 5, pp. 243–257, 2006.
- [21] A. K. Al-Jiboory and G. G. Zhu, "Improved synthesis conditions for mixed $\mathcal{H}_2/\mathcal{H}_{\infty}$ gain-scheduling control subject to uncertain scheduling parameters," *International Journal of Control*, pp. 1–19, Jun. 2016.
- [22] Y. Altun, "A new extended LMI-based robust gain scheduled state feedback \mathcal{H}_{∞} controller design," *International Journal of Control, Automation and Systems*, vol. 15, no. 3, pp. 967–975, 2017.
- [23] P. Apkarian and P. Gahinet, "A convex characterization of gain-scheduled \mathcal{H}_{∞} controllers," *IEEE Transactions on Automatic Control*, vol. 40, no. 5, pp. 853–864, 1995.
- [24] G. Cai, C. Hu, B. Yin, H. He, and X. Han, "Gain-scheduled \mathcal{H}_2 controller synthesis for continuous-time polytopic LPV systems," *Mathematical Problems in Engineering*, vol. 2014, 2014.
- [25] T. He, A. K. Al-Jiboory, S. S.-M. Swei, and G. G. Zhu, "Switching state-Feedback LPV control with uncertain scheduling parameters," in *Proceedings of the 2017 American Control Conference (ACC)*, pp. 2381–2386, 2017.
- [26] M. Sato, "Gain-scheduled output-feedback controllers using inexactly measured scheduling parameters," in *Proceedings of the 2010 49th IEEE Conference on Decision and Control (CDC)*, pp. 3174–3180, Dec. 2010.
- [27] M. Sato, "Gain-scheduled state-feedback controllers using inexactly measured scheduling parameters: stabilizing and \mathcal{H}_{∞} control problems," *SICE Journal of Control, Measurement, and System Integration*, vol. 3, pp. 285–291, Jul. 2010.
- [28] M. Sato, "Discrete-time gain-scheduled output-feedback controllers exploiting inexact scheduling parameters via parameter-dependent Lyapunov functions," in *Proceedings of the 50th IEEE Conference on Decision and Control and European Control Conference (CDC-ECC)*, pp. 1938–1943, Dec. 2011.

- [29] M. Sato, "Gain-Scheduled output-feedback controllers using inexactly measured scheduling parameters for linear parametrically affine systems," *SICE Journal of Control, Measurement, and System Integration*, vol. 4, no. 2, pp. 145–152, 2011.
- [30] M. Sato, Y. Ebihara, and D. Peaucelle, "Gain-scheduled state-feedback controllers using inexactly measured scheduling parameters: \mathcal{H}_2 and \mathcal{H}_{∞} problems," in *Proceedings of the 2010 American Control Conference (ACC)*, pp. 3094–3099, Jun. 2010.
- [31] M. Sato and D. Peaucelle, "Gain-scheduled output-feedback controllers using inexact scheduling parameters for continuous-time LPV systems," *Automatica*, vol. 49, no. 4, pp. 1019–1025, 2013.
- [32] P. Zhao and R. Nagamune, "Switching LPV controller design under uncertain scheduling parameters," *Automatica*, vol. 76, pp. 243–250, feb 2017.
- [33] K. Zhou, J. C. Doyle, and K. Glover, *Robust and Optimal Control*. Upper Saddle River, NJ, USA: Prentice-Hall, Inc., 1996.
- [34] C. W. Scherer, "Mixed $\mathcal{H}_2/\mathcal{H}_{\infty}$ control for time-varying and linear parametrically-varying systems," *International Journal of Robust and Nonlinear Control*, vol. 6, no. 9-10, pp. 929–952, 1996.
- [35] T. He, A. K. Al-Jiboory, G. G. Zhu, S. S.-M. Swei, and W. Su, "Guaranteed \mathcal{H}_{∞} performance LPV ICC control with application to Blended-Wing-Body model," in 2018 AIAA/ASCE/AH-S/ASC Structures, Structural Dynamics, and Materials Conference, no. 210049 in AIAA SciTech Forum, American Institute of Aeronautics and Astronautics, Jan. 2018.
- [36] G. J. Balas and J. C. Doyle, "Robustness and performance trade-offs in control design for flexible structures," *IEEE Transactions on Control Systems Technology*, vol. 2, no. 4, pp. 352–361, 1994.
- [37] F. Blanchini, S. Miani, and C. Savorgnan, "Stability results for linear parameter varying and switching systems," *Automatica*, vol. 43, no. 10, pp. 1817–1823, 2007.
- [38] C. Briat and M. Khammash, "Stability analysis of LPV systems with piecewise differentiable parameters," *IFAC-PapersOnLine*, vol. 50, no. 1, pp. 7554–7559, 2017.
- [39] G. S. Deaecto, "Dynamic output feedback \mathcal{H}_{∞} control of continuous-time switched affine systems," *Automatica*, vol. 71, pp. 44–49, 2016.
- [40] G. S. Deaecto and J. C. Geromel, "Stability analysis and control design of discrete-time switched affine systems," *IEEE Transactions on Automatic Control*, vol. 62, no. 8, pp. 4058–4065, 2017.
- [41] X. Zhao, P. Shi, Y. Yin, and S. K. Nguang, "New results on stability of slowly switched systems: A multiple discontinuous Lyapunov function approach," *IEEE Transactions on Automatic Control*, vol. 62, no. 7, pp. 3502–3509, 2017.

- [42] S. Qu, T. He, and G. G. Zhu, "LPV modeling and switched control for EGR valves with dry friction," in *Proceedings of the 2019 IEEE Conference on Control Technology and Applications (CCTA)*, pp. 400–405, Aug. 2019.
- [43] E. A. Yazdi and R. Nagamune, "A parameter set division and switching gain-scheduling controllers design method for time-varying plants," *Systems and Control Letters*, vol. 60, no. 12, pp. 1016–1023, 2011.
- [44] E. A. Yazdi, M. Sepasi, F. Sassani, and R. Nagamune, "Automated multiple robust trackfollowing control system design in hard disk drives," *IEEE Transactions on Control Systems Technology*, vol. 19, no. 4, pp. 920–928, 2011.
- [45] M. Hanifzadegan and R. Nagamune, "Switching gain-scheduled control design for flexible ball-screw drives," *Journal of Dynamic Systems, Measurement, and Control*, vol. 136, no. 1, p. 14503, 2013.
- [46] M. B. A. Jabali and M. H. Kazemi, "Uncertain polytopic LPV modelling of robot manipulators and trajectory tracking," *International Journal of Control, Automation and Systems*, vol. 15, no. 2, pp. 883–891, 2017.
- [47] H. Li, Y. Huang, G. G. Zhu, and Z. Lou, "Linear parameter-varying model of an electrohydraulic variable valve actuator for internal combustion engines," *Journal of Dynamic Systems, Measurement, and Control*, vol. 140, 08 2017. 011005.
- [48] M. Postma and R. Nagamune, "Air-fuel ratio control of spark ignition engines using a switching LPV controller," *IEEE Transactions on Control Systems Technology*, vol. 20, pp. 1175–1187, Sep. 2012.
- [49] S. Zhang, J. Yang, and G. G. Zhu, "LPV Modeling and mixed constrained $\mathcal{H}_2/\mathcal{H}_{\infty}$ control of an electronic throttle," *IEEE/ASME Transactions on Mechatronics*, vol. 20, no. 5, pp. 2120–2132, 2015.
- [50] C. Yuan and F. Wu, "Robust switching output-feedback control of time-varying polytopic uncertain systems," *International Journal of Control*, vol. 89, no. 11, pp. 2262–2276, 2016.
- [51] R. Skelton, T. Iwasaki, and K. Grigoriadis, *A unified algebraic approach to linear control design*. Taylor & Francis, 1998.
- [52] J. P. Hespanha and A. S. Morse, "Stability of switched systems with average dwell-time," in *Proceedings of the 38th IEEE Conference on Decision and Control (CDC)*, vol. 3, pp. 2655–2660, Dec. 1999.
- [53] S. Lim and K. Chan, "Analysis of hybrid linear parameter-varying systems," in *Proceedings* of the 2003 American Control Conference (ACC), vol. 6, pp. 4822–4827 vol.6, June 2003.
- [54] J. P. Hespanha, D. Liberzon, and A. S. Morse, "Hysteresis-based switching algorithms for supervisory control of uncertain systems," *Automatica*, vol. 39, no. 2, pp. 263–272, 2003.
- [55] H. Ye, A. N. Michel, and L. Hou, "Stability theory for hybrid dynamical systems," *IEEE Transactions on Automatic Control*, vol. 43, no. 4, pp. 461–474, 1998.

- [56] H. Lin and P. J. Antsaklis, "Stability and stabilizability of switched linear systems: A survey of recent results," *IEEE Transactions on Automatic Control*, vol. 54, no. 2, pp. 308–322, 2009.
- [57] J. P. Hespanha and A. S. Morse, "Stability of switched systems with average dwell-time," in *Proceedings of the 38th IEEE Conference on Decision and Control (CDC)*, vol. 3, pp. 2655–2660, IEEE, 1999.
- [58] B. Lu, F. Wu, and S. Kim, "Switching LPV control of an F-16 aircraft via controller state reset," *IEEE transactions on control systems technology*, vol. 14, no. 2, pp. 267–277, 2006.
- [59] M. Hanifzadegan and R. Nagamune, "Switching gain-scheduled control design for flexible ball-screw drives," *Journal of Dynamic Systems, Measurement, and Control*, vol. 136, no. 1, p. 014503, 2013.
- [60] P. Chen, "The design of smooth switching control with application to V-STOL aircraft dynamics under input and output constraints," *Asian Journal of Control*, vol. 14, no. 2, pp. 439–453, 2012.
- [61] M. Hanifzadegan and R. Nagamune, "Smooth switching LPV controller design for LPV systems," *Automatica*, vol. 50, no. 5, pp. 1481–1488, 2014.
- [62] T. He, G. G. Zhu, S. S.-M. Swei, and W. Su, "Smooth-switching LPV control for vibration suppression of a flexible airplane wing," *Aerospace Science and Technology*, vol. 84, pp. 895–903, 2019.
- [63] C. Hoffmann and H. Werner, "A survey of linear parameter-varying control applications validated by experiments or high-fidelity simulations," *IEEE Transactions on Control Systems Technology*, vol. 23, no. 2, pp. 416–433, 2015.
- [64] A. K. Al-Jiboory, G. G. Zhu, and C. Sultan, "LMI control design with input covariance constraint for a tensegrity simplex structure," in *ASME Dynamic Systems and Control Conference*, p. V003T52A004, Oct. 2014.
- [65] A. K. Al-Jiboory, A. White, S. Zhang, G. G. Zhu, and J. Choi, "Linear matrix inequalities approach to input covariance constraint control with application to electronic throttle," *Journal of Dynamic Systems, Measurement, and Control*, vol. 137, p. 091010, Sep. 2015.
- [66] G. Pipeleers, B. Demeulenaere, J. Swevers, and L. Vandenberghe, "Extended LMI characterizations for stability and performance of linear systems," *Systems and Control Letters*, vol. 58, no. 7, pp. 510–518, 2009.
- [67] A. K. Al-Jiboory, A. White, S. Zhang, G. G. Zhu, and J. Choi, "Linear matrix inequalities approach to input covariance constraint control with application to electronic throttle," *Journal of Dynamic Systems, Measurement, and Control*, vol. 137, pp. 91010–91019, Sep. 2015.
- [68] P. Apkarian and R. J. Adams, "Advanced gain-scheduling techniques for uncertain systems," *IEEE Transactions on Control Systems Technology*, vol. 6, no. 1, pp. 21–32, 1998.

- [69] T. He, G. G. Zhu, S. S.-M. Swei, and W. Su, "Simultaneous design of smooth switching state-feedback LPV control," in *Proceedings of the 2018 American Control Conference (ACC)*, pp. 3368–3373, Jun. 2018.
- [70] R. C. L. F. Oliveira, P. Bliman, and P. L. D. Peres, "Robust LMIs with parameters in multi-simplex: existence of solutions and applications," in *Proceedings of the 47th IEEE Conference on Decision and Control (CDC)*, pp. 2226–2231, Dec. 2008.
- [71] R. C. L. F. Oliveira and P. L. D. Peres, "Parameter-dependent LMIs in robust analysis: Characterization of homogeneous polynomially parameter-dependent solutions via LMI relaxations," *IEEE Transactions on Automatic Control*, vol. 52, pp. 1334–1340, Jul 2007.
- [72] C. W. Scherer, "LMI Relaxations in robust control," *European Journal of Control*, vol. 12, no. 1, pp. 3–29, 2006.
- [73] P. Apkarian and H. Tuan, "Parameterized LMIs in control theory," *SIAM Journal on Control and Optimization*, vol. 38, no. 4, pp. 1241–1264, 2000.
- [74] C. W. Scherer and C. W. J. Hol, "Matrix sum-of-squares relaxations for robust semi-definite programs," *Mathematical Programming*, vol. 107, pp. 189–211, 2006.
- [75] P. Gahinet, P. Apkarian, and M. Chilali, "Affine parameter-dependent Lyapunov functions and real parametric uncertainty," *IEEE Transactions on Automatic Control*, vol. 41, pp. 436–442, Mar. 1996.
- [76] J. Löfberg, "YALMIP: A toolbox for modeling and optimization in MATLAB," in *Proceedings of the CACSD Conference*, (Taipei, Taiwan), pp. 284–289, Sep. 2004.
- [77] J. F. Sturm, "Using SeDuMi 1.02, a MATLAB toolbox for optimization over symmetric cones," *Optimization Methods and Software*, vol. 11, no. 1, pp. 625–653, 1999.
- [78] C. Hoffmann and H. Werner, "Complexity of implementation and synthesis in linear parameter-varying control," *IFAC Proceedings Volumes*, vol. 47, no. 3, pp. 11749–11760, 2014.
- [79] T. He, G. G. Zhu, and S. S.-M. Swei, "Sequential design of switching \mathcal{H}_{∞} LPV state-feedback control,," in *Proceedings of the 2019 American Control Conference (ACC)*, pp. 4547–4552, Jul. 2019.
- [80] W. Jiang, C. Dong, and Q. Wang, "Smooth switching linear parameter-varying control for hypersonic vehicles via a parameter set automatic partition method," *IET Control Theory Applications*, vol. 9, no. 16, pp. 2377–2386, 2015.
- [81] F. D. Bianchi and R. S. Sánchez-Peña, "A novel design approach for switched LPV controllers," *International Journal of Control*, vol. 83, no. 8, pp. 1710–1717, 2010.
- [82] M. J. Lacerda, E. S. Tognetti, R. C. L. F. Oliveira, and P. L. D. Peres, "A new approach to handle additive and multiplicative uncertainties in the measurement for \mathcal{H}_{∞} LPV filtering," *International Journal of Systems Science*, vol. 47, no. 5, pp. 1042–1053, 2016.

- [83] B. Lu, H. Choi, G. D. Buckner, and K. Tammi, "Linear parameter-varying techniques for control of a magnetic bearing system," *Control Engineering Practice*, vol. 16, no. 10, pp. 1161–1172, 2008.
- [84] A. M. Mohamed and I. Busch-Vishniac, "Imbalance compensation and automation balancing in magnetic bearing systems using the Q-parameterization theory," *IEEE Transactions on Control Systems Technology*, vol. 3, no. 2, pp. 202–211, 1995.
- [85] H. M. Balini, J. Witte, and C. W. Scherer, "Synthesis and implementation of gain-scheduling and LPV controllers for an AMB system," *Automatica*, vol. 48, no. 3, pp. 521–527, 2012.
- [86] T. He, G. G. Zhu, and S. S.-M. Swei, "Smooth switching LPV dynamic output-feedback: A simultaneous design approach," *International Journal of Control, Automation and Systems*, 2020. in press.
- [87] W. Su, C. E. S. Cesnik, and C. E. S. Cesnik, "Nonlinear aeroelasticity of a very flexible Blended-Wing-Body aircraft," *Journal of Aircraft*, vol. 47, pp. 1539–1553, sep 2010.
- [88] A. K. Al-Jiboory, G. G. Zhu, S. S. M. Swei, W. Su, and N. T. Nguyen, "LPV modeling of a flexible wing aircraft using modal alignment and adaptive gridding methods," *Aerospace Science and Technology*, vol. 66, pp. 92–102, 2017.
- [89] J. S. Shamma, "An overview of LPV systems," in *Control of Linear Parameter Varying Systems with Applications* (J. Mohammadpour and C. W. Scherer, eds.), pp. 3–26, Boston, MA: Springer US, 2012.
- [90] T. He, A. K. Al-Jiboory, G. G. Zhu, S. S.-M. Swei, and W. Su, "Application of *ICC* LPV control to a blended-wing-body airplane with guaranteed \mathcal{H}_{∞} performance," *Aerospace Science and Technology*, vol. 81, pp. 88–98, 2018.
- [91] A. White, G. G. Zhu, and J. Choi, "Optimal LPV control with hard constraints," *International Journal of Control, Automation and Systems*, vol. 14, no. 1, pp. 148–162, 2016.
- [92] G. G. Zhu, K. M. Grigoriadis, and R. E. Skelton, "Covariance control design for Hubble Space Telescope," *Journal of Guidance, Control, and Dynamics*, vol. 18, pp. 230–236, mar 1995.
- [93] C. M. Agulhari, R. C. L. F. Oliveira, and P. L. D. Peres, "Robust LMI parser: a computational package to construct LMI conditions for uncertain systems," in *XIX Brazilian Conference on Automation (CBA 2012)*, (Campina Grande, PB, Brazil), pp. 2298–2305, 2012.
- [94] A. K. Al-Jiboory, G. G. Zhu, and J. Choi, "Guaranteed performance state-feedback gain-scheduling control with uncertain scheduling parameters," *Journal of Dynamic Systems, Measurement, and Control*, vol. 138, no. 1, p. 014502, 2016.
- [95] T. He, G. G. Zhu, S. S.-M. Swei, and W. Su, "Optimal sensor placement for vibration control of a flexible aircraft wing," in *Proceedings of the 2019 IEEE Conference on Control Technology and Applications (CCTA)*, pp. 789–794, Aug. 2019.

- [96] S. Leleu, H. Abou-Kandil, and Y. Bonnassieux, "Actuators and sensors positioning for active vibration control in flexible systems," *IFAC Proceedings Volumes*, vol. 33, no. 26, pp. 935–940, 2000.
- [97] M. van de Wal and B. de Jager, "A review of methods for input/output selection," *Automatica*, vol. 37, no. 4, pp. 487–510, 2001.
- [98] R. Potami, *Optimal Sensor/Actuator Placement and Switching Schemes for Control of Flexible Structures*. PhD thesis, Worcester Polytechnic Institute, Worcester, MA, 2008.
- [99] T. He, G. G. Zhu, S. S.-M. Swei, and W. Su, "Active vibration suppression of BWB airplane using smooth switching LPV control," in *AIAA Scitech 2019 Forum*, AIAA SciTech Forum, American Institute of Aeronautics and Astronautics, Jan. 2019.
- [100] M. Shamaiah, S. Banerjee, and H. Vikalo, "Greedy sensor selection: Leveraging submodularity," in *Proceedings of the 49th IEEE Conference on Decision and Control (CDC)*, pp. 2572–2577, IEEE, 2010.
- [101] S. T. Jawaid and S. L. Smith, "Submodularity and greedy algorithms in sensor scheduling for linear dynamical systems," *Automatica*, vol. 61, pp. 282–288, 2015.
- [102] W. K. Gawronski, *Dynamics and control of structures: A modal approach*. Springer Science & Business Media, 2004.
- [103] A. Das and D. Kempe, "Submodular meets spectral: Greedy algorithms for subset selection, sparse approximation and dictionary selection," *arXiv preprint arXiv:1102.3975*, 2011.
- [104] K. Zhou and Z. Ren, "A new controller architecture for high performance, robust, and fault-tolerant control," *IEEE Transactions on Automatic Control*, vol. 46, no. 10, pp. 1613–1618, 2001.